POLITECNICO DI TORINO

Master's Degree in Mechatronic Engineering

Master's Degree Thesis

Implementation and optimization of an innovative control algorithm for the electrification of vintage vehicles powered by an Internal Combustion Engine

Supervisors

Prof. Marco VACCA

Eng. Bruno VADALÀ

Candidate

Michele DANESE

April 2024

Ai miei genitori

Abstract

A retrofit kit serves as a system facilitating the transformation of a traditional internal combustion engine vehicle into a fully electric one. This thesis project aim to enhance a tailored algorithm designed for a vehicle control unit (VCU), an integral part of a conversion kit intended for installation in vintage cars. Specifically, the development of both Powertrain Control Module (PCM) and Battery Management System (BMS) features and how they communicate with each other is addressed. The algorithm is developed within the LabVIEW environment and subjected to testing based on the model-based design approach. The initial section involves a thorough requirements analysis of the PCM and BMS algorithms and presents their preliminary implementation. The PCM developed features encompass throttle mapping, torque output control for an inverter, execution of vehicle-management functions through a state machine, management of charging phase enablement and fault handling. The latter two are related to the BMS developed functions, which include organizing battery management through a state machine, contactors management, current limits computation, state of charge estimation and cells balancing management. Subsequently, a battery module is modeled based on available data and it's used to carry out the model-in-the-loop testing phase to check the algorithm functionality.

Contents

List of Tables

List of Figures

Chapter 1

Introduction

The energy and transportation sectors are intended to face significant challenges over the next decade. Decarbonization and pollution reduction have transitioned from being optional to imperative, necessitating the deployment of innovative technologies and solutions to reach the ambitious targets set by the European Union (EU). Electric mobility emerges as a pivotal opportunity to realize environmental goals through more sustainable transportation. With the EU's focus on CO2 reduction targets and the growing share of renewable energy sources in the generation mix, it is increasingly inevitable that Electric Vehicles (EVs) will dominate the automotive industry. The "Fitfor55 package," released by the EU in July 2021, mandates a 55% reduction in average emissions from new cars by 2030 and complete elimination by 2035 compared to 2021 levels. Consequently, all new cars entering the European market must be zero-emission vehicles by 2035 [1]. However, due to the high purchase price, these vehicles still remain a niche product. An interesting solution, to encourage their widespread use, could be the Electric Retrofit, the transformation of a car already on the road with an Internal Combustion Engine (ICE) into an electric one. The production of such Retrofit kit supports the concept of circular economy that aim to reduce the deleterious practice of scrapping, giving a substantial contribution to the abatement of global warming and improving the vehicle recycling [2].

The aim of this thesis project is to further develop an existing prototype Vehicle Control Unit (VCU) integrated into a retrofit kit. The implemented algorithm is designed to regulate various aspects of an electric vehicle, encompassing both the powertrain and the battery system. Concerning the powertrain, the algorithm will generate a torque request signal to be transmitted to the inverter, taking into account throttle and brake positions, as well as the current speed of the vehicle. Subsequently, the control strategy will restrict the maximum available torque based on factors such as motor temperature, shaft speed, state of charge, and potential faults. On the battery side, the algorithm will continuously monitor the battery's status by analyzing voltage, temperature, and current measurements. Additionally, it will ensure the safety of the vehicle by preventing battery faults during the charge and discharge phases. The algorithm will also manage cell balancing to guarantee uniform voltages among all cells, and it will govern the contactors for the purpose of connecting and disconnecting the battery with the rest of

the architecture. State of charge estimation is another integral aspect incorporated into the algorithm, closely related to enabling the charging phase.

The software has been developed within the LabVIEW environment and is designed to run on the Miracle[2], a fast prototyping control unit that is directly compatible with this programming language. Finally, battery management logics are tested using a simulated LabVIEW model of a battery module, subjected to the Model-in-the-Loop (MIL) testing phase according to the V-cycle methodology.

1.1 eRSS features

The e-RSS (electrified retro-smart system) consists of a modular and configurable platform that incorporates electric driving technologies into vintage vehicles. The conversion system is composed of an Inverter, Electric Motor, Battery Pack, Charger and a VCU that is specifically designed for this application. The VCU manages both all the powertrain functionality, regulating the power flow in the system and ensuring that the vehicle can operate safely in all conditions, and all battery management functionality, monitoring the battery pack status ensuring both safety and efficiency in its operation. The installation of the eRSS kit enables the end consumer to fully satisfy the following needs:

- *Low Environmental Impact Mobility:* the use of electric cars aligns with environmental conservation efforts, promoting "zero emissions" and mitigating noise pollution.
- *Reduced Automobile Management Costs:* this includes decreased maintenance expenses, leading to savings on repairs and inspections. Additionally, benefits such as stamp duty relief, reduced insurance costs, and free parking on designated areas contribute to a substantial reduction in overall ownership expenses
- *Extended Automobile Lifecycle:* the less complex nature of electric car engines, compared to traditional combustion engines, results in lower maintenance frequency, enhancing the overall longevity of the vehicle
- *Freedom of Movement in Traffic-Restricted Areas:* retrofitted cars grant the freedom to access all restricted traffic zones (ZTL) in Europe without constraints or additional costs. This not only provides practical benefits but also contributes to the improvement of urban traffic conditions, making city driving a more pleasant experience.

1.2 Retrofit Policy

The retrofit decree published by the “Ministero delle Infrastrutture e dei Trasporti” in 2015 defines the procedures for national approval, for the purpose of certification, and the installation procedures of electric retrofit systems on vehicles falling within

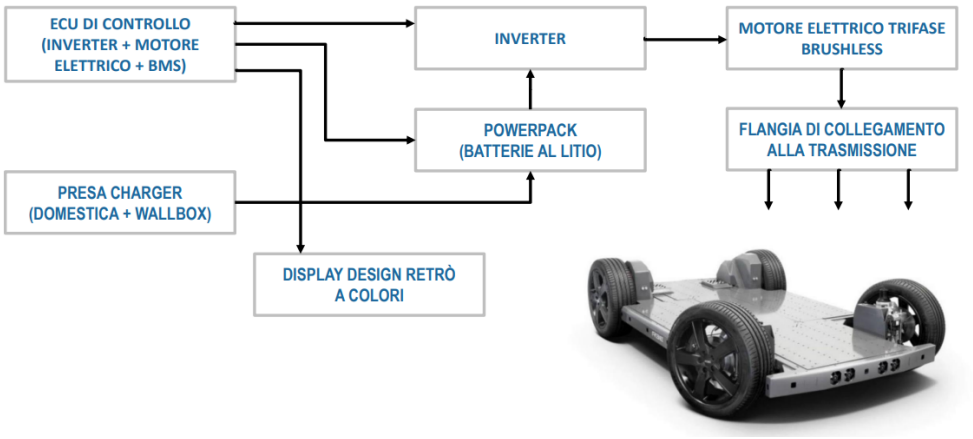

Figure 1.1: eRSS Architecture

the international categories M1, M1G, M2, M2G, M3, M3G, N1, and N1G, originally registered with a thermal engine. The retrofit system has to comprise at least [3]:

1. An electric powertrain (electric machine and its power converter), mounted upstream of the transmission components.
2. A battery pack (inclusive of the electric and thermal management system for the accumulators and a disconnecting and protective system) designed to exclusively provide energy and traction power.
3. An interface with the grid for recharging the battery pack.
4. Any other subsystems necessary for the proper functioning of the converted vehicle.

This thesis work concerns the design of a retrofit kit tailored for M1-type vehicles, which can accommodate no more than 8 passengers and can be driven with a B license. It is therefore necessary to follow all the associated guidelines; in particular, Annex C of the decree outlines the approval process for electric retrofit systems, establishing some European regulations, constraints, which extend to the algorithm we will develop. Some of these limitations include:

- The power of the electric powertrain must fall within the closed interval 65% to 100% of the maximum power of the original ICE.
- The arrangement of the electric powertrain and related components must not substantially alter the vehicle's balance concerning mass distribution on the axes. This must remain within +/- 20% compared to that of the original vehicle for each axis, while the overall mass must not exceed 8% more.
- The conventional fuel tank (gasoline or diesel) and those for LPG or CNG, must be removed or rendered unusable before installing the electric retrofit system.
- The active and passive safety devices of the base vehicle must not be modified.

Chapter 2

EVs Overview

An electric vehicle (EV) is a type of vehicle propelled by one or more electric motors, relying on electrical energy stored in batteries or other energy storage devices. The key components of an electric vehicle include the electric motor, power electronics for controlling the motor, and the energy storage system (typically a battery pack).

2.1 EVs Classification

Electric vehicles can be classified according to the degree of electrification, which generally refers to the extent to which the vehicle relies on electricity. Categories include:

- **Hybrid Electric Vehicles (HEVs):** these vehicles combine an internal combustion engine with an electric motor. They can operate on either the engine alone, the electric motor alone, or a combination of both.
- **Plug-in Hybrid Electric Vehicles (PHEVs):** similar to HEVs, PHEVs have both an internal combustion engine and an electric motor. However, PHEVs can be charged externally and have a larger electric-only driving range.
- **Battery Electric Vehicles (BEVs):** BEVs are fully electric vehicles that rely solely on electric power stored in batteries. They do not have an internal combustion engine and produce zero tailpipe emissions.
- **Fuel Cell Electric Vehicles (FCEVs):** FCEVs use hydrogen fuel cells to generate electricity, which powers an electric motor. They emit only water vapor as a byproduct.

2.1.1 HEVs

As shown in the figure 2.1, among the main components of this architecture we can find the internal combustion engine, the gas exhaust system and the gasoline tank. Regarding the components essential for the control and operation of electric propulsion, they show remarkable similarities to those identified in the BEV architecture. However,

unlike the latter, these components exhibit reduced performance due to their limited use. Based on the degree of hybridization, Hybrid Electric Vehicles can be classified as Micro-Hybrid, Mild Hybrid, Full Hybrid or Plug-in Hybrid Electric Vehicles. These vehicles are briefly described [4]:

- *Micro Hybrid Electric Vehicles:* micro-hybrid EVs typically operate in a voltage range of 12 V to 48 V, with an electrical power capacity often less than 5 kW, and thus have mainly only auto start-stop functionality. In braking and idling scenarios, the ICE automatically shuts down, contributing to a potential 5-10% improvement in fuel economy, especially in urban driving conditions. Some of these vehicles, taking advantage of the increased power capacity of a 12 V battery, incorporate some degree of regenerative braking capability, which allows the recovered energy to be stored in the battery. The implementation of most micro-hybrid electric systems involves improvements to the alternator starting system. This modification alters the conventional belt arrangement and reinforces the alternator, enabling engine starting and battery charging. Lead-Acid batteries are widely used on these vehicles. The main advantage of micro-hybrid vehicles lies in their cost-effectiveness, although a major disadvantage is the inability to recover the full regenerative braking energy.

- *Mild Hybrid Electric Vehicles:* unlike micro-hybrid EVs, mild hybrid EVs are usually equipped with an independent electric drivetrain capable of providing 5-20 kW of electric propulsion power. The electric propulsion system operates in a voltage range of 48 V to 200 V. Mild hybrid electric vehicles leverage an electric motor to assist the ICE during intense acceleration phases and efficiently recover most of the regenerative energy during deceleration phases. Common implementations include the belt starter-generator, mechanically linked through the alternator belt in a manner similar to micro-hybrids, and the starter-generator, mechanically linked via the engine crankshaft. Nickel-Metal Hydride and Lithium-Ion batteries are often used in these hybrid electric vehicles. One distinctive feature of mild hybrid electric vehicles is the absence of an exclusive electric-only propulsion mode. Improvement in fuel economy, ranging from 15 to 20%, result from engine shutdown at stops, using electrical power for initial vehicle start-up, optimizing engine operational points, and minimizing transients.

- *Full Hybrid Electric Vehicles:* here, the electric drive system typically exceeds 40 kW of power and operates at a voltage level exceeding 150 V to enhance operational efficiency and accommodate component/wire size.The electric powertrain in a full hybrid electric vehicle has the capability to exclusively power the vehicle for brief periods, especially when the combustion engine operates less efficiently. The energy storage system is designed to capture and store regenerative braking energy during various deceleration scenarios. These vehicles can also offer a purely electric driving range of up to two kilometers, catering to specific needs such as silent cruising in designated areas and achieving zero emissions for driving in tunnels and indoor spaces. In comparison to traditional ICE vehicles, full hybrid electric vehicles demonstrate a potential improvement of up to 40% in overall fuel economy during city driving conditions.

A second classification on HEVs can be made on how the power of the electric motor is combined with that of the ICE:

- *Series type configuration:* the vehicle operates with the ICE coupled to a generator, which charges the batteries and/or supplies electrical energy to the electric motor. Subsequently, the electric motor delivers all the torque required for wheel propulsion. This type is most commonly used in PHEVs.
- *Parallel type configuration:* here, the vehicle is driven by either an ICE, an electric motor, or both simultaneously. The electric motor operates as a generator during regenerative braking or when the thermal engine generates excess power beyond what is necessary for vehicle propulsion, thereby recharging the batteries.
- *Combined type configuration:* although having the advantageous features of series and parallel configurations, the combined architecture is relatively more complicated and expensive.

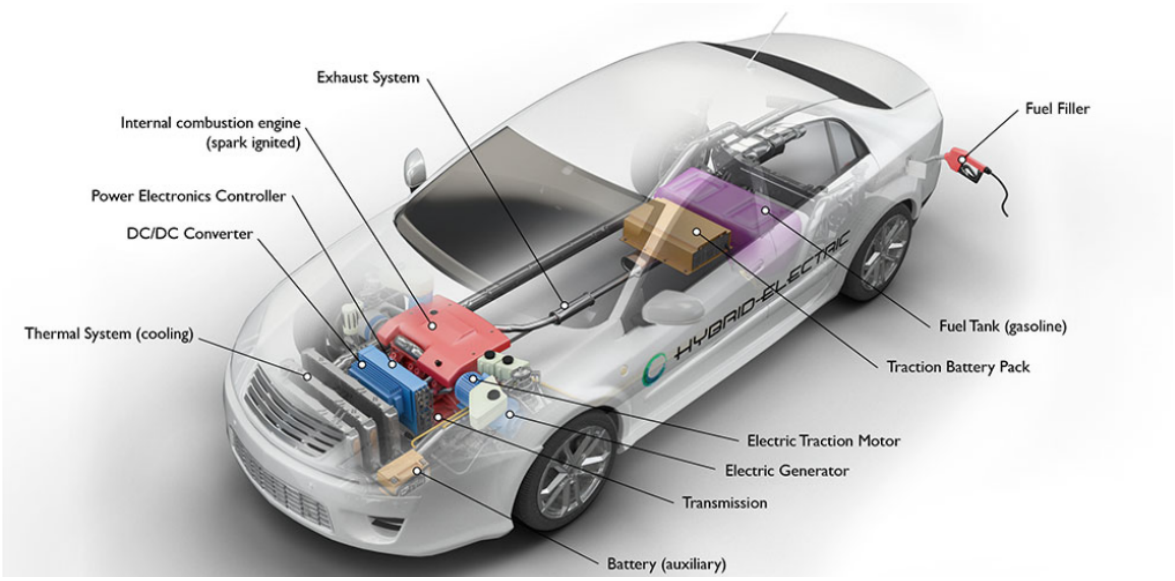

Figure 2.1: HEV Architecture [5]

Due to the fact that the electric motor is generally less bulky than the thermal motor, a freedom of choice in where to put it is allowed. Depending on the distance between the electric motor and the wheels we can define different classes:

- **P0:** configuration implemented through an enhanced belt starter–generator system to handle frequent start–stop operation. Electric motor before thermal one.
- **P1:** configuration with an electric motor mounted on the drive shaft, downstream of the ICE, before the clutch. In P0 and P1, the power of the electric motor is not high, in fact they are typical architectures of micro hybrid electric vehicles.

The efficiency of P1 architecture is higher than P0 because it lacks belt-pulley transmission.

- **P2:** P2 hybrid joint is located on the input gear shaft of the transmission. This implies the addition of a clutch, which makes the car very versatile; most mild hybrid electric vehicles use this architecture.
- **P3:** configuration in which the electric motor is placed immediately after the gearbox. Propulsion efficiency is improved.
- **P4:** since the motor/generator is mounted on the rear axle, and there are fewer and fewer entrained organs, the P4 architecture is the most efficient implementation to recover regenerative braking energy and enhance the vehicle. Possible to cruise in electric-only.
- **P5:** configuration in which the electric motor is placed directly inside the wheels. It allows the elimination of the differential and half-shafts; the main disadvantage is an increase in wheel weight, which worsens comfort and road holding. Little adopted solution.

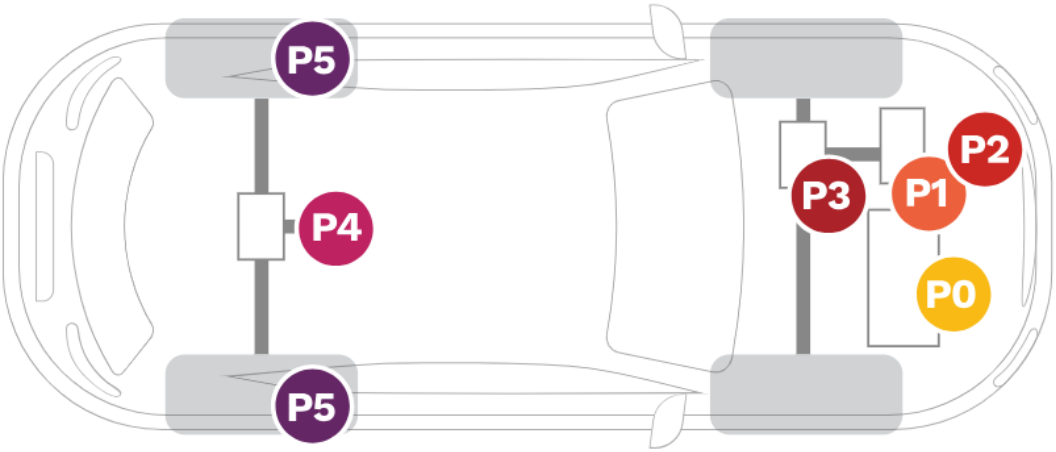

Figure 2.2: Powertrain Arrangements [6]

2.1.2 PHEVs

Plug-in Hybrid Electric Vehicles are a middle ground between HEVs and BEVs. Compared to the hybrid vehicles seen so far, which could recharge the battery through regenerative braking and ICE, PHEVs can also recharge the battery pack by connecting the car to the charging station through a specific socket. The electric powertrain of PHEVs typically has an electric power capacity of between 80 and 150 kW. This capacity allows the vehicle to operate exclusively in electric mode, providing an electric range of between 20 and 60 km. During driving, the vehicle initially enters electric mode, using the energy stored in the battery. When the battery reaches a certain level of

depletion, the ICE come in to propel the vehicle. At the same time, the battery performs the dual function of providing additional electrical energy and capturing regenerative braking energy, as in a full hybrid electric vehicle. This multifaceted approach aims to improve fuel economy, dynamic performance, and reduce emissions. The fundamental components, shown in figure 2.3, are identical to those present in hybrid vehicles, with the exception of the on-board charger and charging socket. These additions facilitate the charging of larger batteries, thereby optimizing the efficiency of electric propulsion.

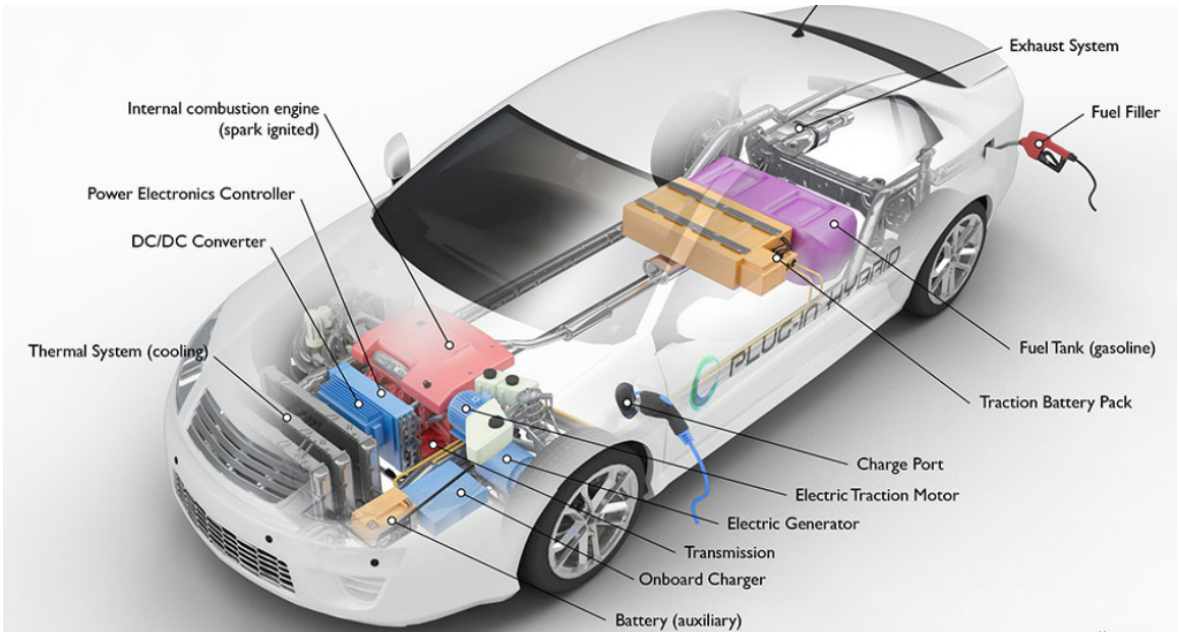

Figure 2.3: PHEV Architecture [5]

2.1.3 BEVs

Vehicles exclusively powered by electric drive systems fall under the category of Battery Electric Vehicles. Unlike ICE vehicles, BEVs feature a large battery, usually Lithium-Ion, that serves as the primary source of energy for the electric motor. As a result, they do not have a fossil fuel tank and exhaust system for combustion emissions. While BEVs demonstrate high fuel efficiency and minimal environmental impact, their driving range tends to be less than that of conventional combustion engines. Charging the battery is achieved by connecting the vehicle to the power grid through a wall socket or a designated charging station. The efficiency and range of BEVs are influenced by various factors. Extreme temperature conditions can impact the battery's energy capacity, leading to a reduction in the vehicle's range. Additionally, the driving environment plays a crucial role; city driving proves advantageous as it allows for energy regeneration through regenerative braking. At the opposite, highway driving tends to decrease the range faster due to increased energy consumption in countering aerodynamic forces at higher speeds.

As seen in the figure 2.4, the main components are:

- Electric Traction Motor
- Inverter
- Battery Pack
- On-board Charger
- DC-DC Converter
- Charging Port
- Auxiliary Battery to provide electricity to power vehicle accessories

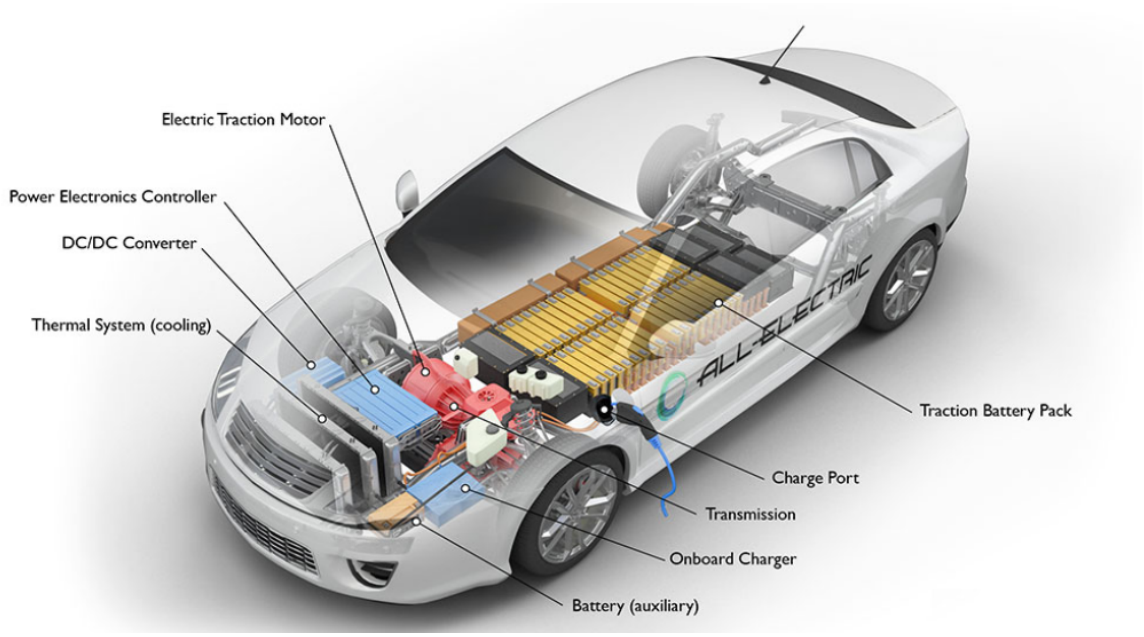

Figure 2.4: BEV Architecture [5]

2.1.4 FCEVs

Fuel Cell Electric Vehicles represent a cutting-edge paradigm in sustainable transportation. These vehicles leverage hydrogen as a fuel source, utilizing fuel cells to electrochemically convert hydrogen and oxygen into electricity to power an electric motor. The only emission from this process is water vapor, making FCEVs a promising solution for reducing greenhouse gas emissions and mitigating environmental impact. The main components of an FCEV include a fuel cell stack, a series of electrodes separated by a polymer electrolyte membrane where electrochemical reactions take place, a tank where hydrogen is stored, a battery pack that stores lost energy captured during regenerative braking, and an electric drive system responsible for propelling the vehicle. Like conventional ICE vehicles, they can refuel in about 5 minutes and

boast a driving range of more than 300 km. As technology continues to evolve, fuel cell electric vehicles are set to play a key role in the transition to a more sustainable and environmentally conscious mobility ecosystem.

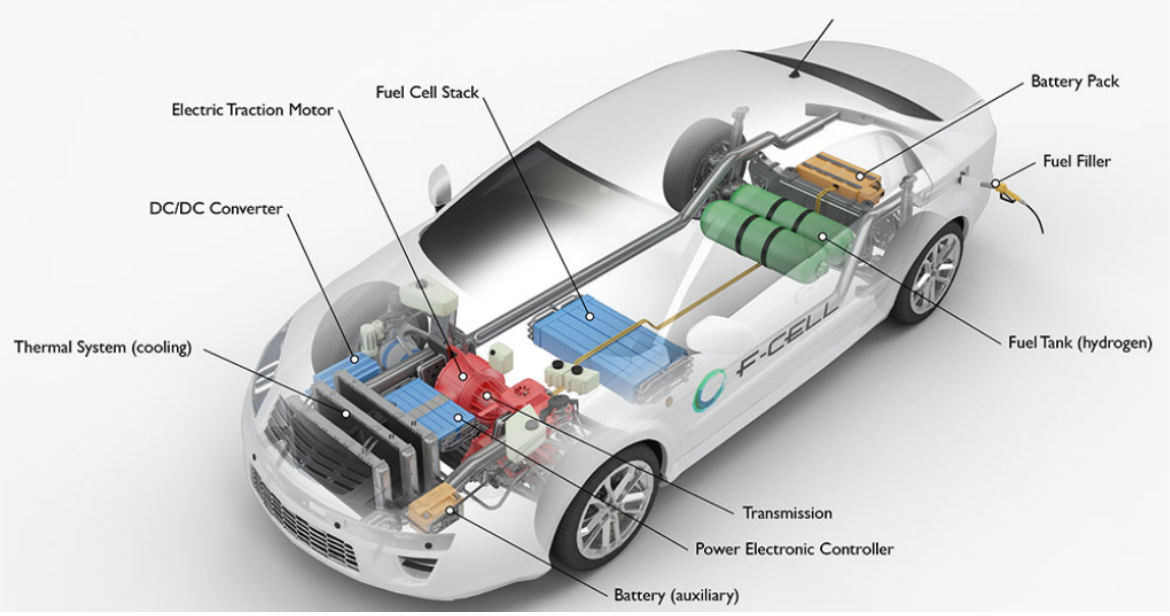

Figure 2.5: FCEV Architecture [5]

2.2 BEV Architecture

The architecture consists of several key components that work in harmony to provide efficient and sustainable electric propulsion. It includes the following elements:

1. **Battery Pack:** the heart of a BEV, advanced lithium-ion battery technology is typically used. This high-capacity battery stores electrical energy to power the electric motor.

2. **Electric Traction Motor:** it is responsible for converting electrical energy from the battery into mechanical energy to drive the vehicle's wheels. The electric motor operates silently and efficiently.

3. **Power Electronics:** set of units used to manage the flow of electricity between the battery and the electric motor. It includes:

   (a) **Inverter:** it controls the speed and torque of the electric motor by converting direct current from the battery into three-phase alternating current for the electric car. When the vehicle is in energy recovery (braking), the inverter performs the opposite conversion, from three-phase alternating current (AC) to direct current (DC).

(b) **DC-DC Converter:** responsible for lowering the high voltage (e.g. 400 V) to the low voltage network (12 V).

4. **Charging Interface:** fundamental component that enables the vehicle to replenish itself with electricity. The charging system includes:

   (a) **On-board Charger (OBC):** responsible for converting alternating current from the power source into direct current to charge the vehicle's battery.

   (b) **Charging Port:** BEVs are equipped with a charging port that allows the vehicle to be connected to an external power source to recharge the battery. Charging can be done at home, through public charging stations or rapid charging networks.

5. **Energy Management and Control system:** electronic control units, ECUs, that manage different aspects of the vehicle, including:

   (a) **Powertrain Control Unit (PCU):** this ECU implements the algorithm that determines the relationship between the input commands, such as the throttle, and the output torque request to be sent to the inverter to drive the motors.

   (b) **Battery Management System (BMS):** it monitors the temperature, voltage and current of the battery pack cells, ensuring safe operation and extending battery life.

6. **Transmission:** it transfers mechanical energy from the electric drive motor to the wheels. Many BEVs use a single-speed transmission since electric motors provide high torque across a broad range of speeds, eliminating the need for traditional multi-speed transmissions.

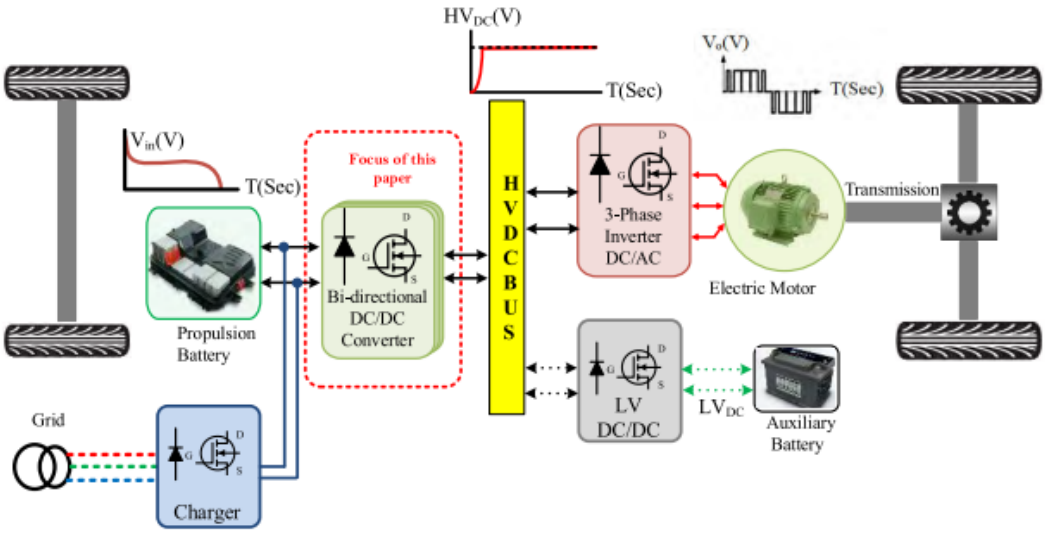

Figure 2.6: Simplified block diagram of BEV Drivetrain [7]

2.2.1 Battery Pack

The Energy Storage System (ESS) used in electric vehicles is mainly a battery composed of rechargeable cells.
The battery cell is the essential component of a battery pack and produces an electrical potential determined by factors such as electrode chemistry, temperature, and state of charge. Within the cell, electrochemical energy can be stored and converted into electrical energy when connected to an external load. Cells can be connected in series or parallel to obtain a higher voltage or capacity, respectively. Multiple cells combined form a battery module. They can come in various shapes and sizes, influencing the entire design of the battery pack. However, the most common configurations in automotive applications include cylindrical, prismatic, and pouch designs.

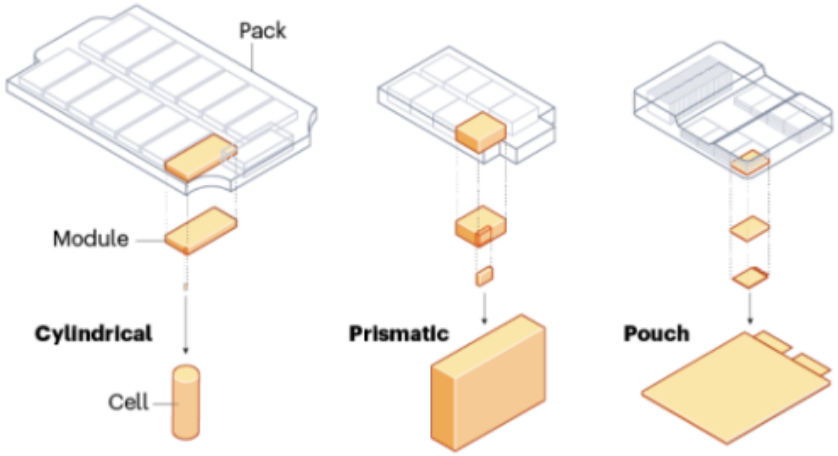

Figure 2.7: Arrangement of battery cells into modules and assembly into battery packs [8]

Each module is characterized by a set of cells, temperature, voltage, and current sensors, a cooling and heating system, and a physical casing that houses the battery cells and associated components. The casing provides protection from shock, vibration, and other environmental factors as well as electrical isolation. In addition, the module incorporates a cell balancing circuit to ensure uniform performance across all cells.
The combination of modules, on the other hand, forms the battery pack. It is the final system that supplies power to the vehicle. Typically, a battery pack reaches an average voltage ranging from a few hundred to several hundred volts (e.g., 200-800 V). They can be incorporated into electric vehicles (EVs) using different installation configurations. Some of the main methods commonly used are [9]:

(a) *Floor Integrated:* the battery pack that is a removable, yet integral, part of the floor requires a special protective structure and floor design. This configuration offers advantages in terms of maximizing interior space and cooling. It is one of the most widely used configurations.

(b) *Platform:* unlike the floor integrated, it has a more distributed battery cell

distribution, but the battery is not removable. Therefore, the platform is not integrated into the floor structure but becomes the floor structure.

(c) *Tunnel Mounting:* this configuration places the battery pack along the center tunnel of the vehicle, which usually runs between the front and rear seats.

(d) *Rear Mounting:* the battery pack is strategically placed at the rear of the electric vehicle. Placing the battery in the rear can limit the available interior space, potentially impacting passenger and cargo space.

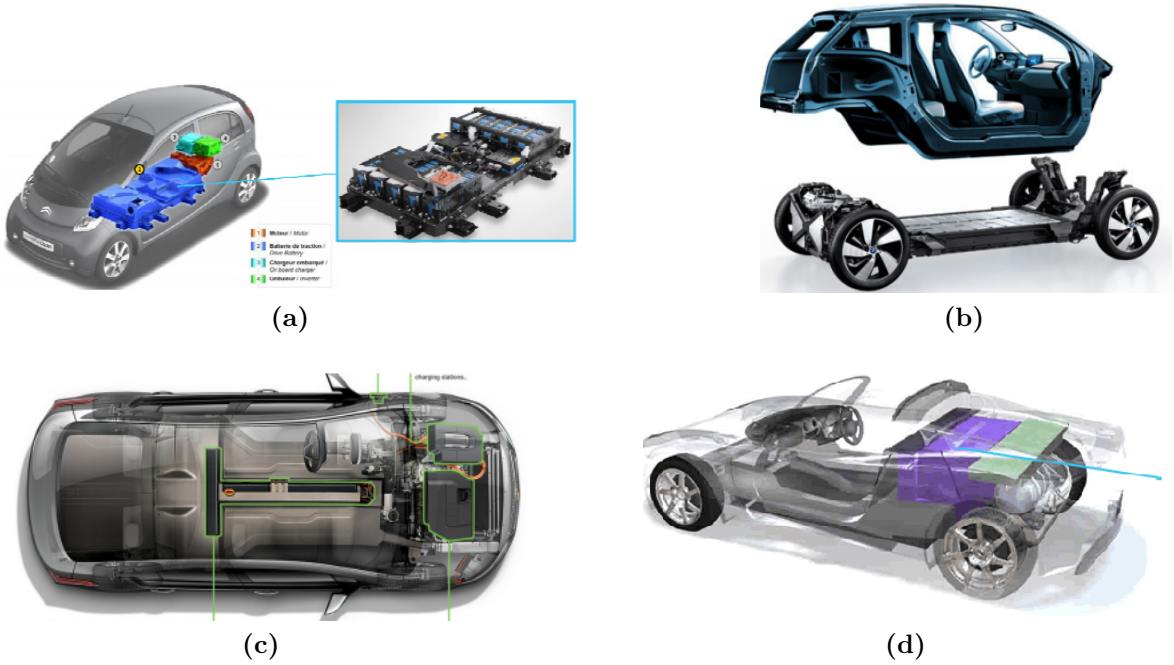

Figure 2.8: Battery Pack configurations: (a) Floor Integrated; (b) Platform; (c) Tunnel Mounting; (d) Rear Mounting

The battery pack connects to both the inverter and the OBC through a series of contactors, switches that can be operated by a control system. They are essentially a relay. There are two main types of contactors: Normally Open (NO) and Normally Closed (NC). An NO contactor prevents the passage of current when the actuation circuit is not powered. At the opposite, an NC contactor connects the external circuit when the contactor's actuating coil is not energized. Therefore, we use EV contactors as NO to switch off the circuit in case of loss of actuation circuit supply.
Before the main contactor closes, a pre-charge contactor is often used to gradually introduce power into the system, mitigating inrush currents and ensuring a smoother connection. The coordination of these contactors is typically orchestrated by the battery management system which we will analyze in more depth later.

2.2.2 Electric Traction Motor

An electric machine is an electromechanical device that converts energy into electrical and mechanical forms. When energy is converted from electrical to mechanical to propel the vehicle's wheels, it is referred to as a "motor". During braking, the machine reverses the flow of energy, converting mechanical energy from the wheels into electrical energy stored in the battery. This phenomenon is called regenerative braking, and in this case the electric machine acts as a "generator". Regenerative braking mode is a distinctive feature of EVs. The conversion of energy in both directions - electric to mechanical and vice versa - involves electrical, mechanical, and magnetic losses that affect overall efficiency. Although some energy is inevitably lost during the conversion process, electric machines generally exhibit high efficiency compared with other energy conversion devices.
Electric motors offer advantages over ICEs, providing full torque at low speeds, and their instantaneous power rating can be two or three times the rated power, contributing to excellent acceleration. Electric motors are of two types: DC motor and AC motor. Despite the ease of control of DC motors, their size and maintenance requirements are making their use obsolete not only in the automotive industry. As for AC and brushless motors, although their control is more complex, they are widely used. This is due to the new vector control techniques developed for sinusoidal machines, which make the control of AC motors similar to that of DC motors through reference frame transformation techniques [10]. AC motors can be classified into:

- **Asynchronous motor:** commonly referred to as an induction motor (IM).
- **Synchronous motor:** it can be further classified into:
  - *Permanent Magnets motor (PMSM)*
  - *Switched Reluctance motor (SRM)*

AC machines require an alternating power supply, which can be obtained from a DC source through a DC/AC inverter. These machines can be single-phase or multi-phase types. Single-phase AC machines are used for low-power applications, while higher-power machines are always in a three-phase configuration. In both asynchronous and synchronous machines, the stator windings have a similar configuration and are responsible for creating the rotating magnetic field (RMF). The stator, a static part of the EM, consists of two distinct parts: the stator core and the stator windings. The stator core consists of a series of grooved silicon steel sheets, called foils, stacked and designed to guide magnetic flux and minimize losses caused by eddy currents. The thickness of the foil is inversely proportional to the magnetic field strength generated. Inside the grooves, a set of insulated electrical coils forms the stator windings. They are powered by three-phase AC (balanced triad of currents) which, together with the geometric arrangement of the polar pair, generate a rotating magnetic field whose speed is called the "synchronism speed" and is equal to the following expression:

$$\omega_s = \frac{2\pi f}{p} \tag{2.1}$$

where:

- f is the frequency of the supply currents.
- p is the number of polar pairs; number of windings for each phase. Each North-South pair is defined as a polar pair.

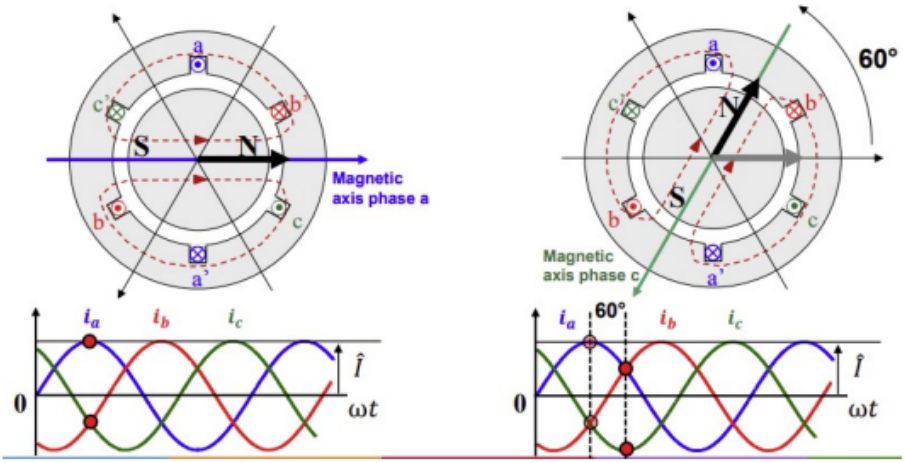

Figure 2.9: RMF generated by a balanced triad of currents

Asynchronous motor

Based on the structure of the rotor, the moving part of the EM, two types of induction motors are distinguished.

(a) **Squirrel cage:** copper rods are housed in the rotor slots, which are soldered to two front rings, also made of copper, to form a cage. Thus connected, the cages form a short circuit that is run through by currents induced by the rotating magnetic field. In addition, it does not have its own number of poles, but naturally matches the number of poles of the stator.

(b) **Wound:** a winding with a number of phases that may also differ from that of the stator winding is housed in the rotor slots. The rotor winding is connected in the shape of a star with the terminals headed by three conducting rings, insulated both from each other and from the shaft on which they are keyed. On the rings rest the brushes by which the phases of the rotor winding are connected to three external, variable, star-connected resistors. The set of the three variable resistors forms the starting rheostat, whose main purpose is to limit the currents drawn by the motor during starting and to increase starting torque. In normal operation, the rings are short-circuited and the rotor behaves like a cage rotor. At startup, however, all resistors are introduced, which are then gradually excluded as the rotor accelerates. This starting maneuver allows the mechanical characteristic to be shifted along the x-axis until the maximum torque matches the starting torque.

Due to its more robust structure and cost-effectiveness, the squirrel cage is more widely used today than its competitor despite start-up problems.

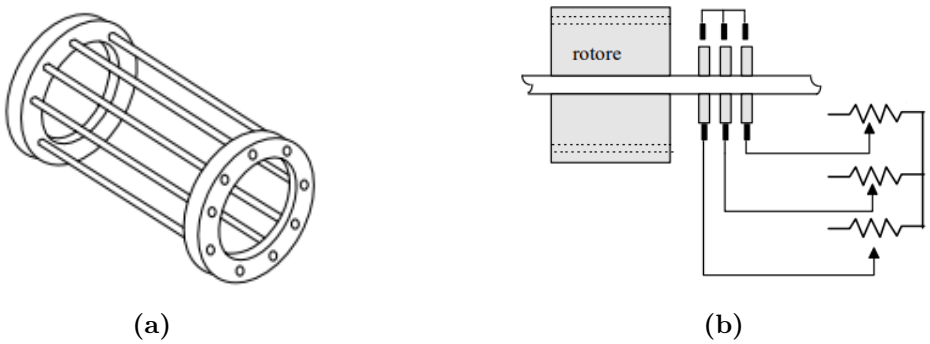

(a) **(b)**

Figure 2.10: (a) Squirrel cage rotor; (b) Wound rotor

As we have seen, when three-phase current flows through the stator, a rotating magnetic field of constant modulus is generated. By Faraday's law, since we have a variable electromagnetic field in a closed circuit, an induced voltage will be created on the rotor. As a result of this phenomenon, an induced current will be generated on the rotor, which, being in a magnetic field, will produce, by Lorentz's law, a pair of electromagnetic forces that will rotate the rotor. It will rotate at a lower speed than synchronism, because if it were equal, the change in flux and consequently the induced currents and driving torque would cancel out. The difference between the rotating stator magnetic field ω_s and the rotational speed of the rotor ω_r can be expressed by the slip, defined as:

$$s = \frac{\omega_s - \omega_r}{\omega_s} \tag{2.2}$$

It represents the fraction of revolutions lost by the rotor relative to the rotating magnetic field, for each of its revolutions.
The characteristic curve of a motor, figure 2.11, is the graph that relates the driving torque (or power) delivered by the motor to the rotational speed of the rotor. As an alternative to the number of revolutions, slip can be represented, remembering that for $s = 0$ the rotor speed is equal to the synchronous speed (theoretical value), while for $s = 1$ the rotor is still. The mechanical characteristic turns out to be anti-symmetric with respect to slip values: $T_m(-s) = -T_m(s)$. The electromagnetic torque results positive, concordant with the direction of field rotation, for positive values of the slip, otherwise negative. It follows that the electromagnetic torque has direction concordant with the direction of rotation of the rotor (**Motoring Region**) only for slip values between 0 and 1, while it opposes motion in all other cases. For negative slip (the rotor rotates in the direction of field rotation but at a higher speed) or greater than 1 (the rotor rotates in the opposite direction to that of field rotation), the machine absorbs mechanical power; this mechanical power can be returned, net of losses, to the stator supply network in the form of electrical energy (**Generating Region**) or dissipated entirely within the machine itself (**Breaking Region**). In the starting phase, i.e., when the rotor is still,

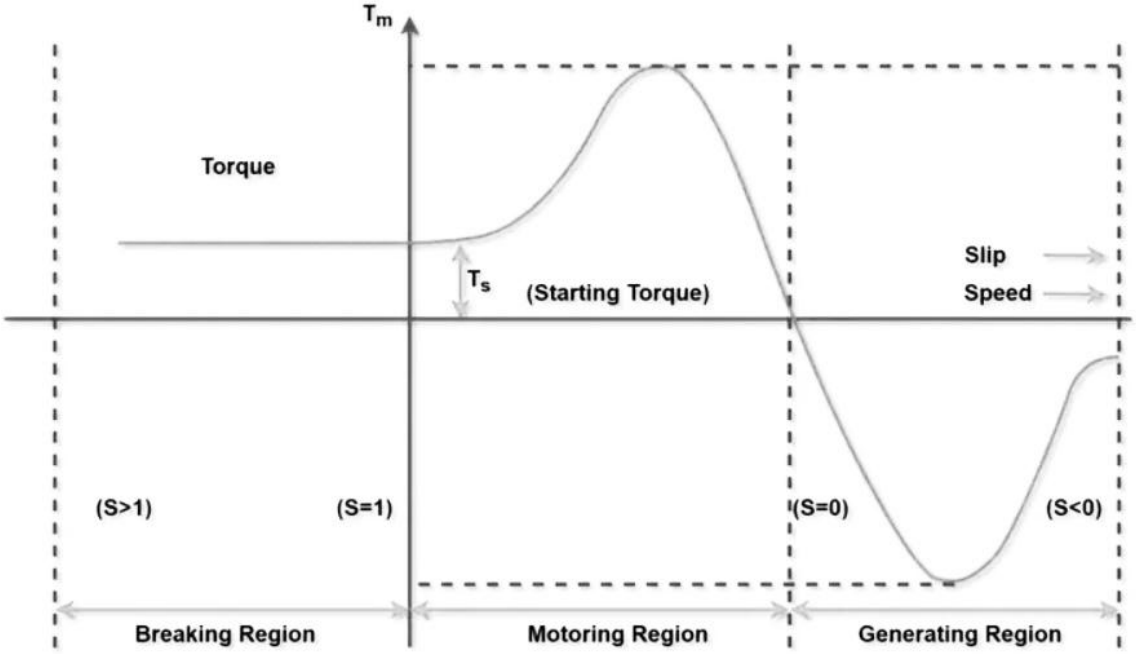

Figure 2.11: Torque-speed characteristic

as indicated by the Motoring Region, there is a starting torque T_s that, if greater than the resisting torque T_r, allows the motor to start and move up to the steady-state speed, in which the electromagnetic torque T_m equals the resisting torque (including internal motor friction). The achieved steady state is stable and corresponds to the decreasing section of the curve. So, the working point is given by the intersection with the resistant torque curve. In the stable section, if there is a perturbation that increases T_r, because of this excess resistance, the rotational speed tends to slow down, but this slowing down causes the driving torque to increase. This increase in driving torque restores the operating conditions to the previous operating point as soon as the perturbing cause ceases.

Control strategies for an induction motor are critical to ensure optimal performance, energy efficiency and operational stability. One of the most common types is constant voltage/frequency speed control, in which the frequency and voltage applied to the motor are adjusted to achieve the desired speed. Using the inverter allows the frequency to be set, allowing the speed to vary according to 2.1. At the same time, managing the voltage so that the V/f ratio remains constant allows the motor speed to vary with constant flux. Since electromotive force and torque are directly proportional to flux, maintaining flux at a constant level ensures constant torque. By continuing to increase the voltage and frequency proportionally, the nominal value of the voltage is reached, beyond which it cannot go. To continue increasing the speed, simply increase the frequency by fixing the voltage at the nominal value: the flux decreases as well as the torque.
Other speed control strategies include adjusting the number of poles (in cage rotor motors, it is possible, by means of appropriate switches, to vary the number of pole

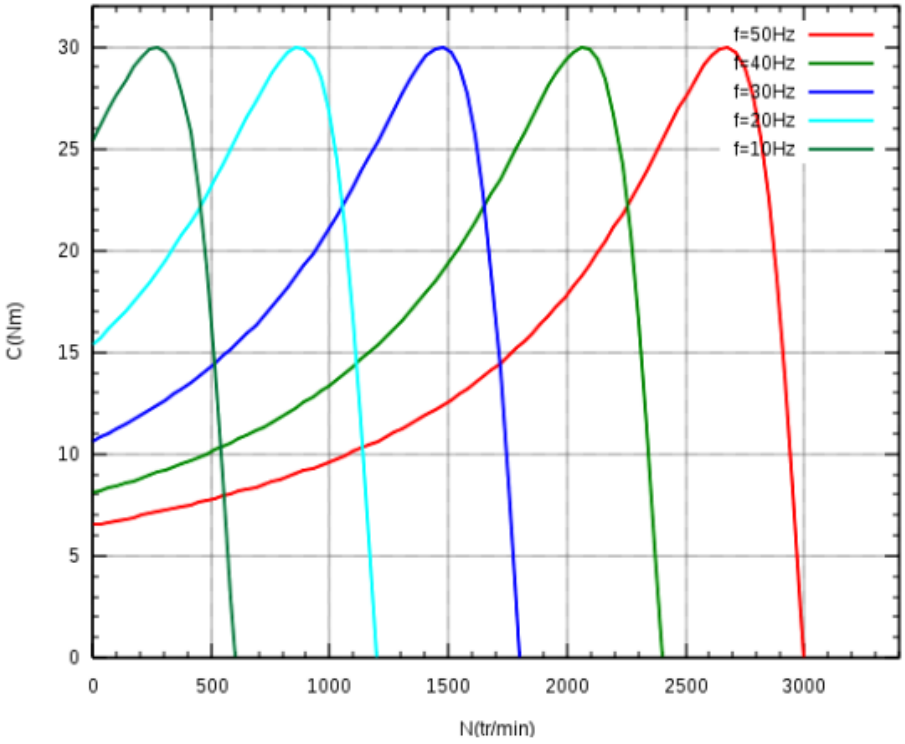

Figure 2.12: Constant torque control range (V/f control strategy) [11]

pairs of the stator winding) and injecting emf into the rotor circuits (it is possible to change the mechanical characteristic of the IM with a wound rotor by inserting an emf at the rotor frequency into each rotor phase, adjustable in rms and phase). Recent advances in control strategies have led to alternatives that show dynamic responses superior to the previously mentioned approaches, such as the Field-Oriented Control (FOC) method.

Synchronous motor

As the name suggests, synchronous motors have a rotor that rotates at a constant rotational speed, synchronized with the rotating magnetic field created by the stator circuit. Unlike the stator coils, the rotor coils are powered by a direct current that generates magnetic fields of alternating polarity. The opposite poles of the stator and rotor magnetically attract each other. The rotating magnetic field attracts the magnetic field generated by the rotor, causing it to rotate synchronously. Therefore, synchronous machines are only able to generate torque at synchronous speed, as can be seen from figure 2.13. Recall that this speed is related to the frequency and the number of pole pairs of the machine according to the relationship 2.1. From the figure, it can be seen that the motor has no starting torque, so it needs additional mechanisms to allow starting until synchronous speed is reached. Above a certain size, synchronous motors do not have the ability to self-start. This is due to the inertia of the rotor, which prevents it from instantly aligning with the rotating magnetic field due to its rapid

pace. Since a synchronous motor does not inherently generate average torque at rest, it cannot accelerate to synchronous speed without an additional mechanism. In larger

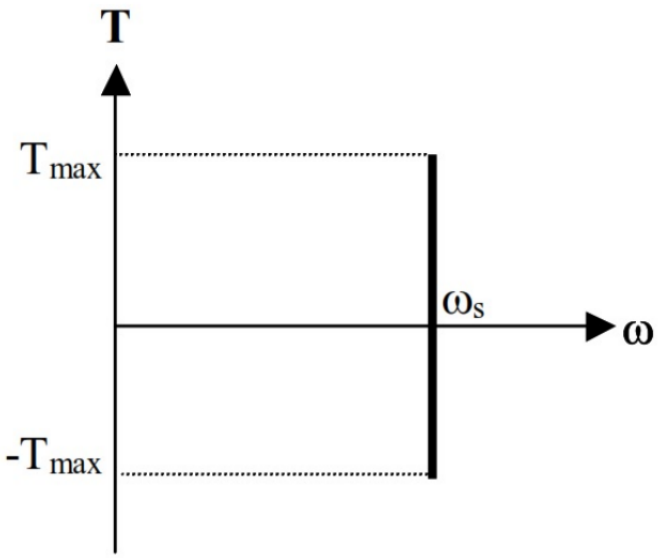

Figure 2.13: Torque-speed characteristic

motors, a squirrel-cage induction winding is incorporated not only to allow the motor to start, but also serves to damp oscillations in the motor's operating speed. As the rotor approaches synchronous speed, the previously turned off motor coils are energized, thus synchronizing the motor. Through the use of the inverter, the starting process has been simplified. The inverter allows both the frequency and the supply voltage to be adjusted. In this way, starting from a zero frequency and increasing it very gradually, it is possible to accelerate the motor from a standstill.
In this type of motor, the rotor configuration generally involves the use of permanent magnets (PMs). The motors that use magnets to produce air-gap magnetic flux instead of field coils are called PM motors. This configuration not only eliminates copper losses from the rotor, but also eliminates the need for maintenance of the field excitation circuit. PM motors can be classified into two main groups:

- **Permanent Magnet Synchronous Motor (PMSM).** The permanent magnet synchronous motor (PMSM) operates like a synchronous motor, characterized by sinusoidal waveforms of mmf, voltage and current. The incorporation of rare-earth magnetic materials increases the flux density in the air gap, consequently increasing the motor's power density and torque-to-inertia ratio. In applications requiring high-performance motion control, PMSM excels, offering fast response, significant power density, and superior efficiency. The PMSM, similar to the induction and DC machines, is fed from a power electronic inverter for its operation. PMSMs are classified according to the location and shape of PMs in rotors. The three common arrangements of PMs in rotors are: surface-mounted, inset and interior, as shown in figure 2.14. The distinction between surface-mounted and inset magnets lies in the placement of the magnets inside the rotor. In the case of inset magnets, they

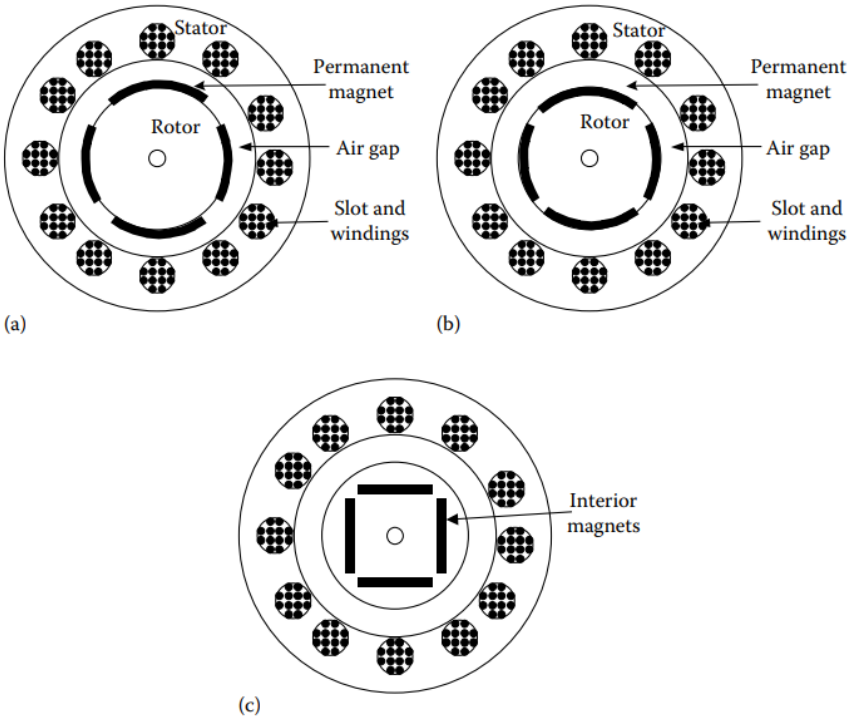

Figure 2.14: PM arrangements: (a) surface-mounted; (b) inset; (c) interior

are placed inside slots on the rotor surface, which provide greater security for the magnets but still remain exposed to the air gap. In the surface-mounted variant, the magnets are glued with epoxy or wedge-attached to the cylindrical rotor. Another category is that of interior PMSMs, which have the magnets embedded in the rotor, giving them anisotropic properties.
The main drawback of this type of motor is that it requires complex control strategies, since the magnetic field of the rotor cannot be controlled. To achieve this type of control, vector control techniques, also called Field-Oriented Control, are used. The basic idea of the vector control algorithm is to decompose a stator current into a magnetic field-generating part and a torque generating part. Both components can be controlled separately after decomposition.
The torque generated by the PMSM results from the iteration between the magnetic field of the stator and that of the rotor. The stator magnetic field is represented by the magnetic flux/stator current. The magnetic field of the rotor is represented by the magnetic flux of PMs that is constant, except for the field weakening operation [12]. It is defined as:

$$T = \vec{B}_s \times \vec{B}_r \tag{2.3}$$

This expression shows that the torque is maximum if the stator and rotor magnetic fields are orthogonal. The goal is to align the stator flux with the q-axis, orthogonal to the rotor flux. For this purpose, the component of the stator current in quadrature with the rotor flux is controlled to generate the desired torque, while the direct component is set to zero. The direct component of the stator current

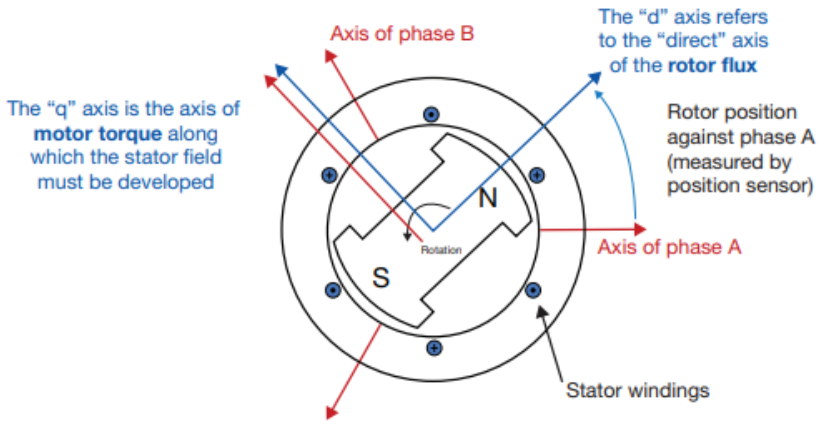

Figure 2.15: FOC vector explanation

can be used in some cases for field weakening, which has the effect of opposing the rotor flux and reducing the back-emf, allowing operation at higher speeds. As we know, the current flowing in the stator windings is a time- and speed-dependent three-phase current. So the goal is to describe this current flow in a time-invariant system of two coordinates (d and q). To do this, two transformations are used; the

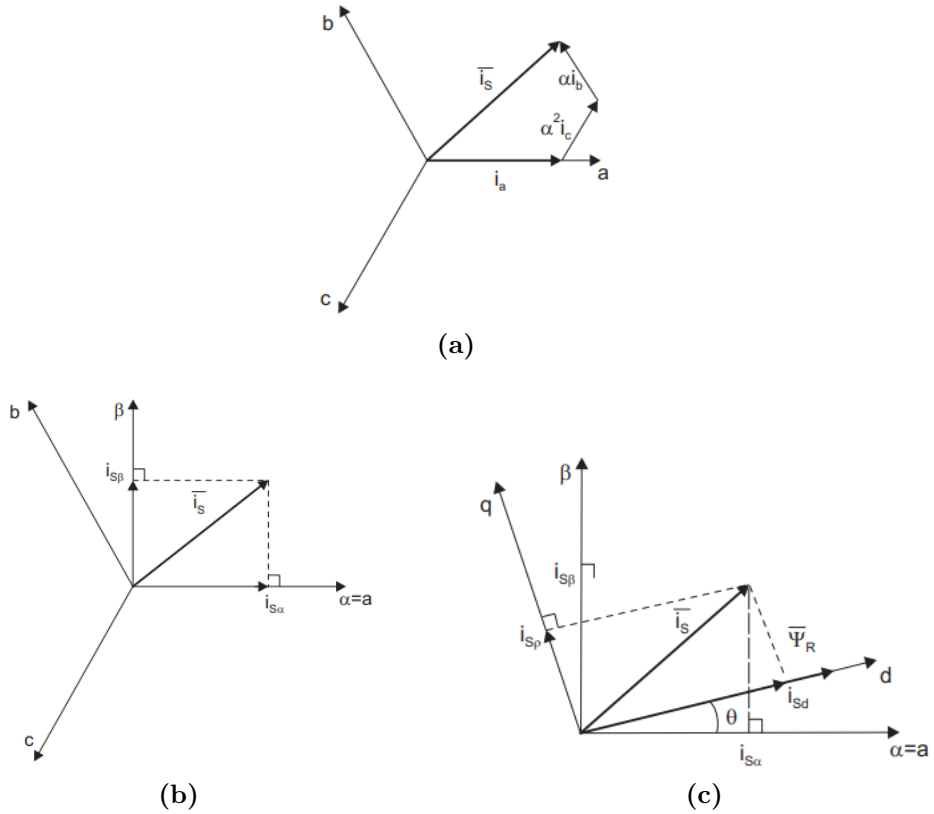

Figure 2.16: (a) 3-phase frame; (b) Clarke transformation; (c) Park transformation [13]

Clarke Transformation obtaining a system of two coordinates (α - β) dependent on time and the *Park Transformation* to make the system time-invariant (d - q). Now, the two currents, quadrature and direct currents, depend on the components of the current vector (α, β) and the position of the rotor flux θ, respectively. The rotor position information is needed to efficiently perform the control of the PMS motor, but incorporating a rotor position sensor on the shaft may compromise the robustness and reliability of the overall system in some applications. Therefore, the aim is to avoid relying directly on this mechanical sensor for position measurement and instead use indirect techniques for rotor position estimation. After the two transformations, the system can be controlled by DC quantities as in a separately excited DC motor.

- **Permanent Magnet Brushless DC Motor (PMBLDC).** The PM AC motors with trapezoidal back-emf waveforms are the PM brushless DC motors. The trapezoidal waveforms are derived from the concentrated rather than sinusoidally distributed windings used in PMSMs. The popularity of these machines comes from the ease of control. Rectangular pulses of current are used to alter the magnetic field of the stator at discrete locations. A set of three Hall sensors mounted on the stator can easily give the position information; this avoids the need for a high-resolution encoder or position sensor, as required in PMSMs. However, the trade-off for position sensor simplification is reflected in motor performance. Vector control is not possible in PM BLDC machines because of the trapezoidal shape of the back-emfs. Essentially, the motor operates as a DC motor under the guidance of its electronic controller, which is why it has been called a brushless DC motor.

Not only because of their outstanding performance, simplicity of design, low cost, robustness, and fault tolerance, but especially because of the absence of rare-earth-based materials, which avoids the drawbacks associated with the high costs and environmental impact of mineral extraction and refining, **Switched Reluctance Motors** have attracted increasing interest in electric vehicle (EV) applications. In fact, the rotor of these motors is made of ferromagnetic material and its section is suitably shaped to create preferential paths for the passage of the magnetic flux produced at the air gap by the stator winding. The stator and rotor of a reluctance motor must have different numbers of poles. Typically, the stator has a higher number of poles than the rotor; for example, with a 8/6 ratio as in the figure 2.17. For the rotor to begin to rotate, a change in magnetic resistance from its position must occur. This magnetic resistance, also known as reluctance, is why the motor is referred to as a reluctance motor. Applying a voltage to the stator winding creates a current flow that generates magnetic flux through both the stator and the rotor. The rotor then turns in the direction where the magnetic resistance for magnetic flux is minimized, producing torque. The torque decreases to zero as the rotor aligns with the position of least magnetic resistance. To achieve continuous rotation, a voltage must be applied to the next winding in sequence. Despite the many advantages over other conventional AC machines, they have one significant disadvantage: acoustic noise, resulting from radial vibration and torque ripple. The latter results from the high phase currents that the motor requires.

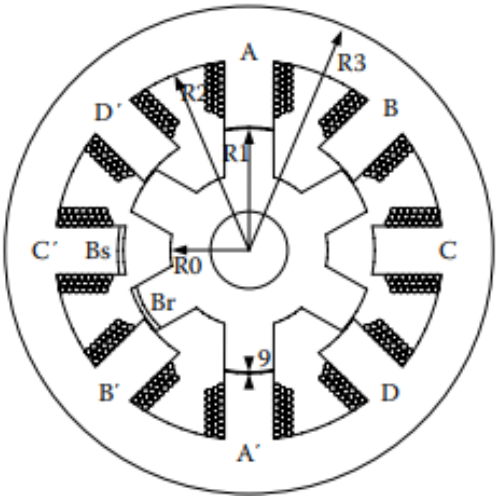

Figure 2.17: Cross section of SR motor

2.2.3 Power Electronics

Power electronics generally combine electronic components, electrical power, and control strategy. It deals with the design and implementation of circuits and systems that can efficiently manipulate electrical energy through the use of semiconductor devices such as Diodes, Thyristors, Bipolar Junction Transistor (BJT), Insulated Gate Bipolar Transistor (IGBT) and Metal Oxide Semiconductor Field Effect Transistor (MOSFET). The main objectives include voltage regulation, frequency conversion and power flow control, helping to improve the energy efficiency and reliability of various electrical systems. Specifically, one of the main functions of these circuits is to convert electrical energy between DC and AC or vice versa, as well as to adjust the signal strength according to the specific needs of the downstream devices connected to the converter. In the field of electric vehicles, the most commonly used converters are:

- DC/AC converter *(Inverter)*
- AC/DC converter *(Rectifier)*
- DC/DC converter

Inverter

A DC-AC inverter aims to convert DC power to AC power, ensuring that the output has the desired voltage magnitude and frequency. During regenerative braking, however, it takes on a reverse function, converting the energy captured by the motor into charging energy for the battery (AC to DC). In electric vehicle (EV) systems, the inverter plays a key role as a central component of the AC motor drive, with the main task of supplying power to the traction motor. In this context, IGBTs are commonly employed as power electronic switches. In more advanced systems requiring higher efficiency and higher switching frequencies, MOSFETs can also be used. As shown in figure 2.18, the three-phase inverter circuit consists of six power switches and six diodes. So, it has eight

switching states in which three switches are always active in each state, ranging from state 0, in which all output terminals are connected to the negative DC bus, to state 7, in which they are all connected to the positive bus. These eight switching states are listed in table 2.1. The inverter can be connected to the motor in two configurations: Δ or Y, as can be seen in the right side of the figure.

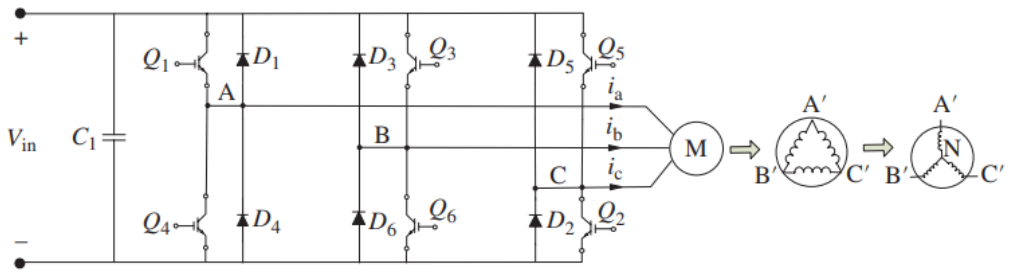

Figure 2.18: 3-phase Inverter

State	Switch State	V_{AB}	V_{BC}	V_{CA}
0	Q_2 Q_4 Q_6 ON Q_1 Q_3 Q_5 OFF	0	0	0
1	Q_1 Q_2 Q_3 ON Q_4 Q_5 Q_6 OFF	0	V_{in}	$-V_{in}$
2	Q_2 Q_3 Q_4 ON Q_1 Q_5 Q_6 OFF	$-V_{in}$	V_{in}	0
3	Q_3 Q_4 Q_5 ON Q_1 Q_2 Q_6 OFF	$-V_{in}$	0	V_{in}
4	Q_4 Q_5 Q_6 ON Q_1 Q_2 Q_3 OFF	0	$-V_{in}$	V_{in}
5	Q_5 Q_6 Q_1 ON Q_2 Q_3 Q_4 OFF	V_{in}	$-V_{in}$	0
6	Q_6 Q_1 Q_2 ON Q_3 Q_4 Q_5 OFF	V_{in}	0	$-V_{in}$
7	Q_1 Q_3 Q_5 ON Q_2 Q_4 Q_6 OFF	0	0	0

Table 2.1: Inverter switching states

Pulse Width Modulation (PWM) is the main technique used by the inverter to produce the desired sinusoidal signal. Initially, however, a three-phase square-wave voltage is generated at the output of the inverter. In order to operate effectively, the electric motor requires a sinusoidal input voltage. Consequently, it becomes essential to expand

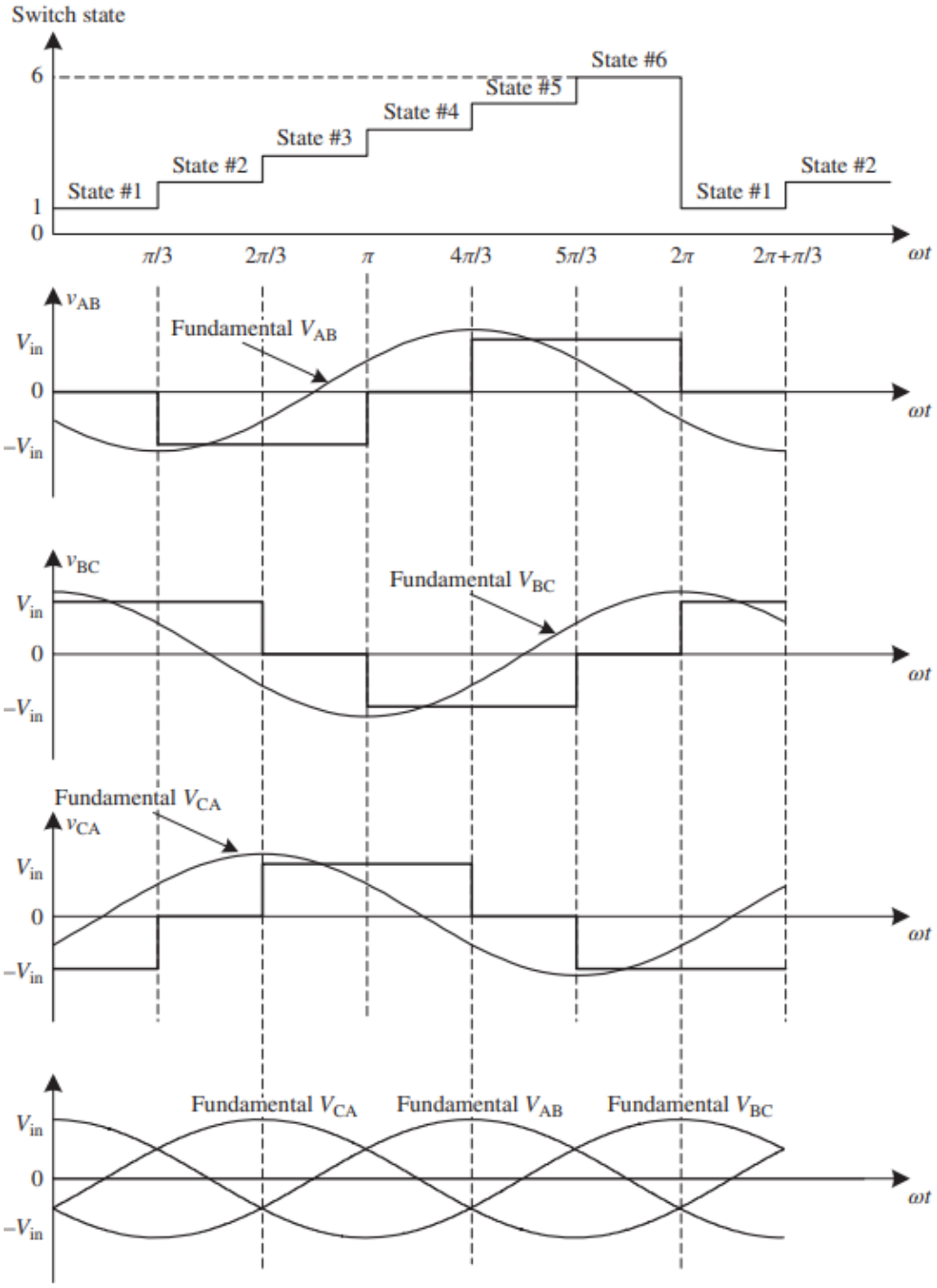

Figure 2.19: Inverter voltage waveforms [4]

the voltages obtained using Fourier series. Next, a filter is applied to the output to selectively capture only the fundamental component and suppress all other harmonics. This yields three voltages, each of which has a sinusoidal waveform, which together form our three-phase signal. Figure 2.19 illustrates the voltage characteristics at the

three output terminals and the corresponding fundamental harmonics.
To more closely meet the needs of electric motors, advanced inverter topologies, such as multilevel inverters, are available. They can provide reduced instantaneous error and better sine wave approximation.

DC/DC converter

Within an electric vehicle, a DC-DC converter plays a crucial role in transforming the high voltage provided by the primary battery system into a lower voltage. This lower voltage is essential for charging a 12 V auxiliary battery and providing power to various accessories such as headlights, windshield wipers, and horns. As already seen in DC-AC inverters, the PWM control strategy is also used in DC-DC converters. The working principle of DC–DC converters can be illustrated by figure 2.20. To obtain the average output voltage V_o, it is essential to keep the frequency $(1/T_s)$ of control of the switch constant. Consequently, adjusting the average output voltage V_o, involves adjusting the on-time of the switch. It can be calculated with the following equation:

$$V_o = \frac{1}{T_s}\int_0^{T_{\text{on}}} V_{\text{in}}\, dt = \frac{T_{\text{on}}}{T_s} V_{\text{in}} = DV_{\text{in}} \tag{2.4}$$

The longer the switch remains on in a given signal period Ts, the higher the average output voltage of the device. In PWM control, this characteristic can be described by the duty ratio, D, defined as the ratio of the on duration to the switching period, T_s:

$$D = \frac{T_{\text{on}}}{T_{\text{on}} + T_{\text{off}}} = \frac{T_{\text{on}}}{T_s} \tag{2.5}$$

Sometimes, the expression *"duty cycle"* is used to characterize the percentage fraction of time spent in the ON state compared to the total signal period [4]. The higher the duty cycle, the higher the output voltage magnitude, and vice versa. Based on the desired

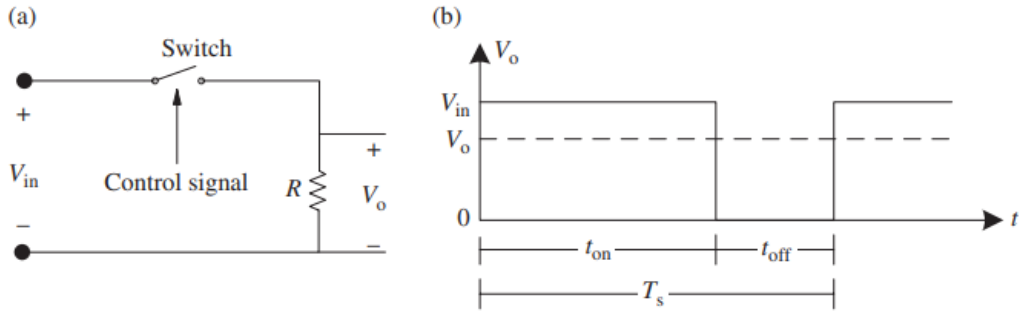

Figure 2.20: Working principle of DC/DC converter: (a) Basic circuit; (b) Control signal

characteristics of the output signal, there are various types of DC-DC converters, each characterized by the ability to create a load voltage, positive or negative, higher or lower than the signal at the input terminal. The most common types are:

- **Buck (Step-Down) Converter:** it lowers the input voltage to a lower output voltage level.
- **Boost (Step-Up) Converter:** it increases the input voltage to a higher output voltage level.
- **Buck-Boost (Step-Down/Up) Converter:** it can reduce or increase the input voltage depending on the load needs.
- **Cuk Converter:** combination of a buck and a boost converter that offers polarity reversal without the use of a transformer.

A crucial consideration in controlling PWM switching is that the frequency of the PWM signal must be significantly higher than any factor affecting the load to avoid discontinuous effects on the system. Depending on the characteristics of the load, a DC-DC converter can operate in two distinct modes:

– *Continuous Conduction Mode (CCM):* the current through the inductor, a fundamental component of the DC/DC converter, never drops to zero during the entire switching period.

– *Discontinuous Conduction Mode (DCM):* the current through the inductor reaches zero before the end of the switching period. This means that during part of the switching period, the inductor is devoid of current.

Therefore, the switch control signal must be designed appropriately to ensure that the converter operates effectively in both operating modes.
Compliance with vehicle safety regulations requires that the 12 V power system be isolated from high voltages. Accordingly, the implemented DC-DC converter must take the form of an isolated buck converter. Among the numerous types of isolated DC-DC converters, one of the most used is the full-bridge converter, shown in the figure 2.21. To achieve good galvanic isolation between the input and output of the converter, a transformer is added inside the power electronic circuit. This converter has two switching periods and four operational modes listed in table 2.2.

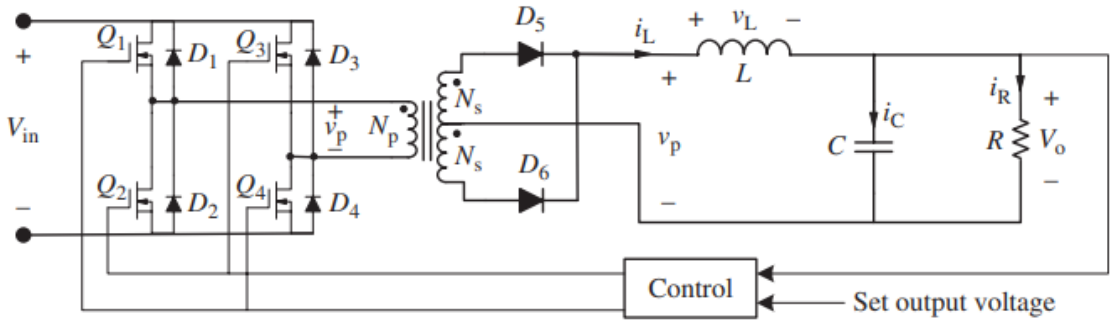

Figure 2.21: Full-bridge isolated buck converter

First subinterval First switching period	Q_1 Q_4 D_5 ON Q_2 Q_3 D_6 OFF	$v_p = V_{\text{in}}$
Second subinterval First switching period	All switches OFF D_5 D_6 ON	$v_p = 0$
First subinterval Second switching period	Q_2 Q_3 D_6 ON Q_1 Q_4 D_6 OFF	$v_p = -V_{\text{in}}$
Second subinterval Second switching period	All switches OFF D_5 D_6 ON	$v_p = 0$

Table 2.2: Isolated buck converter switching states

At the steady state operation to the inductor L, the shaded area A equals the shaded area B in figure 2.22, which produces the following relationship between input voltage and output voltage:

$$V_o = \frac{N_s}{N_p} V_{\text{in}} \frac{T_{\text{on}}}{T_s} = \frac{N_s}{N_p} V_{\text{in}} D \tag{2.6}$$

It is important to highlight that the waveforms provided are derived without considering the magnetizing current of the transformer. In practical analysis where the magnetizing current of the transformer must be considered, the actual waveforms may deviate from the ideal ones.

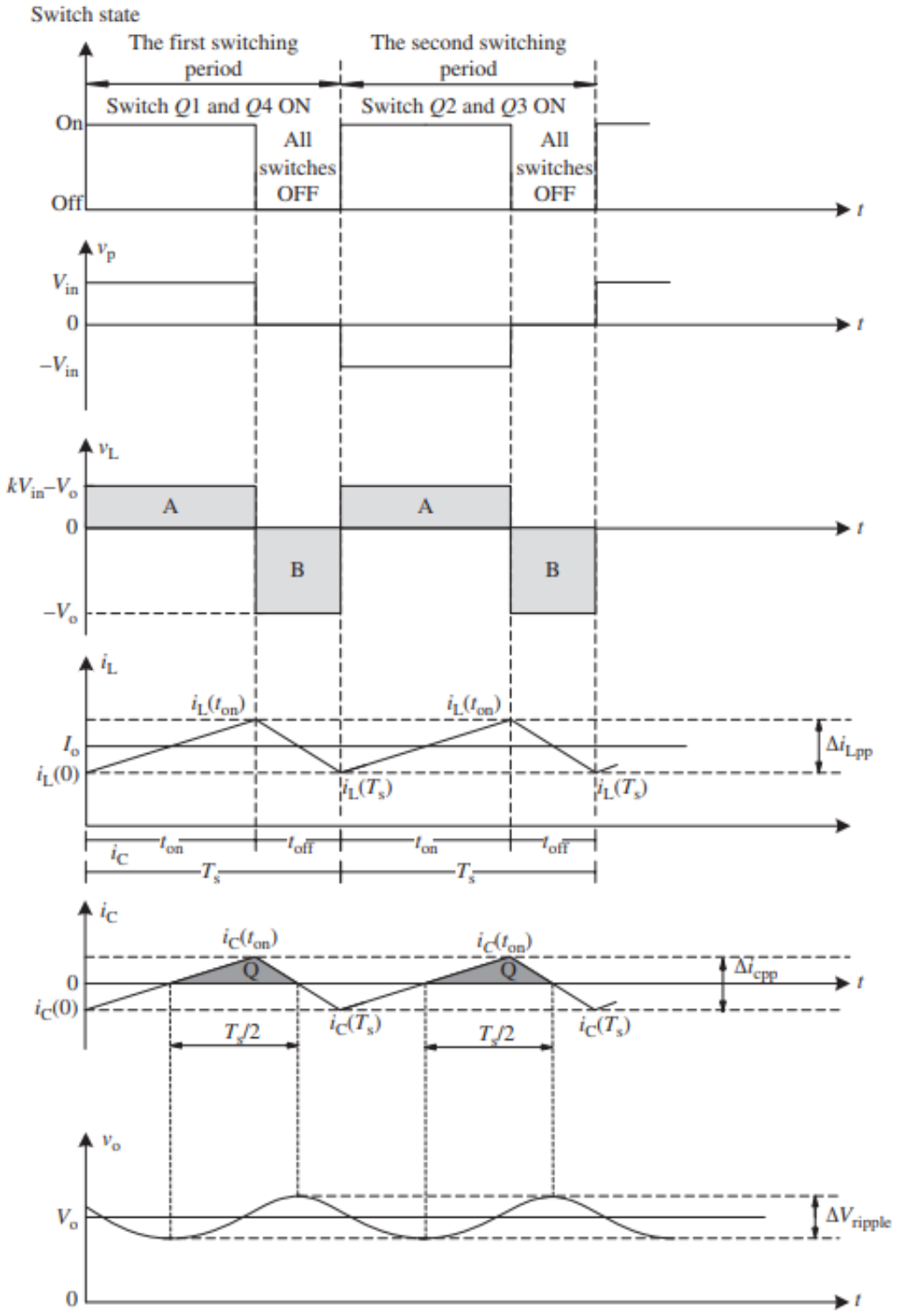

Figure 2.22: Isolated buck converter waveforms [4]

2.2.4 Charging Interface

The charging challenge, along with battery capacity, is a significant aspect for battery electric vehicles. Continuing advances in charging technology, along with the expansion of charging infrastructure, are improving the convenience and speed of charging electric vehicles [14]. Battery charging for EVs can be classified into:

- **Conductive Charging:** this configuration allows a physical connection between the car and the charging stations, called Electric Vehicle Supply Equipment (EVSE). These differ mainly according to the application and the power supplied to the vehicle:
  - *Wallbox*; designed for domestic use, mainly single-phase AC, capable of delivering different power values up to 7,4 kW.
  - *AC Charging Station*; capable of providing three-phase power up 43 kW, is often installed in public places designated for vehicle charging or in dedicated areas. Typically, they also incorporate a charging management system, especially when multiple vehicles are connected to the same EVSE, in order to distribute energy efficiently.
  - *DC Charging Station*; category specifically designed for DC charging, bypassing the vehicle's on-board charger, as the AC-DC converter is built into the charging station. They also require appropriate protections and may incorporate a cable cooling system to handle the high current delivered by the EVSE. The power output of these stations ranges from 20 kW to several hundred kW.

  These systems can be automated using robotic structures that establish a wired connection by attaching a connector to the car.

- **Inductive Charging:** commonly called wireless charging, is emerging as a more versatile and convenient charging method. Unlike a direct wired connection, wireless connection eliminates the sparking problems associated with plugging and unplugging. Instead of the conductive charging system there is an integrated receiving coil and an external transmitting coil on the road surface. The ground coil, exploiting the phenomenon of electromagnetic induction, generates very strong alternating magnetic fields which induce currents in the on-board coil. These currents allow the vehicle to be charged. However, this solution seems to present several problems for the high powers both in terms of efficiency and infrastructure.

- **Battery Swapping:** it is one of the most time-saving and easy charging methods. At a Battery Swapping Station (BSS), electric vehicle owners can simply exchange their depleted battery for a fully charged one. A BSS features essential components, including a distribution transformer, AC-DC converters, battery chargers, robotic arms, charging racks, maintenance systems, control systems, and other equipment dedicated to exchanging and charging batteries. However, the development of Battery Swapping Stations still presents challenges, including the need to standardize electric vehicle battery packs, promote consumer acceptance of the BSS model, and establish reliable methods for estimating battery health.

Each represents distinct modes of energy transfer. The different charging methods require specific infrastructure and equipment to meet the requirements of these vehicles.

On-board battery charger

The on-board battery charger is a crucial component of the EV architecture, with the task of converting the AC voltage signal from the power grid into a reduced power DC signal suitable for charging the vehicle's battery pack. Charging is divided into three levels: Level 1, Level 2, and Level 3, which are distinguished by charging capacity, AC voltage signal amplitude, maximum current in the charging circuit, and the type of socket used to connect the on-board charger to the charging station. Notably, Level 3 charging can also be DC fast charging, where the charger is located in the charging station and the power flow is up to several hundred kW. OBCs can be classified according to two criteria: power flow direction and power transfer technology. In terms of direction of flow, they are classified as unidirectional, which simplify hardware complexity, interconnections and tend to reduce battery degradation, and bidirectional, which support both grid charging and feed-in of energy stored by batteries (V2G), with stabilization of energy through a specialized conversion circuit. In terms of energy transfer, OBCs are further divided into conductive and inductive. Currently, most of them use AC-DC galvanic converters, providing a high level of safety and interoperability with the various AC power modes available.
This section describes the one-way OBC type, which is a converter dedicated only to the vehicle charging process. The fundamental structure of the charger includes several components, each of which is designed to perform a specific function:

- *EMI filter:* Electromagnetic Interference (EMI) filter is a component designed to attenuate and suppress unwanted electromagnetic noise or interference generated during the charging process due to the presence of the switches. It helps to ensure that electrical signals and frequencies produced by the charger comply with regulatory standards and do not interfere with other electronic devices or systems.

- *In-rush current protection:* downstream of the EMI filter, there is a resistor connected in parallel to a switch, which has the function of limiting the inrush current during power-up of the charger. This element is essential because, during initial turn-on, the capacitors are in a discharged state, creating a short-circuit scenario that can lead to significant current flow, jeopardizing the overall integrity of the charger. The switch serves to bypass the resistor once the capacitors reach a specific state of charge, preventing excessive power dissipation.

- *Full wave rectifier:* his role is is to convert sinusoidal AC voltage to DC voltage, and the prevalent circuit topology for rectification is the full-bridge rectifier. Various power electronics components, including diodes, thyristors or MOSFETs, can perform this transformation. However, since there is no need to regulate the output voltage, diodes are the simplest and cheapest elements to implement this function. In addition, a filter capacitor is often connected in parallel with the output of the rectifier to improve the quality of the DC voltage.

- *PFC:* Power Factor Correction (PFC) device allows to minimize harmonic distortions and reactive power in AC-DC conversion to be reduced, thereby increasing system efficiency.
- *Isolated DC-DC converter:* it transforms the DC signal from the PFC into a DC signal suitable for charging the battery pack.

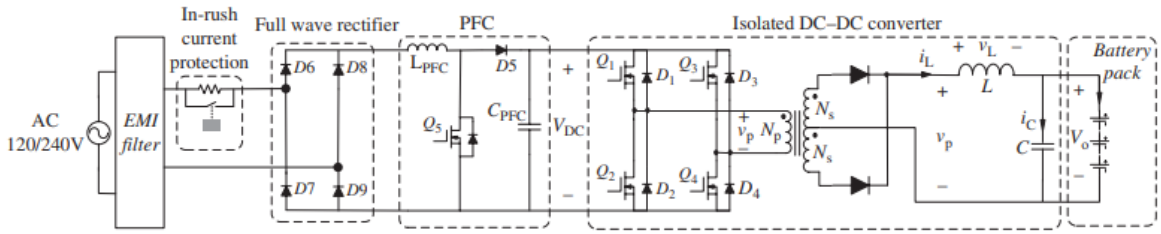

Figure 2.23: On-board battery charger architecture [4]

Charging port

Before describing the types of connectors, it is important to analyze the different conductive charging modes of electric cars established by the IEC 61851 standard. The standard involves control electronics using a "universal" communication system between the station and the vehicle through a PWM circuit, which is necessary to ensure the safety of the charging process, both for people and to prevent damage to the vehicle's battery pack. The charging modes are [15]:

1. **Mode 1:** it allows vehicle charging up to 16 A from standard outlets (Schuko). Thus, there is no source-to-vehicle communication. This mode is suitable for charging micro-electric mobility, with connection generally to a single-phase power grid, in which vehicles with very low battery pack power values, such as scooters and electric bicycles, are included. It does not apply to electric cars.

2. **Mode 2:** an improvement of Mode 1, increases the maximum current up to 32 A (both single-phase and three-phase). A PWM safety device called In-Cable Control Box (ICCB) is present on the vehicle power cable to ensure safe operations during charging. This device does not act on the EVSE side but only on the vehicle side.

3. **Mode 3:** mandatory mode for public environments, involves connecting the electric vehicle to the AC power grid through dedicated public charging stations equipped with a PWM safety system. This mode requires the EVSE to be able to charge the vehicle with both Mode 2 described above and the "fast AC Charging" mode, delivering a maximum charging current of 63 A, under three-phase power conditions.

4. **Mode 4:** it is DC charging up to 200A, 400V. It is designed for public environments and the charger is external to the vehicle.

As with the four modes, the various types of connectors are also established by the IEC 61851 standard. There are both AC and DC charging connectors. For the former (Mode 2 and Mode 3) there are four types of connectors: Type 1, Type 2, Type 3A and Type 3C. Type 1 is found only on the side of the vehicle. Type 2 is found on both the vehicle side and the column side. Type 3A and Type 3C are connectors on the column side only.

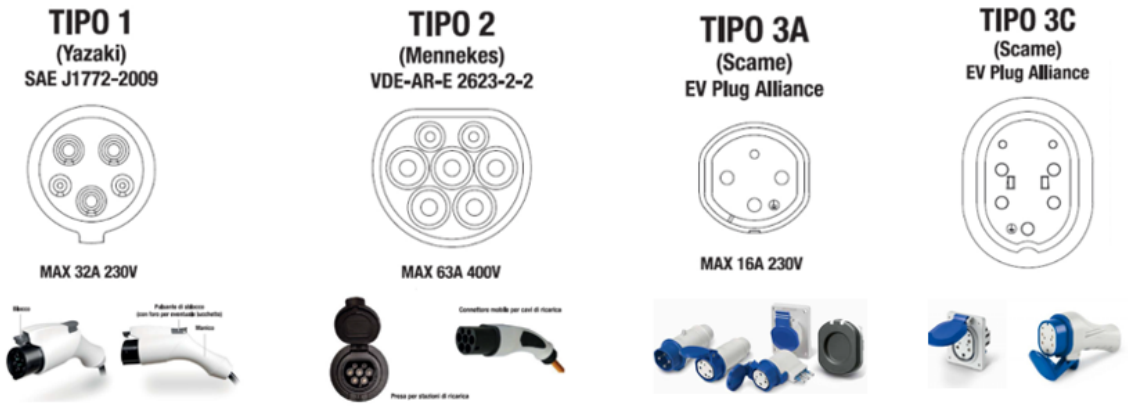

Figure 2.24: Types of AC charging connectors

For the latter (Mode 4) there are two standards: CCS Combo2 and CHAdeMO. The first one, as seen in figure 2.25, allows both DC fast charging and AC slow charging. This is made possible by the presence of 9 pins: 5 power pins for three-phase AC charging, 2 communication pins (Control Pilot and Proximity Pilot), and 2 pins for DC charging.

Figure 2.25: Types of DC charging connectors

Battery Charging Overview

Nowadays, there is a constant search for alternative methods to achieve the fastest possible charging without adversely affecting battery life. This section provides a

simple overview of various conductive charging techniques for EV batteries. Traditional charging methods include constant current (CC), constant voltage (CV), constant power (CP), conical charging and trickle charging. To achieve rapid charging, advanced techniques, such as CC/CV combination, are used. In addition, pulse-charging and negative pulse-charging are used as additional approaches for fast charging. CC charging means charging the battery with a constant flow of current and a variable voltage. This charging method is typically used for Nickel-Cadmium and Nickel-Metal Hydride batteries. CV charging, on the other hand, utilizes constant voltage and variable current until the charging current diminishes to nearly zero. CP charging is a method where a constant charging power is applied. In general, the CC/CV charging technique is the optimal choice for charging Lithium-Ion batteries, the operation of which can be classified into two main processes:

- **Constant Current:** a constant current is applied to charge the battery until the battery voltage rises to a predefined maximum charging voltage (V_{preset})
- **Constant Voltage:** the charging voltage is kept at a constant value, V_{preset}, while the charging current decreases exponentially. The charging process ends when the charging current approaches a value close to zero, typically about 1% of the rated battery capacity.

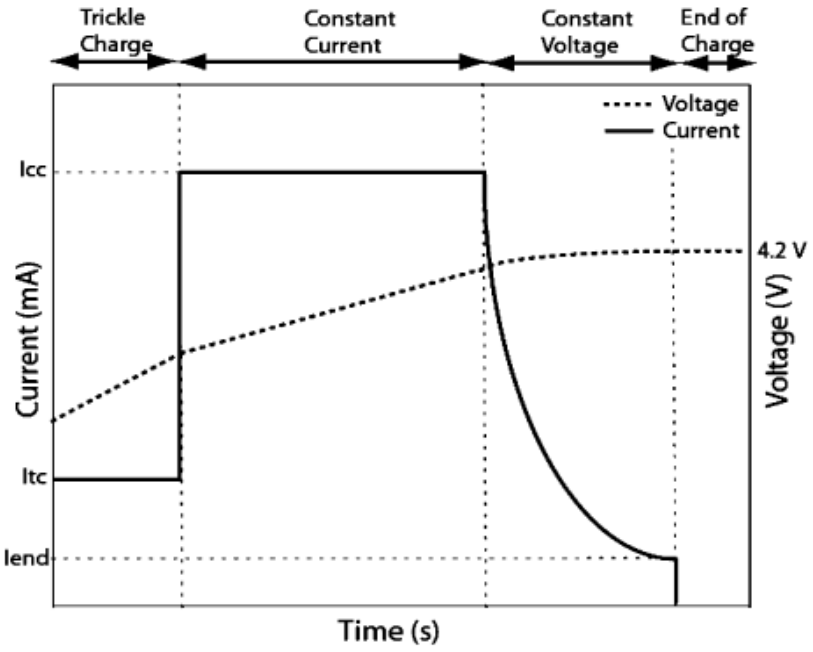

Figure 2.26: Ideal CC/CV charging profile

In addition to these two phases, there may be an additional stage preceding the DC phase, as illustrated in 2.26, known as the "trickle charge" phase. Trickle charging is only necessary when the battery is completely discharged (voltage drops below 3 V). During trickle charging, the battery is recharged with a small current, typically no more than 0.1 times the battery's rated capacity (0.1 C). Here, C represents the rated

capacity of the battery measured in ampere-hours (Ah). Charging currents above 0.1 C could pose risks, as the battery has a high internal impedance at these low voltages and becomes susceptible to thermal runaway [16]. Based on the charging current in the CC mode, the total charging time is varied from 1 hour to 2.5 hours. Generally, lower charging currents in the CC mode lead to higher charging efficiency, longer charging times, and extended battery life.
The CC/CV charging algorithm is well-developed and widely adopted in battery charging, given its simplicity, straightforward implementation, its ability to prevent overvoltage, and its capacity to reduce thermal stress.

Chapter 3

Lithium-Ion Battery

The technological development of Energy Storage Systems, commonly called traction batteries, has a great impact on the electric vehicle industry, as these batteries are used to power the propulsion system of EVs. Unlike auxiliary batteries, which are used to power some accessories, traction batteries must provide continuous power for an extended period. The function of the ESS is to convert chemical energy into electrical energy and vice versa through electrochemical oxidation or reduction reactions to supply/capture electrical energy to/from the vehicle. The stored energy can be captured by regenerative braking or charged from the grid through the charger.

3.1 Cell Overview

As seen in Section 2.2.1, a battery consists of a number of cells assembled in a common container and connected together to function as a source of electrical power. Cells can be arranged in series or parallel to achieve the desired voltage and capacity. A simple cell includes two electrodes located in a container that contains the electrolyte. These electrodes are essential components because, being conductors, they allow the exchange of current within the electrolyte. There are two types of electrodes: the **cathode** (positive) and the **anode** (negative). The cathode requires a high redox potential and specific capacitance, while the anode requires a low redox potential with a high specific capacitance. Both electrodes are immersed in the **electrolyte**, a solution that allows the movement of positive ions (cations) and negative ions (anions). The electrolyte serves as a medium for electron flow and can be in the form of a liquid, solid, polymer or hybrid, commonly consisting of salts, acids or alkaline solutions. In addition, the cell includes a **separator** that allows the movement of ions and prevents a short circuit between the electrodes.
There are two main categories of battery cells: primary cells (non-rechargeable) and **secondary cells** (rechargeable). In the primary cell, the chemical reaction occurs only once. In the secondary cell, the electrodes and electrolyte undergo changes because of the chemical reaction that occurs when the cell supplies current. Unlike the primary cell, the chemical reaction in the secondary cell is reversible, which means that this cell can be recharged by electric current. In addition, while primary cells discharge more slowly and have a high energy density, secondary cells have a lower energy density. The latter

are used in the world of EVs, so, from now on, we will focus only on rechargeable ones. It is important to note that these are not the only forms of electrochemical storage; fuel cells and ultracapacitors are also examples.

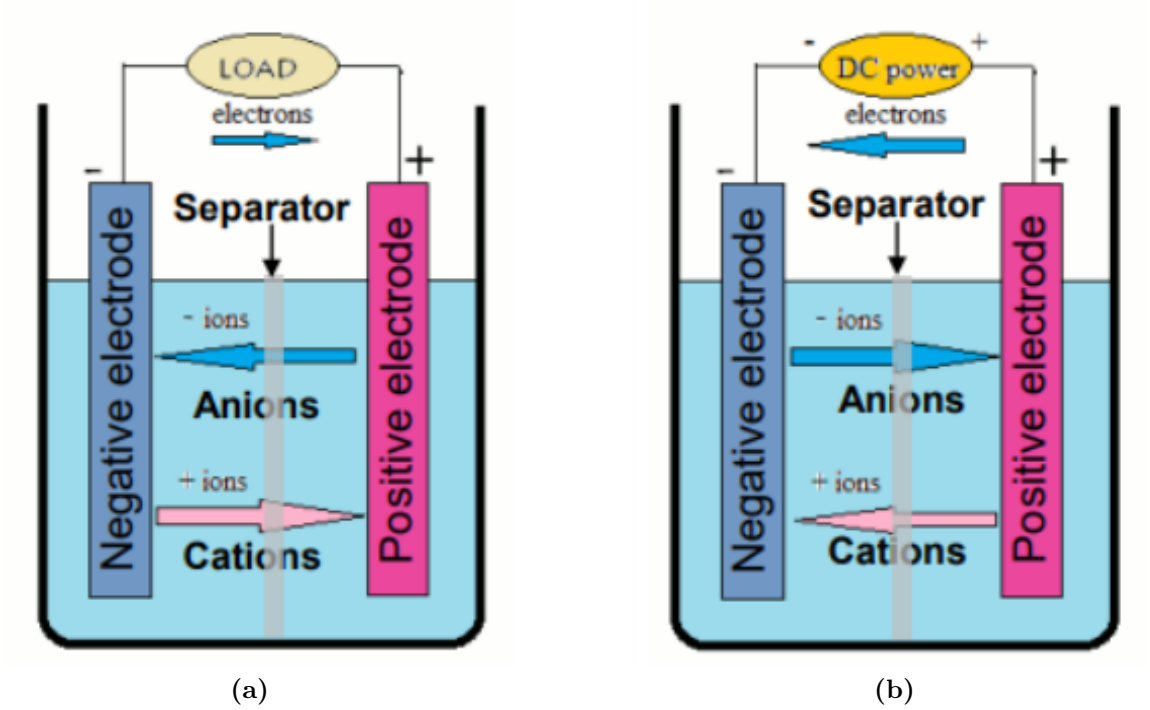

(a) **(b)**

Figure 3.1: Secondary Cell Modes: (a) Discharging; (b) Charging

As can be seen from the figure above, this type of cell works in two different modes: discharge mode and charge mode. During discharge, the battery cell is connected to a load that allows the flow of current from the cathode to the anode, and electrons move from the anode to the cathode. This movement of electrons generates a charge imbalance that is offset by the movement of ions within the cell. Anions move toward the anode to perform an oxidation reaction, donating electrons to the anode. At the same time, cations migrate toward the cathode to undergo a reduction reaction, allowing the cathode to accept electrons. In charge mode, an external voltage source reverses the current flow, leading to the reversal of the chemical reaction [17].

Talking about cell design, there are three main shapes: cylindrical, prismatic and pouch (also called 'coffee-bag') cells.

(a) **Cylindrical:** they have a tubular shape with wound electrodes, offering efficient space utilization in devices. Advantages include mature and cost-effective manufacturing processes, high energy density for long-term device usage, superior heat dissipation that improves safety, robust construction for increased durability, and ease of packaging inside the devices. However, they face limitations in form factor adaptability, potentially subject to mechanical stress or deformation, particularly in custom designs. Despite being resistant to physical damage, their fixed cylindrical

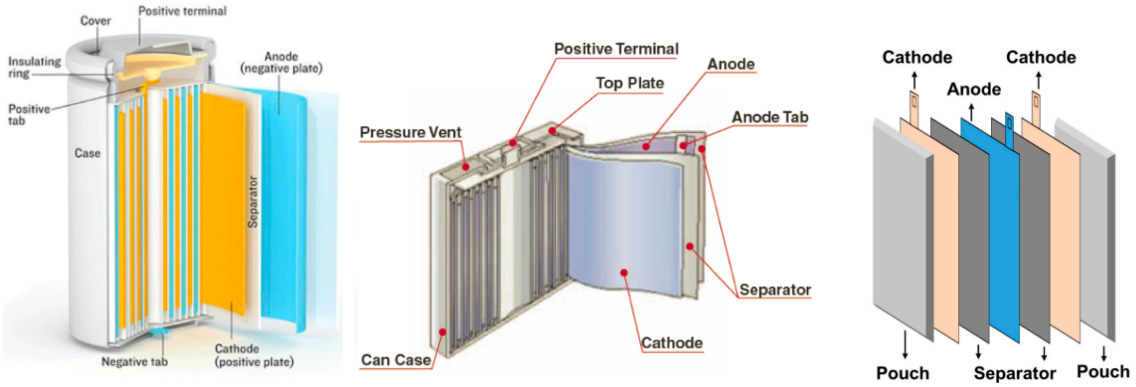

(a) **(b)** **(c)**

Figure 3.2: Cell design: (a) Cylindrical; (b) Prismatic; (c) Pouch

shape may not meet all device requirements, posing challenges in applications with specific form factor needs. Additionally, their radial thermal conductivity limitations lead to smaller individual capacities, requiring multiple cells in EVs, introducing complexity and potential losses.

(b) **Prismatic:** characterized by their flat, rectangular shape, house stacked electrodes in a pouch-like structure. Space optimization for devices with limited room, enhanced packing efficiency in battery modules and streamlined manufacturing processes are the main advantages. However, vulnerability to mechanical stress can affect overall battery life.

(c) **Pouch:** feature flexible pouch-like packaging and house stacked electrodes within a lightweight, customizable pouch. Notably adaptable, they suit various shapes and sizes, ideal for applications prioritizing space optimization. Being lightweight and space-saving, lacking rigid casing, pouch cells excel in weight-sensitive applications. Their safety is improved by aluminum-plastic composite film packaging, which minimizes explosion risks compared to rigid casings. Despite the higher energy density, pouch cells, not having a rigid casing, are susceptible to physical damage, compromising both safety and durability.

3.2 Battery Technologies

With the development of battery technology, an increasing number of different types of power batteries have appeared on the market. However, despite these technological advances, the basic requirements of traction batteries have not significantly changed. The key criteria that must be considered when choosing a battery or ultracapacitor include safety, reliability, longevity, and cost. Energy and power density are also important factors. The former indicates the amount of energy possessed by a battery relative to its weight (equation 3.1), while the latter describes the rate at which a battery can deliver power (cell efficiency). Thus, there are different types of batteries

that have been and are being used for EV applications.

$$EnergyDensity[Wh/kg] = \frac{Voltage_{rated}[V] * Capacity_{rated}[Ah]}{Mass[kg]} \tag{3.1}$$

To obtain an initial comparison, Ragone's plot is employed. This plot, shown below, is used to compare the energy density of various energy storage devices. In this chart, energy density values (Wh/kg) are plotted against power density (W/kg). Note that

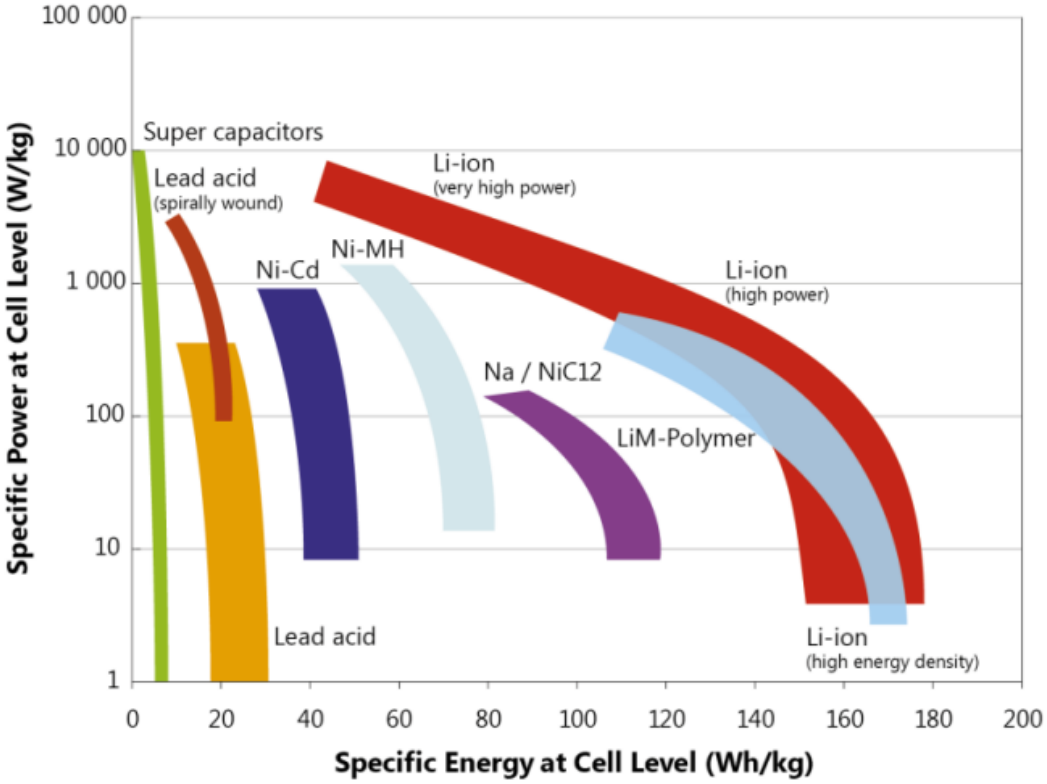

Figure 3.3: Ragone plot

the energy and power density of the final assembled battery pack will be lower than that of the constituent cells [18].

3.2.1 Lead-Acid

The Lead–Acid battery is one of the oldest rechargeable batteries. It has a negative plate made from lead metal Pb and a positive plate from lead dioxide PbO_2, which are both immersed in an electrolyte composed of diluted sulfur acid. The lead-acid battery has the following reversible net reaction:

$$2\,PbSO_4 + 2\,H_2O \rightleftharpoons PbO_2 + Pb + 2\,H^+ + 2\,HSO_4^- \tag{3.2}$$

The main advantages of lead-acid batteries are the low price compared with other batteries, the high open-circuit voltage and easy recycling of materials. One drawback

is the low energy density, which cannot be significantly improved because of the low theoretical value. Other issues, which make it little used nowadays, are high self-discharge rates and low charge/discharge efficiency.

3.2.2 Nickel-Cadmium

Nickel-Cadmium batteries have a slightly higher energy density than lead-acid batteries and a significantly higher power density, but the specific costs are much higher and from an ecological point of view, the use of cadmium is critical. The positive electrode consists of nickel hydroxide and the negative one consists of cadmium hydroxide. The following equation shows the electrochemical reaction that takes place:

$$2\,\mathrm{NiO(OH)} + \mathrm{Cd} + 2\,\mathrm{H_2O} \rightleftharpoons 2\,\mathrm{Ni(OH)_2} + \mathrm{Cd(OH)_2} \tag{3.3}$$

This type of battery is affected by the memory effect problem. That is, the loss of energy storage capacity caused by charging the battery too early. Therefore, to avoid damaging it, it is necessary to let it discharge completely before recharging.

3.2.3 Nickel-Metal Hydride

Nickel-Metal hydride batteries are a further development of nickel-cadmium batteries, with the goal of creating a battery without toxic cadmium but with the advantages of the previous ones. These batteries are composed of nickel hydroxide as a positive electrode, different materials as a negative electrode, and a potassium hydroxide solution ($KOH + H_2O$) as the electrolyte. The presence of hydrogen instead of cadmium in the anode improves the energy density, as can be seen from Ragone's diagram in figure 3.3. The electrochemical reaction can be represented by the following equation:

$$\mathrm{MH} + \mathrm{NiO(OH)} \rightleftharpoons \mathrm{M} + \mathrm{Ni(OH)_2} \tag{3.4}$$

However, these batteries have disadvantages, including lower charging efficiency than other types of batteries and higher self-discharge, which is accentuated in a high-temperature environment. Compared with Ni-Cd, they are less affected by the memory effect. This type of battery is used more for HEVs than for BEVs.

3.2.4 Sodium–Nickel Chloride

Sodium-Nickel Chloride batteries are also called ZEBRA batteries. The name is derived from the "Zero Emission Battery Research Activity" project. It is made of liquid sodium at the operating temperature and a solid ceramic electrolyte which also acts as a separator. The principal redox reaction that occurs in a ZEBRA battery is given by the following equation:

$$2\,\mathrm{NaCl} + \mathrm{Ni} \rightleftharpoons \mathrm{NiCl_2} + 2\,\mathrm{Na} \tag{3.5}$$

It has advantages such as high energy density, low corrosion, high safety, insensitivity to overcharge, long life cycle and low price. It is also characterized by low power density and a self-discharge problem. Its main disadvantage is the high operating temperature

of about 300°C, which requires precise temperature management and good insulation. Cooling to room temperature results in high thermomechanical stress for the ceramic electrolyte (if it breaks down, the cell can no longer be used).

3.2.5 Lithium-Ion

In recent decades, Lithium-Ion batteries have revolutionized the battery industry, emerging as the predominant energy storage solution for several applications, including electric vehicles. This is due to their high efficiency, high power and energy density, low self-discharge rates, absence of memory effect and long life cycle. They are also environmentally friendly, as their components can be recycled. A lithium-ion battery consists mainly of a positive electrode, a negative electrode, electrolytes, separators, binders, and two current collectors. We will examine it in more detail in Section 3.3 below.

3.2.6 Ultracapacitor

Ultracapacitors are known as electrochemical double-layer capacitors that, unlike conventional capacitors, structurally use a double electrical layer, creating a very large surface area to facilitate the storage of a larger amount of charges. With respect to previous batteries, no transformation of chemical energy into electrical energy, or vice versa, takes place. In fact, during the charging phase, they store positive/negative charges on their respective plates, generating a potential. To increase capacitance, dielectric materials are commonly inserted between the plates, allowing higher voltages to be stored. They have a very high power density and outperform almost all battery technologies in terms of cycle life. Unlike a battery, ultracapacitors can withstand millions of charge/discharge cycles, making them particularly suitable for capturing all available energy during regenerative braking. Due to the high power density, they can be charged or discharged at a very high C-rate, and the temperature of the electrodes heated by the current is the only limiting factor. However, the energy density of ultracapacitors is significantly lower than that of batteries, limiting their application to the role of buffers within a system with one or more energy storage devices. Despite an efficiency of more than 97%, which is higher than that of classical electrochemical batteries, they have high self-discharge currents [19].

3.3 Lithium-Ion Cell

Due to the previously mentioned advantages, the lithium-ion battery presents itself as the predominant choice in the automotive industry. The cell of such a battery is characterised by the following structure:

- The **cathode** is the most expensive element in these batteries, being composed mainly of crystalline cobalt, nickel, and manganese. These elements combine to form a multi-metallic oxide material to which lithium is added.

- **Anode** is typically made by mixing an active material, a binding powder, a solvent and additives in a slurry. Graphite is an active material often used in anodes because of its high conductivity, low cost, and ability to reversibly accommodate lithium ions within its many layers due to its unique electronic structure. Alternative negative electrode materials currently used or being evaluated for future applications include lithium titanate ($Li_4Ti_5O_{12}$, LTO battery), hard carbon, a tin/cobalt alloy, and silicon. LTO boasts high durability, thermal stability, and accelerated charging times at the expense of reduced capacity and voltage.

- The space between the two electrodes is filled with an **electrolyte** that plays a key role in transporting lithium ion particles between the cathode and the anode. The most commonly used electrolyte is composed of a lithium salt, such as $LiPF_6$, dissolved in an organic solution. Water is not suitable because of its potential violent reaction with lithium. In addition to the lithium salt, various additives are added to impart the required properties to the electrolyte solution. The precise formulation of the electrolyte varies depending on the specific materials used for the anode and cathode.

- Battery **separator** can be produced with fiberglass fabric or flexible plastic films made from materials such as nylon, polyethylene, or polypropylene. It must be permeable and thin to allow unimpeded passage of charged lithium ions Li^+ during both charging and discharging, and it must be able to prevent the passage of electrons, which will then move through an external load.

3.3.1 Working Principle

Lithium has a high tendency to lose electrons (it has only one electron in the second orbital, which it always wants to lose) and is therefore highly reactive (it reacts easily with water). However, when it is part of a metal oxide, it becomes very stable.

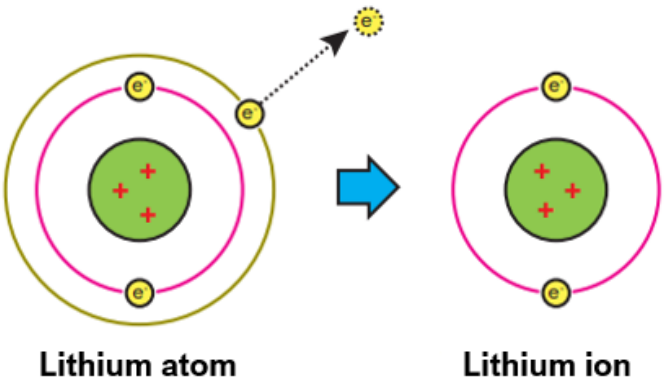

Figure 3.4: Lithium representation

During charging, the electrolyte lets through only Li ions, while electrons (e^-) are attracted to the positive pole of an external energy source and removed from the lithium atoms of the metal oxide. These electrons flow through the external circuit, reaching

the graphite layer. At the same time, positively charged lithium ions Li^+ are attracted to the anode and migrate toward it through the electrolyte. At this point, the electrons have dissociated from the metal oxide, placing the battery in an unstable state; it is now charged.
After removing the external power source and connecting a load, discharge phase, the Li^+ ions want to return to their stable state as part of the metal oxide. As the lithium ions pass through the electrolyte, the electrons move through the circuit, rejoining the cathode. As the lithium ions move through the electrolyte, electrons flow through the load, rejoining the cathode. The operating principle, illustrated in the figure 3.5, can be summarized by the following oxidation-reduction half-reactions:

Cathode reaction:

$$\mathrm{Li_{1-x}MO_2 + xLi^+ + xe^- \rightleftharpoons LiMO_2} \tag{3.6}$$

Anode reaction:

$$\mathrm{Li_yC \rightleftharpoons C + yLi^+ + ye^-} \tag{3.7}$$

Where M represents a metal such as Nickel, Cobalt or Manganese. As can be seen from the last equation, graphite does not play a role in the chemical reaction, but is only a medium for trapping Li^+ ions.

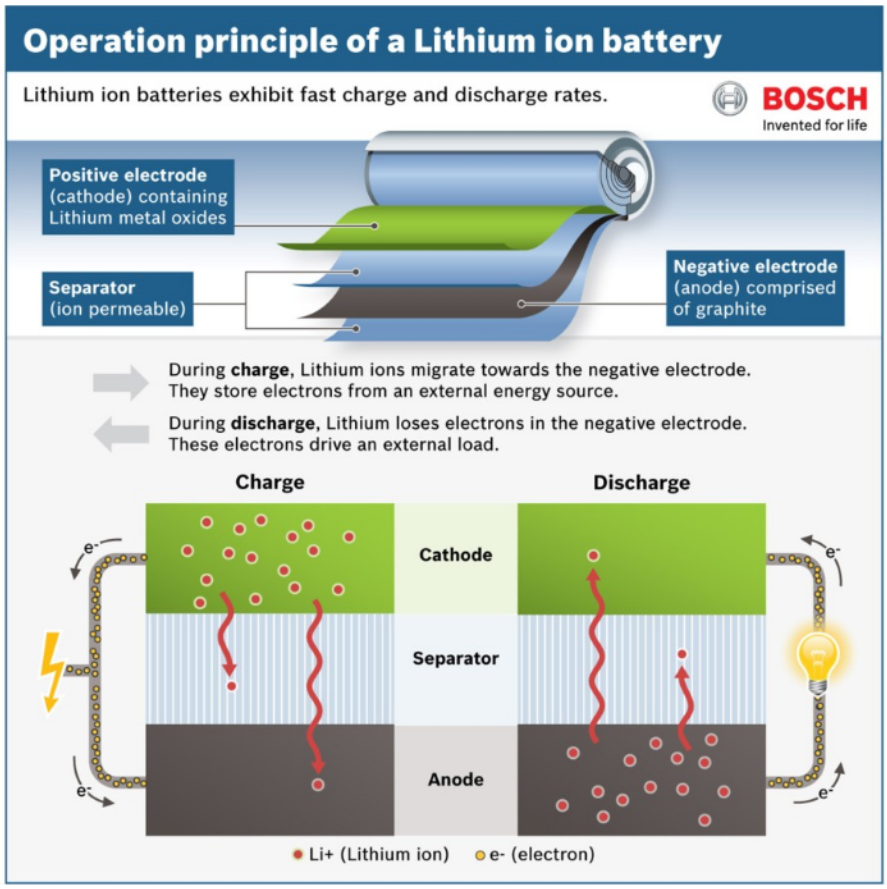

Figure 3.5: Working Principle: Charge and Discharge [20]

3.3.2 Positive Electrode Materials and Characteristic

Battery types are usually named after the positive electrode materials. The performance of current lithium-ion batteries is limited mainly by the characteristics of the cathode. The performance criteria of such batteries in electric vehicle applications require cathode materials with excellent conductivity for both lithium ions and electrons. When the mobility of lithium ions and electrons is faster (higher diffusion coefficient), a battery can achieve both a higher rated power and energy density. To meet performance criteria, current lithium-ion battery cathodes have been developed through different approaches, which can be classified into three distinct families from the point of view of crystal structure: a layered structure typified by $LiCoO_2$ (LCO); a spinel structure such as $LiMn_2O_4$ (LMO); and an olivine structure such as $LiFePO_4$ (LFP). The properties and general characteristics of these cathodes are shown in figure 3.6.

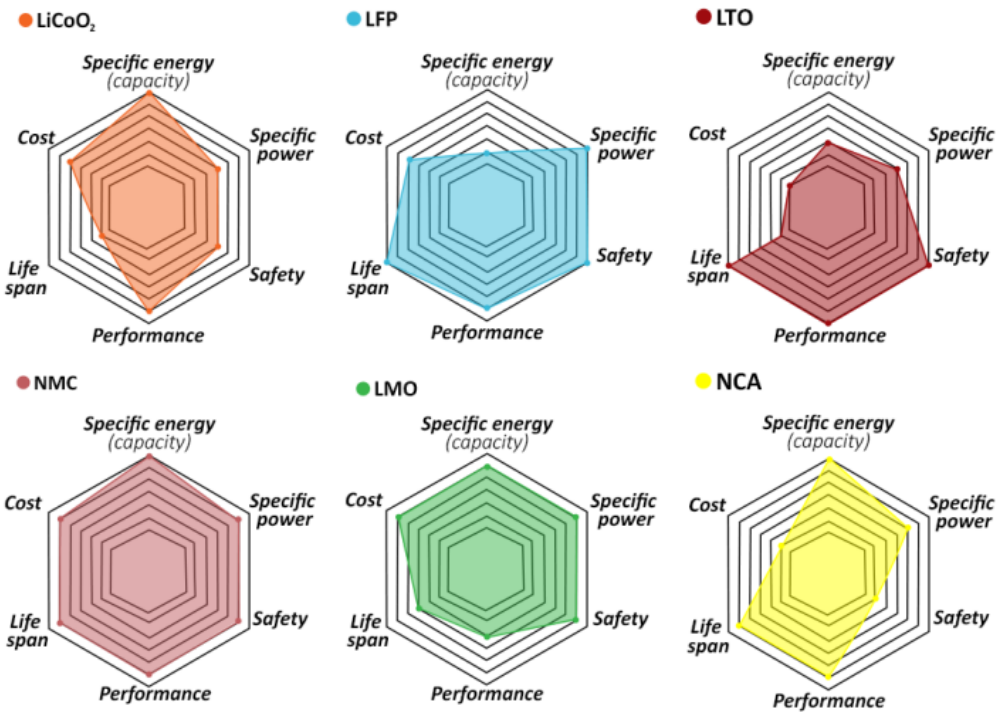

Figure 3.6: Different types of cathodes

Five main cathode materials are used in lithium-ion batteries:

- **Lithium Cobalt Oxide - LCO** ($LiCoO_2$): the first chemistry to be successfully implemented in a cathode. However, the use of cobalt as a cathode material is a problem because of the high price. Characterized by low power density and high energy density, with values between 150 and 200 Wh/kg, cells with this cathode provide high electrical performance but suffer from poor thermal stability due to the volatility of cobalt and have a short lifetime. LCO has a layered crystal structure.
- **Lithium Manganese Oxide - LMO** ($LiMn_2O_4$): it is known for its stability due to the spinel crystal structure, which is more stable and has minimal excess

lithium ions in the fully charged state. These batteries are short-lived but offer high power density and can therefore be recharged quickly. However, instability at higher temperatures persists.

- **Lithium Iron Phosphate - LFP** ($LiFePO_4$): the long life and thermal stability, due to its crystalline structure, make it one of the most widely used lithium-ion batteries. Olivine structures are characterized by stronger covalent bonds between oxygen atoms and other elements, which improve thermal and chemical stability. It is this fundamental difference on the atomic scale that results in increased safety and life cycle [21]. However, as a trade-off, these batteries have one of the lowest energy densities among lithium-ion batteries. Consequently, the operating voltage is also low. Despite the low rated voltage, the potential curve as the state of charge changes is almost flat, ensuring a constant voltage for much of its operation.

- **Lithium Nickel Oxide - LNO** ($LiNiO_2$): it offers the best capacity and power density, but its unstable layered crystalline structure results in reduced lifetime and low thermal stability. Consequently, this cathode type is inadequate for practical applications, and the production of batteries based on this type of cathode has been replaced by more stable alternatives such as NMC cathodes.

- **Lithium Titanate - LTO** ($Li_4Ti_5O_{12}$): it is the only lithium-ion battery in which the composition of the anode changes significantly. Lithium titanate replaces graphite in the anode, and the material is formed into a spinel structure. The cathode can be lithium manganese oxide or NMC. It has low power and energy density compared with other types.

The most important layered oxide classes for EV applications are the NMC and NCA cathodes. The objective of the design of this type of cathode is to obtain the best combination of advantages, while mitigating all the disadvantages, associated with each mentioned monometallic transition oxide. Cost limitation can be achieved by reducing the amount of cobalt, which is the most expensive of all metals. Specifically:

- **Lithium Nickel Cobalt Aluminium Oxides - NCA** ($LiNi_xCo_yAl_{1-x-y}O_2$): it exhibits power and capacity characteristics similar to those of LNO. The addition of aluminum prevents a phase change in the crystal structure, which depends on the concentration of Li, increasing its stability. Despite this, NCA cathodes present safety problems and high costs.

- **Lithium Nickel Manganese Cobalt Oxides - NMC** ($LiNi_xMn_yCo_{1-x-y}O_2$): the combination of nickel and manganese is critical to the success of NMC. While manganese contributes to the development of a spinel structure, leading to low internal resistance, it has the disadvantage of having a relatively low energy density. Nickel has a high energy density but is unstable. When metals are combined, both electrical and structural advantages are achieved. Reducing the cobalt content in NMC is also a current goal due to the high cost of the metal, although decreasing the cobalt percentage lowers the cell voltage. On the other hand, reducing the nominal voltage of the cell tends to increase its life cycles. This is because, when operating at higher voltages, the cell degrades more quickly.

3.3.3 Lithium-Polymer Cell

However, the chemical composition of the cell can be changed not only by the positive electrode, but also by the electrolyte. In fact, replacing the liquid electrolyte with a gel-like lithium polymer results in what is commonly called a lithium polymer ($LiPo$) battery. The operating principle and construction of these batteries are identical to those of lithium-ion batteries. In lithium polymer batteries, the negative electrode consists of graphite and additives bonded onto a metal substrate. The cathode is three-dimensional lithiated cobalt oxides or mixed nickel/manganese/cobalt (NMC) oxides, also bonded to a metal substrate.
One advantage lies in the almost unlimited range of sizes and formats, made possible by the absence of a rigid steel housing and a compact design. In particular, the ability to design extremely thin cells (less than 1 mm) is a distinguishing feature of $LiPo$ battery technology. This allows individual dimensions to be customized and the space reserved for the battery to be utilized to its full potential.
The energy density of these cells is higher than that of other types. Relative to their overall weight, li-polymer cells have a slightly higher energy density than li-ion cells. Like li-ion batteries, they can be easily connected in parallel to allow higher capacities. A further advantage of $LiPo$ cells is their relatively low self-discharge rate. However, they must be protected from overloads, deep discharges and extreme temperatures.
Drawbacks include that, in addition to being more expensive, they can have a slightly shorter life cycle than conventional lithium batteries.
The charging and discharging characteristics of lithium polymer are identical to those of other lithium-ion systems and do not require a dedicated charger. Safety issues are also similar in that protective circuits are required, although batteries with polymer electrolyte contribute to greater safety by reducing the risk of leakage and flammability.

3.3.4 Safety Issues

In general, Li-Ion batteries (LIBs) are temperature-voltage sensitive products. Figure 3.7 shows the behaviors of a typical LIB at various voltages and temperatures. There is a comfortable zone with a voltage range of 2.5 to 4.2 V and a temperature range of -30 to 55 °C, which is the design index formulated by the battery system [22]. Here are outlined the main critical conditions that can occur during the operation of these batteries.

Overcharging. Overcharging often occurs when a battery is forcibly charged beyond the maximum established voltage. In such cases, an excessive amount of lithium is pulled out of the cathode and deposited on the anode. Lithium deposited react with the electrolyte, causing an increase in impedance and thus significant heat generation that will rapidly raise the cell's internal temperature. In the most severe scenarios, the deposited lithium particles can form dendrites that can puncture the separator, causing self-shorting that could trigger a thermal runaway. According to available data, overcharging is the leading cause of EV failures.

Overdischarging. Overdischarge occurs when a cell is discharged to a voltage below

the specified cut-off voltage, which depends on the battery chemistry. This phenomenon can negatively impact the performance of LIBs and, in severe cases, cause safety problems such as internal short-circuits. During anode overdischarge, the solid interphase electrolyte (SEI) decomposes, producing gases such as a carbon dioxide, methane, and carbon monoxide. This process induces swelling of the cell. When the battery is recharged, new SEIs are formed that consume active lithium ions and electrolytes. The formation of these new SEIs alters the electrochemical properties of the anode, leading to degradation of the cell's capacity to the point of total loss of the ability to be recharged.

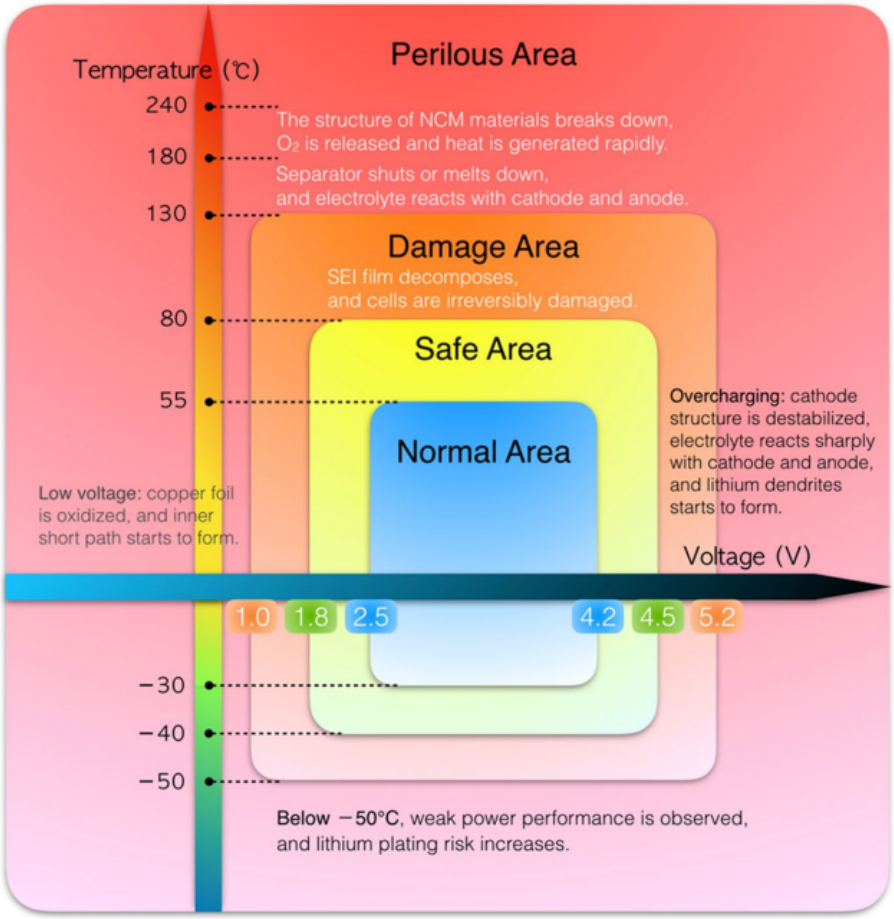

Figure 3.7: The behavior of a LIB at various voltages and temperatures

Low-temperature performance. At freezing temperatures, LIBs suffer from several problems including capacity fade, power attenuation and charging difficulty. These issues are attributed to factors such as low electrolyte conductivity, poor kinetics of charge transfer, increased SEI resistance, and diminished solid-state lithium diffusivity in graphite. The reduced diffusivity of lithium ions, especially at lower temperatures, leads to a decrease in the intercalation rate. This, in turn, promotes lithium plating on the graphite surface during the charging process. A significant portion of the deposited lithium becomes "dead lithium," ceasing to participate in subsequent electrode reactions. This phenomenon is the main cause of capacity fading. Furthermore, the growing

dendrites could pierce the separator membrane and triggering internal short circuits, which could lead to serious safety issues.

Overheating. Overheating leads to severe consequences, starting a series of reactions in the battery system as temperature rises. These reactions, including SEI decomposition, interactions between anode/cathode active materials and the electrolyte, and electrolyte decomposition, contribute to thermal runaway. The order of these reactions is not strictly sequential; some may occur simultaneously. Above 60 °C, SEI decomposition begins, and exposed lithiated anode materials (like LiC_6) react rapidly with the electrolyte. Higher temperatures enhance the dissolution of transition-metal ions, accelerating capacity degradation. Beyond 90 °C, complete SEI decomposition and intensified side reactions generate gases and heat, causing a significant loss of cell capacity and a lower number of life cycles. Further temperature increases may lead to the loss of all cell functions, cell rupture, and leakage of toxic gases and electrolyte solvents.

Overcurrent. During charging/discharging, overcurrent will lead to lithium plating on the negative electrode (LTO technologies are less sensitive). Repeating overcurrent will then create lithium dendrites, which will eventually damage and cross the separator and short-circuit the affected cells, causing thermal runaway.

3.3.5 Cell Characteristics

Various curves are essential for understanding the behavior of the cell during discharge. A typical approach to illustrate the discharge curve is to plot the voltage as a function of State of Charge (SoC) or battery capacity while holding temperature and current constant. The SoC indicates the available charge in a battery or cell at a given time, represented as a percentage. It reads 100% when the battery or cell is fully charged and 0% when it is fully discharged.

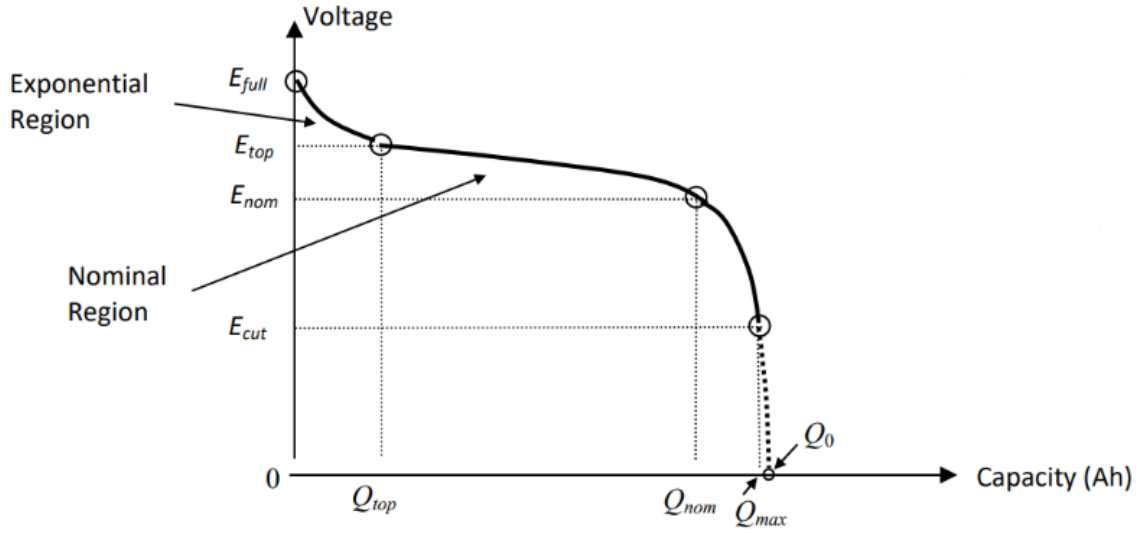

Figure 3.8: Typical cell discharge curve [23]

The parameters present in the discharge characteristic, figure 3.8, are:

- E_{cut}: discharge cut-off voltage;
- E_{nom}: rated voltage;
- E_{top}: exponential point voltage;
- E_{full}: full voltage;
- Q_{top}: exponential point capacity;
- Q_{nom}: rated capacity;
- Q_{max}: maximum capacity;

The voltage starts at the E_{full} value, which represents the fully charged state across the cell. Initially, the voltage decreases exponentially until it reaches the E_{top} value (with a capacity of Q_{top}). Subsequently the voltage follows a more linear trajectory for a significant portion of the discharge, reaching the rated E_{nom} voltage. Towards the end the voltage undergoes a non-linear decrease until it reaches the minimum voltage (E_{cut}). In general, a flat discharge curve is better because it means that the voltage is almost constant throughout the cell's discharge cycle.
Figure 3.9, shown below, represents the cell voltage as a function of SoC. In this plot

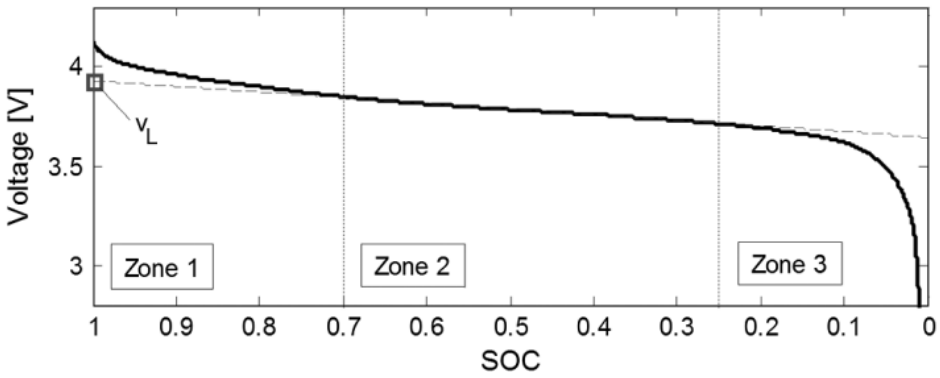

Figure 3.9: Li-Ion cell discharge curve [SOC-Voltage]

it is clear that 80% of the charge is between 3.8 V and 3.9 V. The initial 5% varies between 3.9 V and 4.25 V, while the final 15% ranges from 3.4 V to 3.8 V.
Another important graph is achievable by performing discharge tests at various current values (different C-rates) while keeping the temperature constant. This provides information on how the discharge current affects the battery voltage trend, shedding light on its performance under different load conditions. In figure 3.10, the tests were carried out at room temperature. As the discharge current rises, there is a corresponding decrease in the voltage across the cell. This is due to a voltage drop. If we model the cell as an ideal voltage source with an equivalent impedance in series, an increase in discharge current results in a higher voltage drop across the impedance, leading to a reduction in cell voltage. Naturally, a higher discharge current implies a shorter

discharge time, as more power is required. However, it is important to note that a high discharge current contributes to an increase in operating temperature, which in turn affects the cell voltage. Figure 3.11 illustrates the discharge curves with a current of 3 A at different temperatures. Cells discharged at temperatures below 25°C provide lower voltage and capacity, resulting in less energy production. On the other hand, cells discharged at temperatures above 25°C exhibit higher voltage and capacity. A higher operating temperature, still within the allowable range, allows for better flow of electrons resulting in greater energy production.

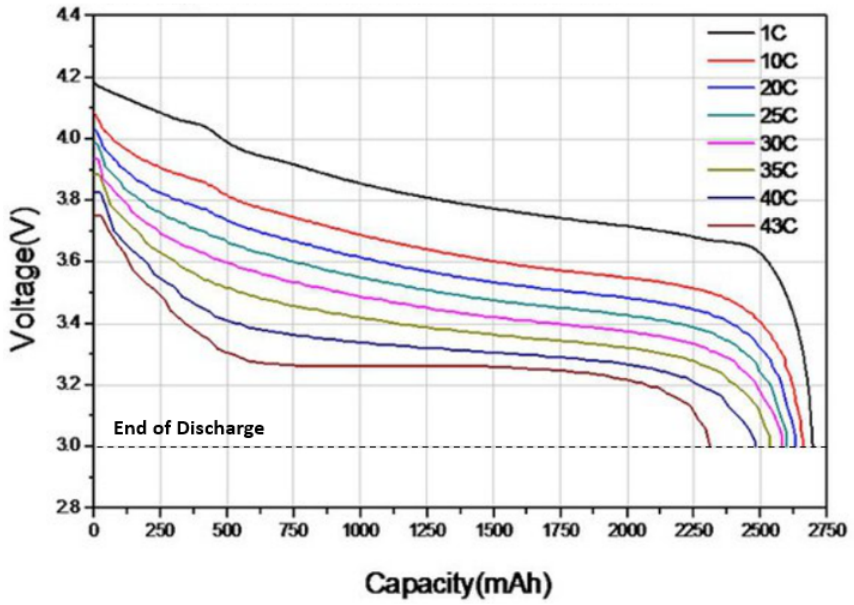

Figure 3.10: Discharge curves at different C-rates

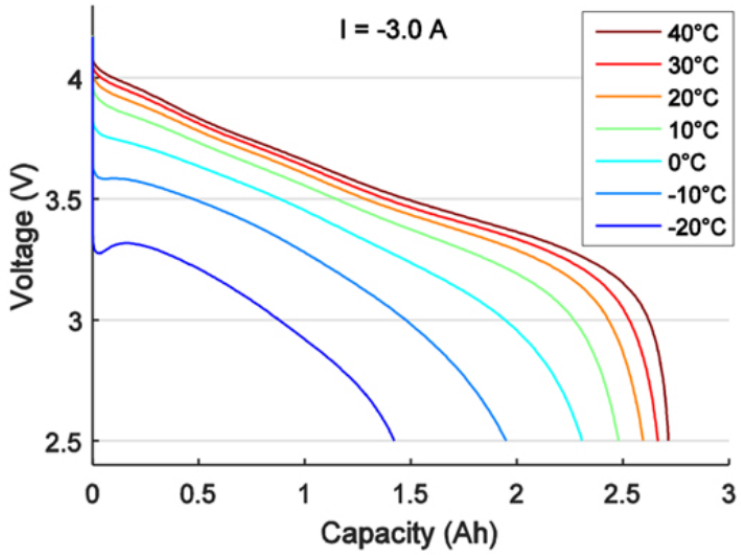

Figure 3.11: Discharge curves at different temperatures

3.3.6 Aging

Aging of lithium-ion batteries is a nonlinear and irreversible process that occurs over time during use, influenced by a combination of both external and internal factors. The most obvious effects of aging are reduced capacity and increased internal resistance. For most applications, the end of life (EOL) of a battery is determined by the minimum allowable residual capacity and the maximum allowable internal resistance and thus depends on the above effects. Generally, there are two types of aging: calendar aging and cyclic aging. The former indicates the gradual degradation of batteries over time, even if they are not used, while the latter concerns the "wear and tear" that batteries experience with each charge and discharge cycle. In other words, every time a battery is used, some degree of aging occurs.
The main factors affecting calendar aging are temperature and state of charge. In general, batteries age faster at higher temperatures and SOC (above 90%). However, it is essential to avoid operating batteries at too low a temperature to prevent problems that have already been addressed, such as lithium plating. Talking about the cyclic aging, it is dominated by the energy throughput, the amount of energy that flows through the battery within a set period of time, where the number of cycles is a crucial factor. However, smaller cycles are less harmful than larger ones. As a result, the battery can withstand more cycles if the depth of discharge (DoD) remains within a limited range. Furthermore, the charging power also affects the cyclic life. Higher charging power or "fast charging" accelerates the aging process [24].
When considering the aging of a lithium-ion battery, it is possible to divide the aging trend, depending on the capacity, into three stages, as shown in figure 3.12.

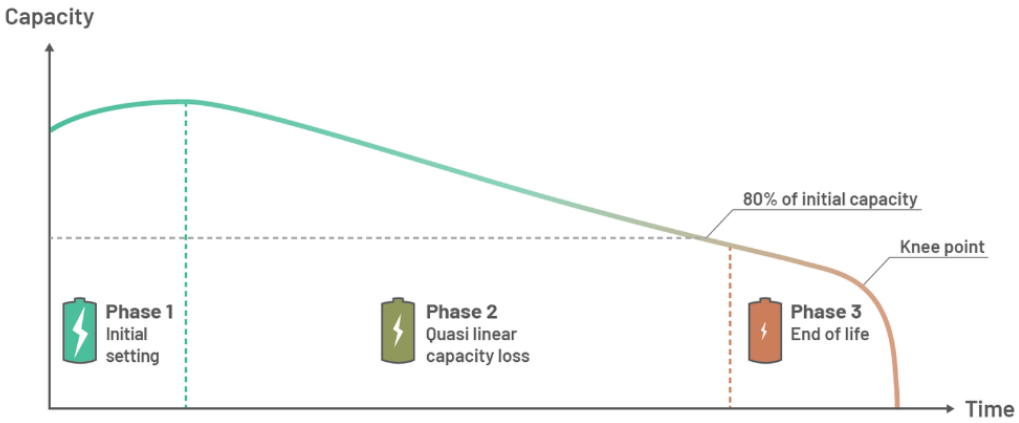

Figure 3.12: Typical battery capacity lifecycle

1. **Initial setting:** in the initial stage of the battery, different chemical processes settle into place. Surprisingly, this can lead to an increase in capacity, even with use. One factor contributing to this increase is the anode protrusion effect, which involves lithium stored in a slightly larger portion of the anode than the electrode, which does not actively participate in chemical reactions.

2. **Quasi linear capacity loss:** in the later stage, there is a pronounced correlation

between capacity loss and battery usage. In general, the relationship tends to be more or less linear when the battery is used under relatively constant operating conditions.

3. **Knee-Point:** the third phase begins at about 80-85% of initial capacity, marked by the occurrence of the "knee point." This is a rapid decline in capacity over a few cycles, indicating the end of battery life.

Chapter 4

SW Environment and Model-Based Approach

The main objective of this chapter is to provide a comprehensive overview of the fundamental principles of the Model-Based Design (MBD) methodology and the software environment, both used in the development of the VCU algorithm.

4.1 Model-Based Design Approach

Model-Based Design offers an effective approach to establish a unified framework for communication throughout the design process, concurrently supporting the development cycle (V-model). The V-shaped model is a popular software design development process, particularly used in the automotive industry. Its name comes from the characteristic V-shaped sequence that features the progression of all phases of product development and testing. As illustrated in the figure, the left side, is devoted to the specification and design phase, while the right side is devoted to the validation and testing of the system. The development flow can be schematized as follows:

1. *Requirement Gathering:* at this stage, the characteristics of the product are defined according to the needs of the end user. The technical specifications are not explicit; however, the points defined serve as the main guideline for the next phase of development.

2. *System Analysis:* here, previously outlined requirements are analyzed and the initial structure of the software is established. In practical situations, users are informed of potential difficulties in meeting certain requirements, which leads to modifications and reanalysis if necessary.

3. *Software Design:* high-level SW design phase. The main building blocks of the software (for this project LabVIEW) are defined.

4. *Module Design:* known as the low-level design phase, specifies the complete internal design of each individual module in the system. Based on the internal designs of the modules, unit tests can be created.

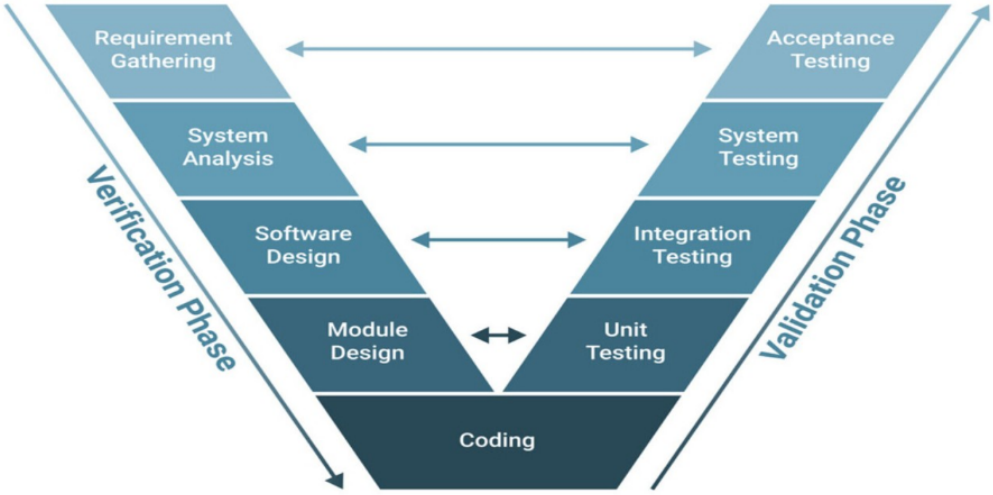

Figure 4.1: V-shape

Next, the developed modules are converted into source code through the use of dedicated compilers; the generated source code is optimized and then incorporated into the control unit. This phase is followed by a testing and validation phase aimed at identifying the main critical issues in the system and implementing the necessary corrections:

1. *Unit Testing:* to check the functionality of the individual modules. This refers to the module design phase described in step 4 of the development flow.
2. *Integration Testing:* validates the system architecture by ensuring that individual units can communicate and function properly once integrated. Specific tests are established during the SW design phase.
3. *System Testing:* overall product performance is evaluated to ensure compliance with specifications.
4. *Acceptance Testing:* performed at the end of the product development chain. These tests are designed at the requirements stage to verify all agreed terms. Finally, the system is integrated into the vehicle and calibrated.

The development and testing flow just described can be divided into four main test phases:

- **Model in the loop (MIL):** during this phase, the control algorithm is developed using simulation software, and an initial testing phase is conducted using a computer-simulated model of the system.
- **Software in the loop (SIL):** at this stage, the source code generated by the controller algorithm is integrated into a software simulation environment on the computer.
- **Processor in the loop (PIL):** here, the generated code is executed on a real processor (ECU), but the plant continues to be simulated.

- **Hardware in the loop (HIL):** last phase of testing, the controller algorithm is still run directly on the ECU as in PIL phase, but now it is connected to a real-time simulator.

As mentioned in the introductory chapter, in the final part of the project only the MIL testing phase will be carry out.

4.2 LabVIEW

LabVIEW (Laboratory Virtual Instrumentation Engineering Workbench) is the integrated development environment for National Instruments' visual programming language made in 1986. Such a graphical language is called the G language. The programming language used in LabVIEW is a high-level programming language. It differs from traditional languages because its syntax is not written but graphical, which is why it is called G-Language (Graphic Language). Each portion of code is called a VI (Virtual Instrument) and is characterized by a block diagram, a front panel and an icon/panel connectors. Within VIs it is possible to insert subroutines, subVIs, making the code highly modular. A G-program or subprogram, does not exist in text form, but can be saved only as a binary file that can be opened and compiled only by LabVIEW. Furthermore, because data can flow simultaneously through nonconsecutive blocks and connection structures, multithreading is implicitly realized, without the need for explicit programmer management. It is important to note that although the language natively supports multithreading, it is possible to force sequential execution through the use of appropriate control structures.
As mentioned, the two main sections of the programming environment are:

(a) **Front Panel:** represents the graphical interface of a LabVIEW program. Within a front panel can be placed controls, indicators, and graphs that allow the user to enter input and read output while running VI. A front panel features a *worksheet* that can be used to insert the various graphical objects that make up the interface, a *toolbar* that contains the main commands for managing the application and for debugging, and a *control palette* that contains all the graphical objects that can be inserted into the panel, grouped by category. Each time a graphical object is inserted on the front panel, an input or output block is automatically generated on the block diagram.

(b) **Block Diagram:** constitutes the programming interface. As already mentioned, G-code is used as the programming language. Like the front panel, the block diagram consists of a *worksheet*, a *toolbar* that has the same commands as the front panel, plus some debugging tools, and a *control palette* that, instead of graphical objects, contains subVIs, control structures, constants, variables, and other useful elements for generating code.

To avoid testing an algorithm directly on a hardware system, the **LabVIEW Control Design and Simulation Module** add-on is used. This module allows you to generate simulation models for the MIL phase. This is made possible by dedicated simulation environments called *Simulation Subsystems*. The block diagram of a simulation

subsystem has a light yellow background to make it distinguishable from the classic LabVIEW block diagram. The main advantage of these subsystems is that they are highly modularizable, making the code easier to understand and navigate. Each behaves as a separate while loop, with a specific step-time that can be used to easily solve discrete differential equations as we will see later.
For the purpose of this project, this add-on will be used to simulate the behavior of a battery pack module to test the battery management logic programmed on the VCU.

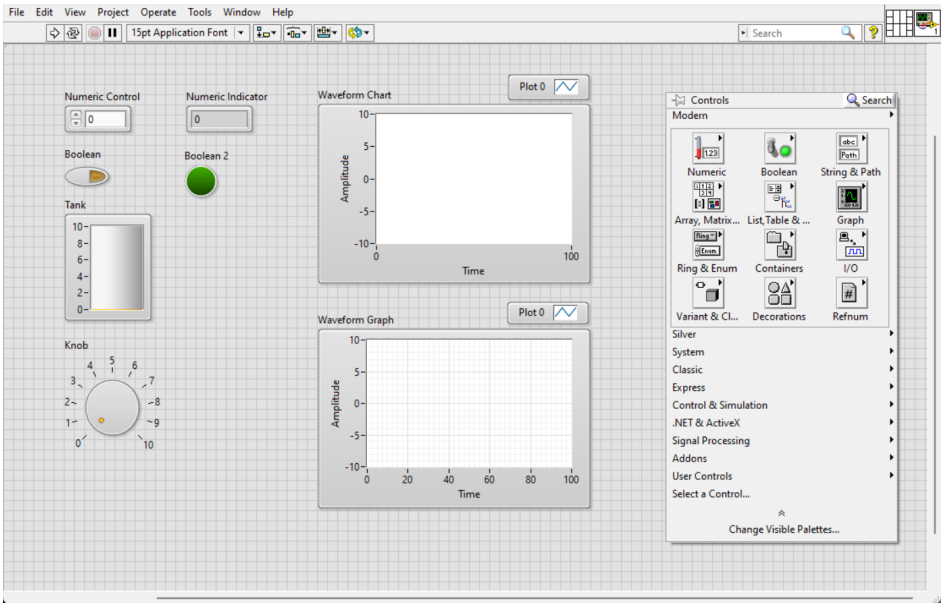

(a)

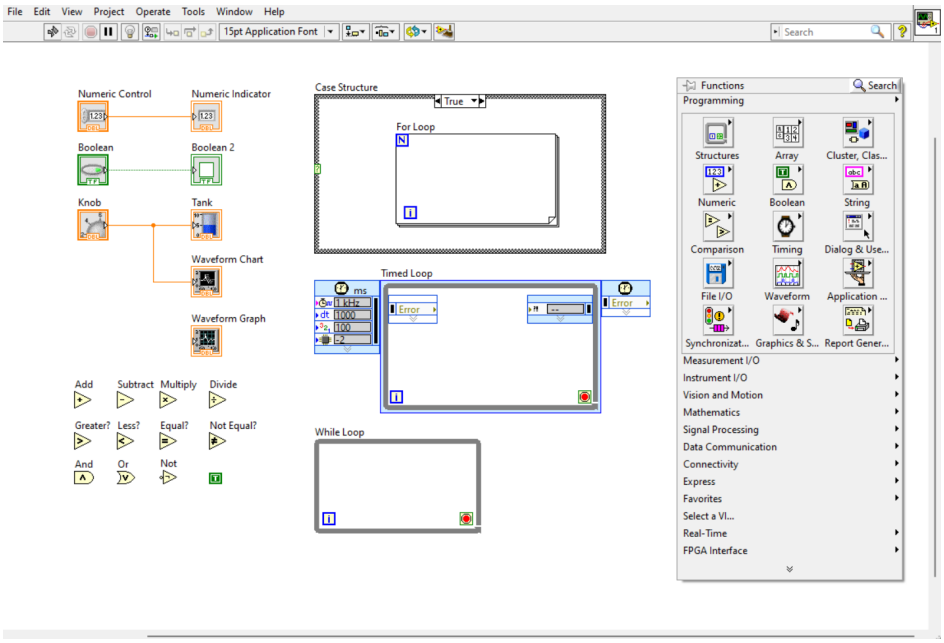

(b)

Figure 4.2: LabVIEW: (a) Front panel; (b) Block diagram

4.3 Miracle^2

The Vehicle Control Unit used for this project is the Miracle^2, a rapid prototyping real-time control unit of Alma-Automotive. Its main features are:

- Dual-Core ARM Cortex A9 real-time processor
- Artix-7 FPGA
- 512 MB RAM
- Power supply 6-26 V DC
- Programmable with NI LabVIEW toolchain
- Standard communication protocols implemented (CAN, Ethernet)

The presence of the FPGA improves controller performance because it enables parallel execution of multiple tasks, not being limited by the number of available processing cores. As mentioned above, the Miracle^2 is compatible with the LabVIEW SW, so it can be easily programmed through the graphics language, which is then automatically translated into the complex VHDL language for the FPGA [25].

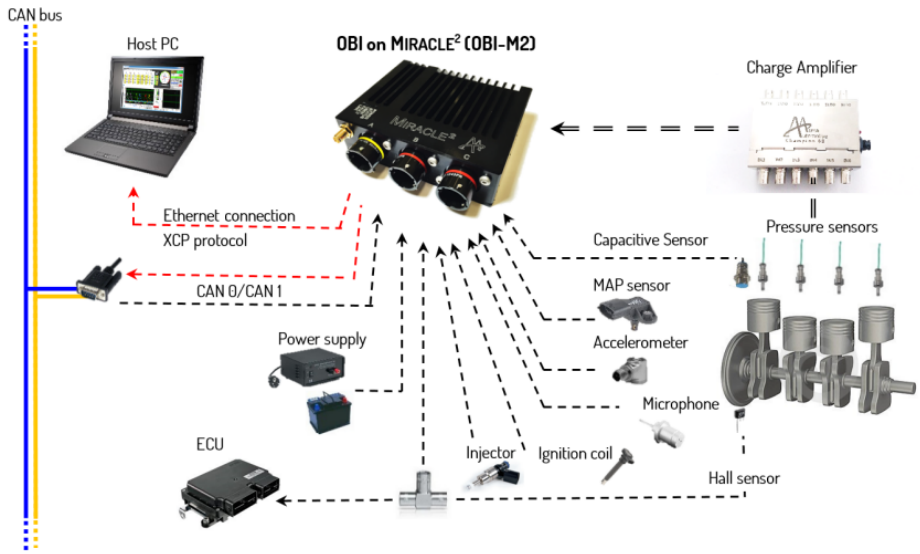

Figure 4.3: Miracle^2 connections

It is possible to connect it to the computer via Ethernet cable or wireless connection.

Chapter 5

VCU Alogrithm Requirements

This chapter outlines the basic requirements that the VCU algorithm must meet to ensure the proper and safe operation of the vehicle. The design procedure follows V-model and the basic principles of model-based design described in the previous chapter.

5.1 Requirements Definition

The VCU that is the subject of this thesis is designed to manage both the powertrain and the battery. To fulfill this purpose, it must have the following characteristics. Regarding powertrain management:

- An output torque request defined as a function of accelerator and brake pedal, current vehicle speed and maximum available torque.
- An algorithm that calculates the maximum available torque in relation to the current state of the vehicle and feedback from the vehicle's different sensors.
- A system that manages charging enablement and governs the general behavior of the vehicle in relation to the state of the battery.
- An algorithm to handle critical system failures by limiting vehicle operation when non-SW-related failures occur.

As for battery management, it must have all the features of a standard BMS:

- A contactors management system to meet safety requirements by isolating the battery in case of failure.
- Current limits defined during both charging and discharging, calculated as a function of voltage and temperature values.
- A thermal management control system that can heat or cool the battery according to the detected temperature.
- An algorithm to estimate the state of charge of the battery.

- An algorithm to manage battery failures by monitoring contactors status, current, voltage and temperature values coming from dedicated sensors.
- A system capable of performing cell balancing operations at the end of charging.

5.2 Powertrain Management

5.2.1 Throttle Mapping

The throttle map is a function that outlines the relationship between pedal position, vehicle speed and torque sent to the inverter. EVs improve mileage with one-pedal driving mode, which allows regenerative braking simply by releasing the accelerator pedal.

One-pedal driving

This driving style prioritizes fuel efficiency, relying heavily on regenerative braking to slow the vehicle. However, because of the limited negative torque that motors can provide compared to hydraulic brakes, the brake pedal remains essential for safety maneuvers and emergency stops. The main advantage lies in efficiently converting a significant portion of the vehicle's kinetic energy into electrical energy stored in the battery. One-pedal driving requires speed-dependent mapping, unlike standard pedal mapping. At low speeds, a modest amount of regenerative torque is applied to stop the vehicle, while at high speeds more braking torque is required to achieve substantial speed reduction, thus minimizing the use of mechanical brakes. A representation of the torque curves is shown in figure 5.1. When using a vehicle with an ICE, users can take

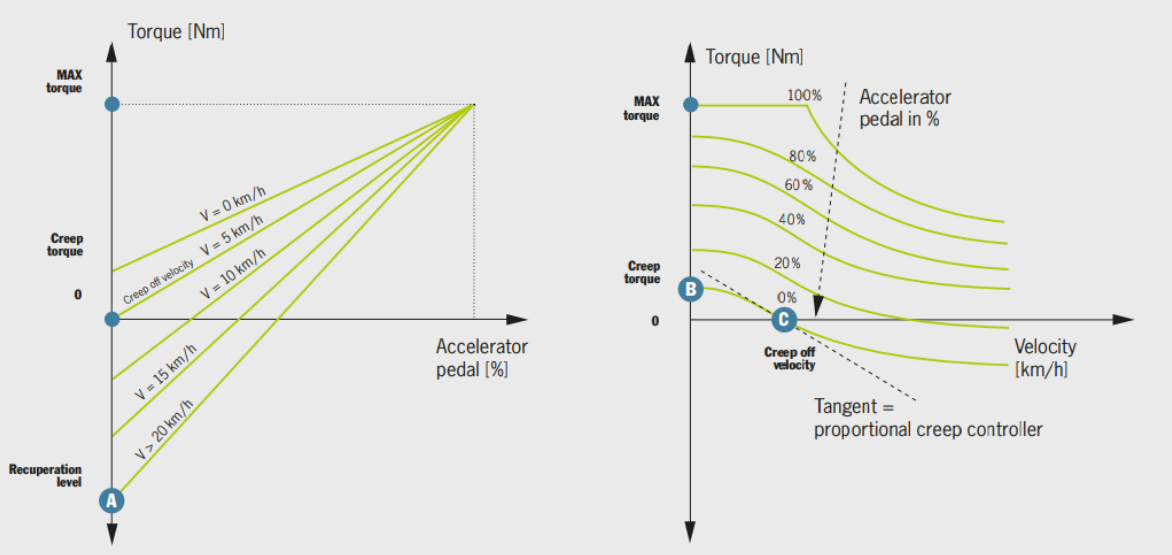

Figure 5.1: Torque curves: throttle pedal view (left); vehicle velocity view (right) [26]

advantage of the torque produced at the idle point of the heat engine by disengaging

the clutch, resulting in what is known as *creep torque*. To replicate this effect in EVs, when the speed of the vehicle drops below a certain threshold, it must be able to deliver a minimum torque. When the vehicle accelerates, the curves undergo alterations that lead to a reduction in the creep torque value. At a given speed, *creep-off velocity* (v_{creep}), a transition point is reached. Here, the creep torque becomes zero, and with a further increase in vehicle speed, negative regenerative torque is activated when the accelerator pedal is lifted. The torque that the motor generates when the throttle pedal value is 0% is called T_i and is a function of the current vehicle speed. The minimum achievable value is $Torque\_0$, which represents the maximum regenerative torque the vehicle can produce. At high speeds, the modulus of T_i gradually decreases from $Torque\_0$ to a minimum torque known as saturation torque (T_{sat}). As a consequence, when accelerating at high speed and lifting the accelerator pedal, the full regenerative torque is not applied instantaneously, but increases gradually as the vehicle slows down, improving driving comfort. As mentioned above, in one-pedal driving, hydraulic braking is provided only when the vehicle speed is below the creep-off velocity or when an unexpected maneuver is required. In these cases, the braking torque complements the regenerative torque applied to the electric motor. To ensure the perfect integration of these two torques for optimal driving comfort, when the brake pedal is pressed, the negative torque must align smoothly with that generated by the release of the accelerator pedal. This implies that all negative torque curves must intersect the torque axis at the value of T_i. By actuating the brake pedal, the torque increases progressively linearly with braking until the maximum regenerative contribution achievable with hydraulic braking is reached as we can see in the graph below. The throttle and brake pedals are mapped on a

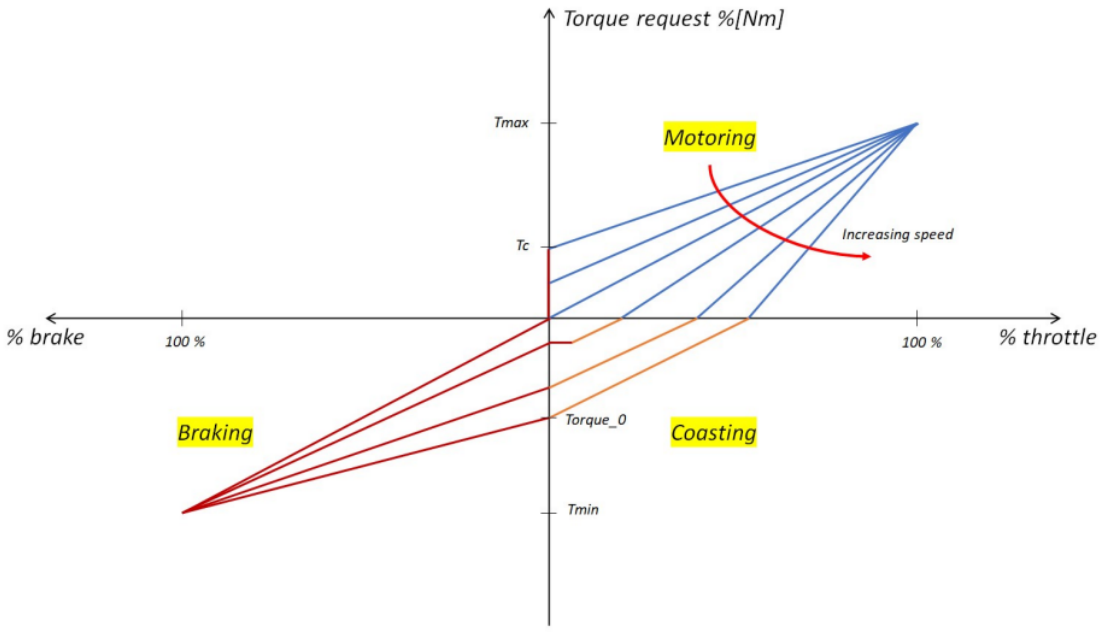

Figure 5.2: Torque profiles

scale from -100% (indicating full braking) to 100% (representing full acceleration).

Torque is mapped to a range from maximum torque (ratio of positive torque to the maximum torque the motor can generate) to relative minimum torque (ratio of negative torque to the maximum regenerative torque available). As in conventional ICE cars, at creep-off velocity the generated torque drops to zero, prompting the user to press the accelerator to further increase speed. Once a certain speed is reached, releasing the throttle decreases the torque, finally becoming negative. This phase, known as *coasting*, turns the motor into an electromagnetic brake. If the brake pedal is applied, the last negative torque value of the coasting phase, T_i, serves as the initial value for the linear braking profile. During braking, the vehicle speed is reduced through a combination of hydraulic and electric brakes.

Reverse torque profile

The reverse torque profile is used for low-speed maneuvers, such as parking. When reverse mode is activated, pressure on the accelerator pedal produces a low negative torque compared to forward conditions. To ensure safe maneuvers, the maximum reverse speed is limited to 20 km/h, and the maximum torque that can be required decreases from T_{max} (stationary vehicle) to 0 (maximum speed). In addition, the reverse mode startup includes safety controls to allow the profile to be activated only when the vehicle is still and free of anomalies. The torque required in this mode is very low, eliminating the need for additional restrictions. There is no regeneration phase, as the recoverable energy in reverse gear is considered negligible.

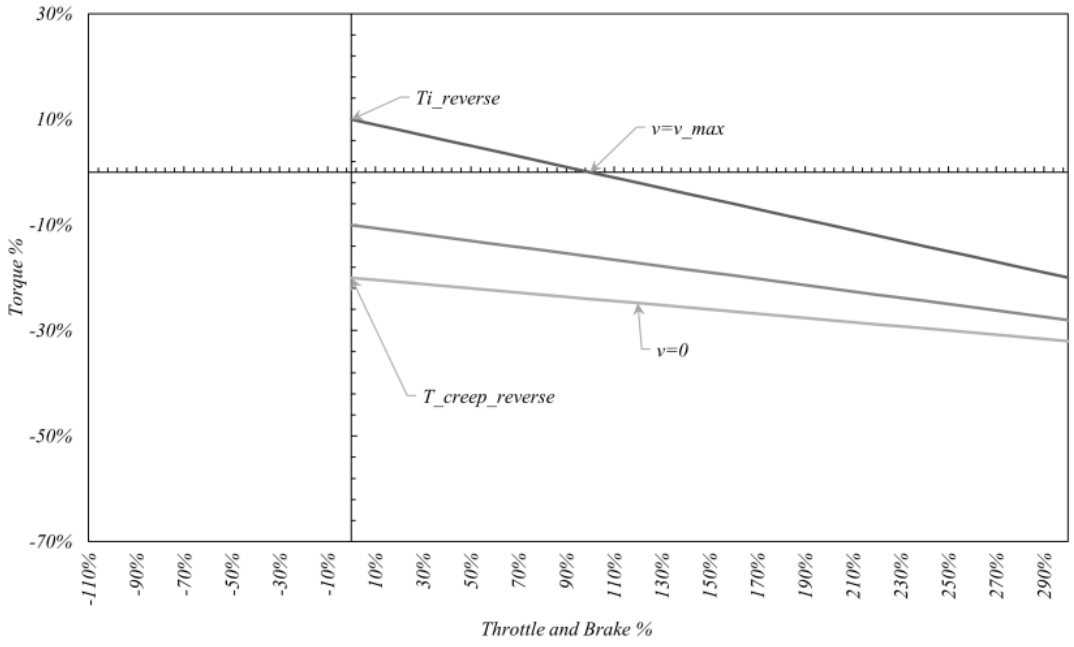

Figure 5.3: Reverse torque profile

5.2.2 Torque Limitation Functions

As we know, the torque that the motor can deliver is not linear with respect to the angular speed of the shaft. In this project, the motor used is a PMSM (SMAC 200-105-19-48 V) manufactured by the Benevelli Group. In this type of motor, torque is limited to a maximum between 0 and 2500 rpm to avoid excessive current flow through the stator windings, which could cause significant thermal loss. Above 2500 rpm, power remains almost constant and torque has an inverse relationship with shaft angular speed.

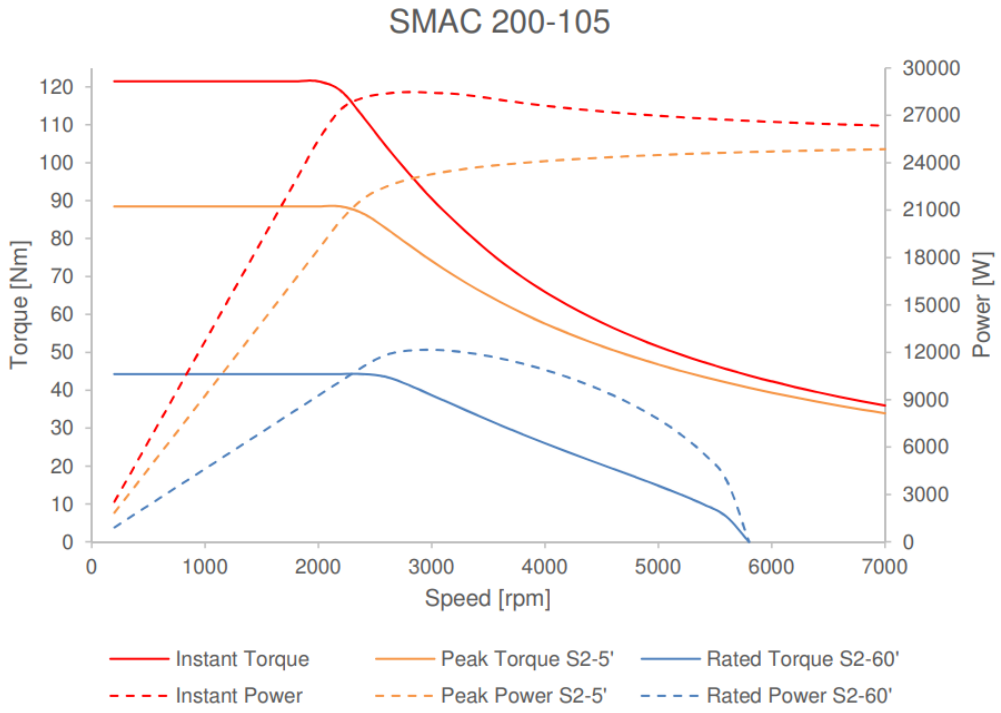

Figure 5.4: SMAC 200-105: Torque-speed curves

The torque value should be limited when one of the following events occurs:

1. The motor has limitations in sustaining the required torque indefinitely. According to the data sheet [27], it can consistently provide a torque of 44 Nm for 1 hour of continuous operation, while the maximum torque of 88 Nm can be sustained for about 5 consecutive minutes. To address all scenarios within these limits, the torque must be linearly limited to a minimum of 44 Nm to safeguard the electric motor from potential thermal damage when the motor temperature approaches critical levels.

2. The motor is approaching ω_{max}, a predetermined value set by default. This value ensures that the vehicle's transmission is rotating at a maximum speed that can be safely sustained.

3. If the system fails, it becomes necessary to limit torque to an extremely low value to mitigate further damage, allowing the driver to perform a safety maneuver that

brings the vehicle to a complete stop. When the vehicle is stopped and a fault is detected, the required torque signal must be reset to 0.

4. The vehicle is not in active driving mode, such as during charging or when it has not been started. In these cases, the motor should not be able to provide any torque.
5. The vehicle is in reverse gear, which means that the full torque of the motor is not available to ensure execution of the maneuver.
6. The state of charge is too low and the maximum torque needs to be reduced to increase mileage.

In the course of normal vehicle operation, multiple limit conditions may coincide. Therefore, to ensure safe operation under all circumstances, the most severe condition should always be applied.

Maximum speed limitation

Because the motor can handle higher speeds, its curve must be constrained by defining the value of the maximum torque required. Maximum torque must be accessible up to a specific percentage of maximum speed, after which torque gradually decreases until it reaches zero. This gradual transition is critical to avoid torque oscillations between the maximum value and zero once maximum speed is reached. Simply limiting the torque to zero would result in undesirable oscillations.

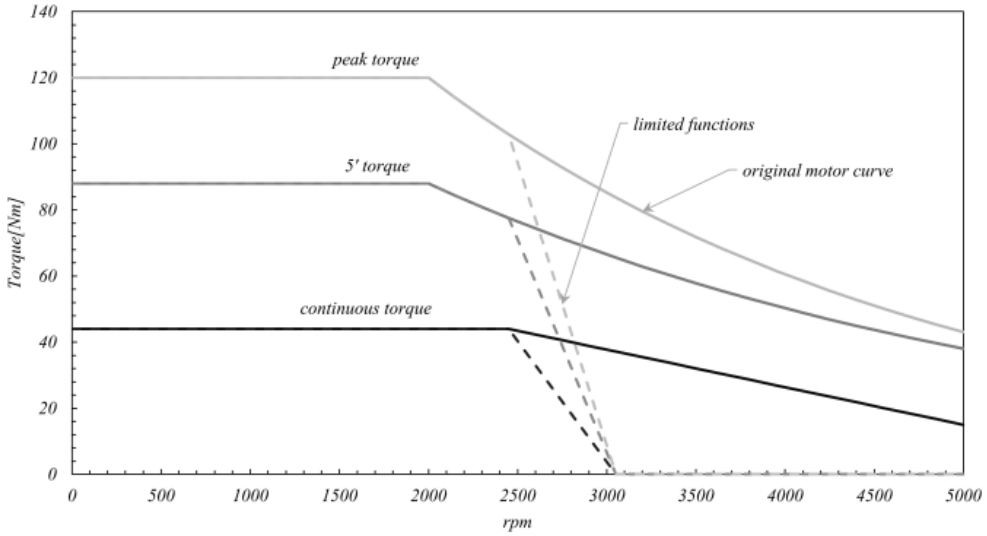

Figure 5.5: Speed limitation

Temperature-Torque limitation

The motor cannot provide maximum torque indefinitely. In its typical operation, the motor converts part of the input active power into mechanical power, while the

remaining energy is dissipated by the Joule effect. When torque exceeds the rated value, internal power losses exceed the capacity of the cooling system, leading to motor overheating. The use of a sensor, such as a thermocouple, on the motor makes it possible to implement a controller that performs safety checks on the motor temperature. This controller can then limit the torque required in the event of overheating to ensure safe operation.

5.2.3 Enabling the Charging Phase

The management of enabling the charging phase must operate in coordination with the battery management part. Recharging should be enabled only if specific conditions related to the state of the battery and, subsequently, the conditions of the pilot contacts are met. To assess whether the battery should be recharged, it is necessary to consider not only the state of charge, but also to verify that individual cell voltages meet specific requirements. When the charging process starts, a continuous exchange of information occurs between the vehicle and the charging station to verify that all parameters remain within specified limits. This data exchange is implemented using a PWM strategy communicated through the pilot control line. Once charging is complete, the vehicle side deactivates the on-board charger, interrupting the flow of energy.

5.3 Battery Management

5.3.1 Contactors Management

A check on the closing and opening contactors is required for safe operation at high voltage. To increase battery life, limiting the transient current during startup is critical to avoid potential unexpected damage. In EV propulsion systems, filter capacitors are connected to the DC link. As a result, an inherent inrush current occurs during insertion or interruption of the main power contact. Therefore, a pre-charge system should be required to control the current increase when using the traction battery under such circumstances. This peak typically lasts a few seconds, depending on the characteristics of the system. Pre-charge control is a standard feature in most electric vehicles. Its circuit diagram can be shown in figure 5.6. A resistor is placed in series with the pre-charge relay to bypass the positive relay for limiting the outrush current. The pre-charge circuit shall operate in the following sequence [28]:

1. During system shutdown, all relay contacts are deactivated.
2. When the system is reactivated, both the pre relay and the negative relay are activated, creating a bridge in the pre-charge circuit and exciting the load through the resistor.
3. If the inrush current is monitored or estimated, the positive relay is activated once that current has been reduced to a safe level.
4. The load is now fed from the battery through two parallel paths. Then, the pre relay is turned off after a specified delay to conclude the pre-charge phase.

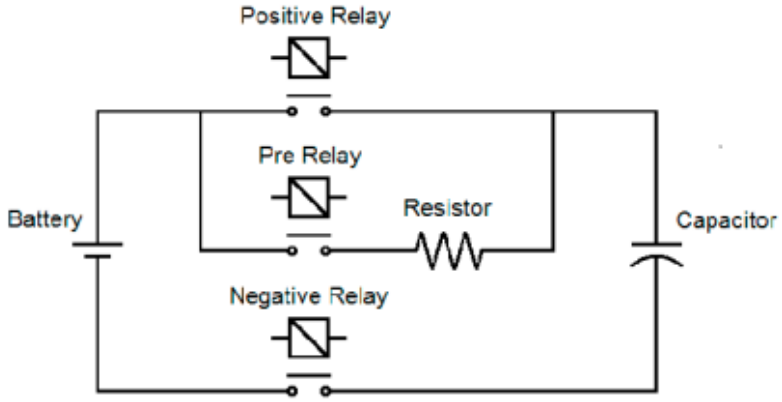

Figure 5.6: Contactors circuit

Contactors are the only moving part of a battery pack, and although simple, there are numerous failures that can interrupt operation. For this reason, their status must be monitored. Defects are typically: contactor permanently closed, permanently open, or overheating.

5.3.2 Cell Protection

Cell protection includes the protections and mechanisms implemented to ensure safe and reliable operation of individual battery cells, as well as their safe and timely management in the event of failure. The main objective of cell protection is to prevent or reduce the risks and potential hazards associated with battery cells, including overcharging, overdischarging, overheating, and short-circuiting. The key elements that must be present in cell protection are:

- **Overcharge protection:** the battery management algorithm should be configured with voltage thresholds, such as the threshold for the maximum allowable safe voltage of the battery cell. To ensure a safety margin, this threshold is usually set slightly below the specified value. Overcharge protection prevents the cell from being charged beyond the recommended voltage range. This protection provides continuous monitoring of the cell voltage during the entire charging process. It reduces the current rate when the voltage reaches the upper threshold and stops the charging process when the voltage exceeds this threshold.

- **Overdischarge protection:** it ensures that a battery cell is not discharged below the predefined voltage threshold, which indicates the lower limit of the safe voltage range for the cell. This limit, which is a little higher than the specified minimum value, is generally established to prevent potential damage to the cell when the voltage drops excessively. When the monitored voltage approaches or falls below the lower voltage threshold, the overdischarge protection mechanism comes into play by disconnecting the battery from the load or moderating the discharge rate by limiting the current flowing from the battery.

- **Overtemperature protection:** temperature protection also requires establishing temperature thresholds, both lower and upper, that define the safe working range for battery cells. As a preventive measure against overheating, the protection mechanism can moderate the rate of charge or discharge or, in extreme situations, disconnect the cell if the temperature exceeds acceptable levels. It is important to note that the safe working temperature range changes between the charging and discharging process.

To constrain the current rate, both during discharging and charging, the battery management algorithm must calculate, based on the measured voltage and temperature values, current limits. These values will be communicated to both the charger and the inverter to inform them what is the maximum current the battery is capable of delivering or receiving.

- **Overcurrent protection:** it protects the cell from excessive discharge or charge currents. In case of sudden overcurrent, the protection system must limit the current or disconnect the battery pack to avoid damage.
- **Short-circuit protection:** it identifies and prevents short circuits within a cell or battery pack, reducing potential hazardous conditions. Programmed resistance thresholds indicate normal cell operation. An indication of a possible short circuit occurs when the monitored resistance falls below certain predefined limits, indicating an unusually low level. In response, the battery management algorithm can isolate the affected cells from the rest of the battery system. Isolation can be achieved by opening a switch or disconnecting the cell to prevent the short circuit from involving other cells.

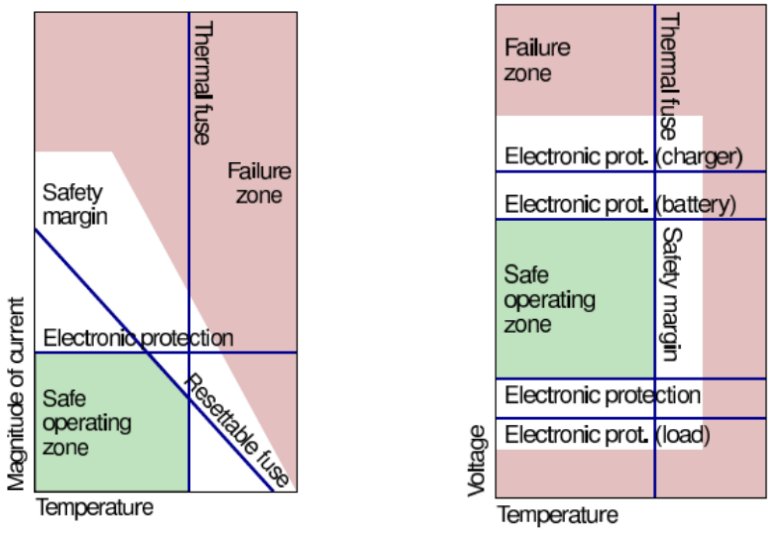

Figure 5.7: Protection: (a) Overcurrent/overtemperature; (b) Overvoltage/overtemperature [29]

5.3.3 State of Charge Estimation

The state of charge provides the driver information about the energy remaining in the energy storage system to power the vehicle before requiring a recharge. It provides a fundamental indication during operation. Because the accuracy and reliability of SOC estimation have a significant impact on vehicle performance and safety, several SOC estimation methods have been developed. Although some are based on cell chemistry, most are based on measurable variables that change with SOC, including battery voltage, current, and temperature.

Coulomb counting method

This method, also called current-based SOC estimation method, represents the most common approach for calculating the state of charge. Given an initial SOC_i, the SOC at time t can be determined by integrating the current with the following expression:

$$SOC(t) = SOC_i + \frac{\eta(i(t), T)}{C_{rated}(T)3600} \int i(t)\, dt \tag{5.1}$$

where $C_{rated}(T)$ is the rated capacity and depends on temperature, and $\eta(i(t), T)$ is the coulombic efficiency of the battery and depends on both the temperature and sign of the current (charge/discharge). The Coulomb counting method is simple and reliable, provided the following three conditions are met under operating conditions: the initial SOC point can be determined accurately, the current flowing through the battery can be measured accurately and the battery capacity can be obtained correctly in real time. Although widely used, this methodology faces some difficulties in automotive applications. As an open-loop estimation method, extended battery use can lead to inaccurate current measurements, introducing significant errors. In addition, the Coulomb counting approach neglects the self-discharge current, relying solely on external current flow. Another complexity arises from the intricate relationship between capacitance, Coulomb efficiency, temperature and age of the battery. As temperature increases, the capacity and efficiency of a battery may increase due to increased electrochemical activity, but this relationship is not linear. Operating temperatures below 10°C significantly affect battery performance. In addition, both capacity and coulombic efficiency decrease as the battery ages.

Kalman filter method

A Kalman filter provides a method of estimating the states of a linear dynamic system, while an Extended Kalman filter (EKF) can be used to estimate the states of a nonlinear system. From a system perspective, a battery system can be considered a nonlinear dynamic system. By correctly formulating the equation of state space and defining the state of charge as the state variable, the EKF technique can be employed to estimate the SOC. The EKF involves two equations. The first equation involves matrices constructed from the Equivalent Circuit Model (ECM) parameters, system state matrices, measurable input matrices, and unmeasurable process noise. The second equation is the measurement equation, which expresses the output voltage in terms of

system state vectors, measurable input matrices and measurable noise. In some EKF methods, an internal filter is established to fine-tune the SOC, while the battery model is adjusted by an external filter. The internal filter, based on the SOC and cell model, suggests a corresponding voltage using the measured current. The SOC is adjusted by comparing the measured voltage with the proposed voltage. As a result, the system feedback is the voltage and the output is the SOC. Over a long period of monitoring the applied current and voltage, the external filter gradually adjusts the system model parameters. With this method, cell aging and other life cycle effects are detected and modeled in real time. An accurate battery model must be established in order to obtain better results from the EKF method and the battery system must be treated as a nonlinear time-variant dynamic system. Most common models will be described in the Chapter 7 [30].

Neural network method

A Neural Network (NN) is a mathematical model, a sub field of artificial intelligence, composed of interconnected artificial neurons inspired by biological neural networks. Its purpose is to predict the output of a nonlinear system using past data from that system. Unlike the Extended Kalman Filter, neural network methods do not rely on physical, electrical, chemical or thermal models and take less time to generate results. NNs include inputs and outputs and are composed of numerous processing units, known as neurons, interconnected with each other. The accuracy of the neural network method depends on the extent to which the network is trained, making the training process a critical step in achieving accurate predictions. The most two common network architectures to estimate the SOC are the nonlinear input-output (NIO) feed-forward network and nonlinear autoregressive with exogenous input (NARX) feed-back network. Figure 5.8 shows the structure of a feed-forward neural network. To represent the input and

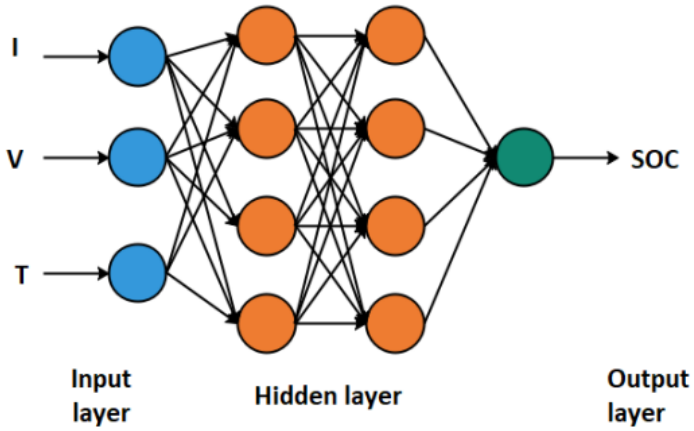

Figure 5.8: NN based SOC estimator

output variables, the neural network includes an input layer with nodes and an output layer, respectively. In addition, there are one or more hidden layers designed to capture the non-linearity between the input and output variables. The nodes between two adjacent layers are interconnected. Processing layers, which include activation functions

at each node, are present only in the output layer and hidden layers. There are various types of activation functions, such as sigmoid function, hyperbolic tangent and ReLU (Rectified Linear Units). In most scenarios, the hyperbolic tangent/sigmoid functions are used as activation functions for the hidden layer, while the linear transfer function is commonly used for the output layer. In regarding to the SOC estimation, the neural network method determines the SOC direct from the voltage, current and temperature. The constructive approach to SOC estimation on neural network involves the following steps:

1. Initialization; determine the size of the input layer and the number of neurons in the hidden layer.
2. Train the neural network using the input (current, voltage, temperature) and output (SOC) variables.
3. Calculate the error between the estimated output and the output obtained from the actual inputs.
4. If the error is within the expected level, the search is finished; otherwise, repeat Step 2.

Since the current, terminal voltage and temperature have the greatest influence on the SOC of the battery, these three parameters are chosen as the input of the network.

5.3.4 Thermal Management

As discussed extensively above, the individual cells in a battery pack must operate, both when charging and discharging, within a safe and well-defined temperature range. A battery thermal management system must then ensure safe and efficient operation by regulating temperature conditions. It has to controls the operating temperature of the cells by either dissipating heat when it is too hot or providing heat when it is too cold.

Cooling system management

The cooling system can be implemented in three different ways: equipped with a forced ventilation system, which allows air exchange between the interior of the battery pack and the external environment, with air cooling system inside the pack or with liquid cooling system inside the pack.

Heating system management

The battery can be warmed by an electric heater. An example of an electric battery heater is the Positive Temperature Coefficient (PTC) heater. The heating element of a PTC heater has a positive temperature coefficient, so its resistance increases with increasing temperature. When current is initially applied to the cold PTC heater element, it has a low resistance and absorbs a considerable current. When it heats up, the resistance increases, reducing the current draw. This inherent characteristic makes PTC heaters safe and efficient. If a PTC heater overheats, it automatically

stops absorbing current and absorbs only the current necessary to maintain the desired temperature. In addition, PTC heaters heat up faster than conventional elements because they take the maximum current when they are cold. An IGBT or other high-current power device is used to turn the heater on and off, while voltage and current sensors monitor the input voltage and current absorption.

5.3.5 Cell Balancing

Cell imbalance is a crucial factor in large battery packs, which contributes to the degradation of battery performance by affecting its State of Health (SoH). Deviations in cell behavior typically result from two phenomena: alterations in internal impedance or reduction in cell capacity due to aging. In either scenario, if a single cell within a battery pack exhibits deviant behavior, it becomes susceptible to overvoltage during high-power charging events. Cells with low capacity or high internal impedance are subject to significant voltage fluctuations during charging and discharging. To address this issue, both active and passive cell balancing technique must be used in electric vehicles to mitigate voltage imbalances and ensure that the battery pack operates safely and efficiently.

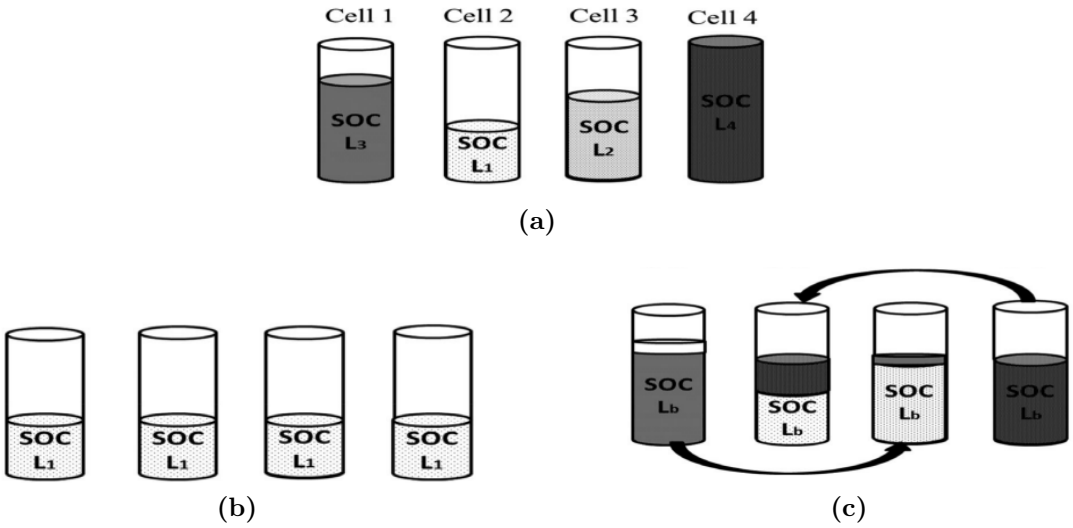

Figure 5.9: (a) Without balancing; (b) Passive balancing; (c) Active balancing

Passive Balancing

This approach employs resistors in a balancing circuit to equalize the voltage of each cell by dissipating energy from cells with higher voltage, ensuring that the overall cell voltages align with the lower voltage. This technique can be classified into fixed shunt resistor and switchable shunt resistor. The latter is commonly used for the Li-ion battery balancing circuit being more reliable than the former. Despite the simplicity of control and implementation, this balancing method generates energy losses due to the high currents flowing through the switches and resistors. For this reason, it can be used

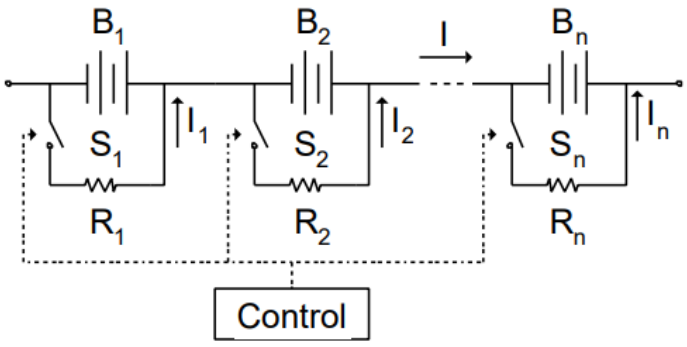

Figure 5.10: Switched resistor method

for low-power applications, with a balance current of less than 10 mA per Ah of cell capacity.

Active Balancing

Active cell balancing methods use an active charge-shuttling element or voltage/current converters to transfer energy from one cell to another. These devices can be controlled analogically or digitally. The main classifications of active cell balancing methods include charge shuttling and energy converting [31].
Charge-shuttling cell balancing mechanisms involve a device that extracts charge from a designated cell, stores it, and then transfers it to another cell. There are various charge transfer schemes, among which the "flying capacitor" is prominent. A variant of the "flying capacitor" method involves intelligent selection of the cells to be balanced. By charging the capacitor from the highest cell and selectively discharging it to the lowest cell, this approach significantly reduces the time required to balance cells, especially when the most charged and most discharged cells are placed at opposite ends of the module. Additional checks are needed to locate and select target cells. This method

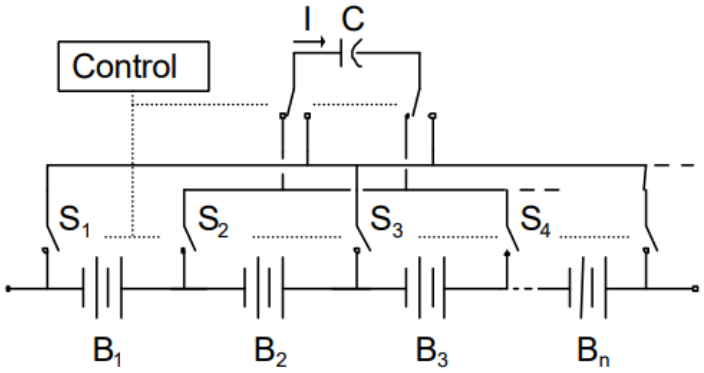

Figure 5.11: Flying capacitor method

requires a large number of switches (N + 2) with N representing the number of cells and only one capacitor. To simplify control, a single capacitor can be used for each

two cells. In this configuration, the capacitor constantly switches between the two cells, facilitating the exchange of charge from the cell with the higher charge to the cell with the lower charge. However, this method requires a considerable amount of time to transfer charge between cells with different charge levels, especially if these cells are placed at opposite ends of the module. This is due to the need to pass the charge through all the cells, resulting in loss of time and efficiency.
Balancing cells through the use of energy conversion devices involves the utilization of inductors or transformers to transfer energy from one cell or group of cells to another cell or group of cells. Two active energy converter methods include the switched transformer and the shared transformer. The switched transformer method shares the same switching topology as the flying capacitor method (figure 5.12). This approach

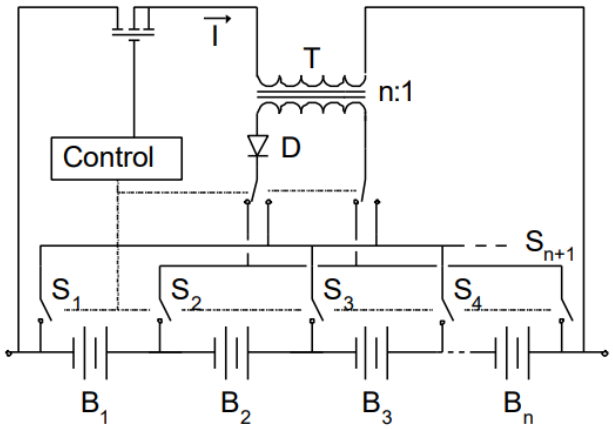

Figure 5.12: Switched transformer method

allows rapid balancing of the lower cells, but at the expense of energy extraction from the entire battery pack. Disadvantages include high complexity, a large number of control components (relays and switches), and reduced efficiency due to switching and magnetic losses. The shared transformer, on the other hand, employs a single magnetic core with designated secondaries for each cell. Current from the cell stack is directed into the primary of the transformer, inducing currents in each of the secondaries. The secondary with the lowest reactance is the one with the highest induced current. As a result, each cell receives a charging current inversely proportional to its relative state of charge. The shared transformer can effectively balance a multi-cell pack with minimal losses. However, the balancing circuit must be designed for the maximum number of cells expected, and the addition of additional secondary taps may not be easily achievable.

Chapter 6

Software Implementation

This chapter is going to provide an overview of the software and strategies implemented to meet the requirements outlined in Chapter 5. Each task will be described in detail, offering an in-depth analysis of the rationale behind the decisions made to meet the specified requirements.

6.1 Powertrain Management Implementation

As discussed earlier, the final goal of the powertrain management algorithm is to determine the value of the requested torque to be sent to the inverter. This value will be a function of the throttle, brake, speed, and overall state of the vehicle.

6.1.1 Finite State Machine

The best way to express the current state of the vehicle is to use a Finite State Machine (FSM). It must be deterministic, which means that the vehicle can only be in one specific state at a time and that only one transition from one state to another will be possible at the same time. The FSM is characterized in each state by input and output variables, the latter of which are used to determine the final torque request and to possibly activate certain subsystems. The FSM logic is illustrated in the flowchart in figure 6.1.
In the LabVIEW environment, a case structure was used to implement a finite-state machine, in which it is possible to switch from one state to another based on the input condition.

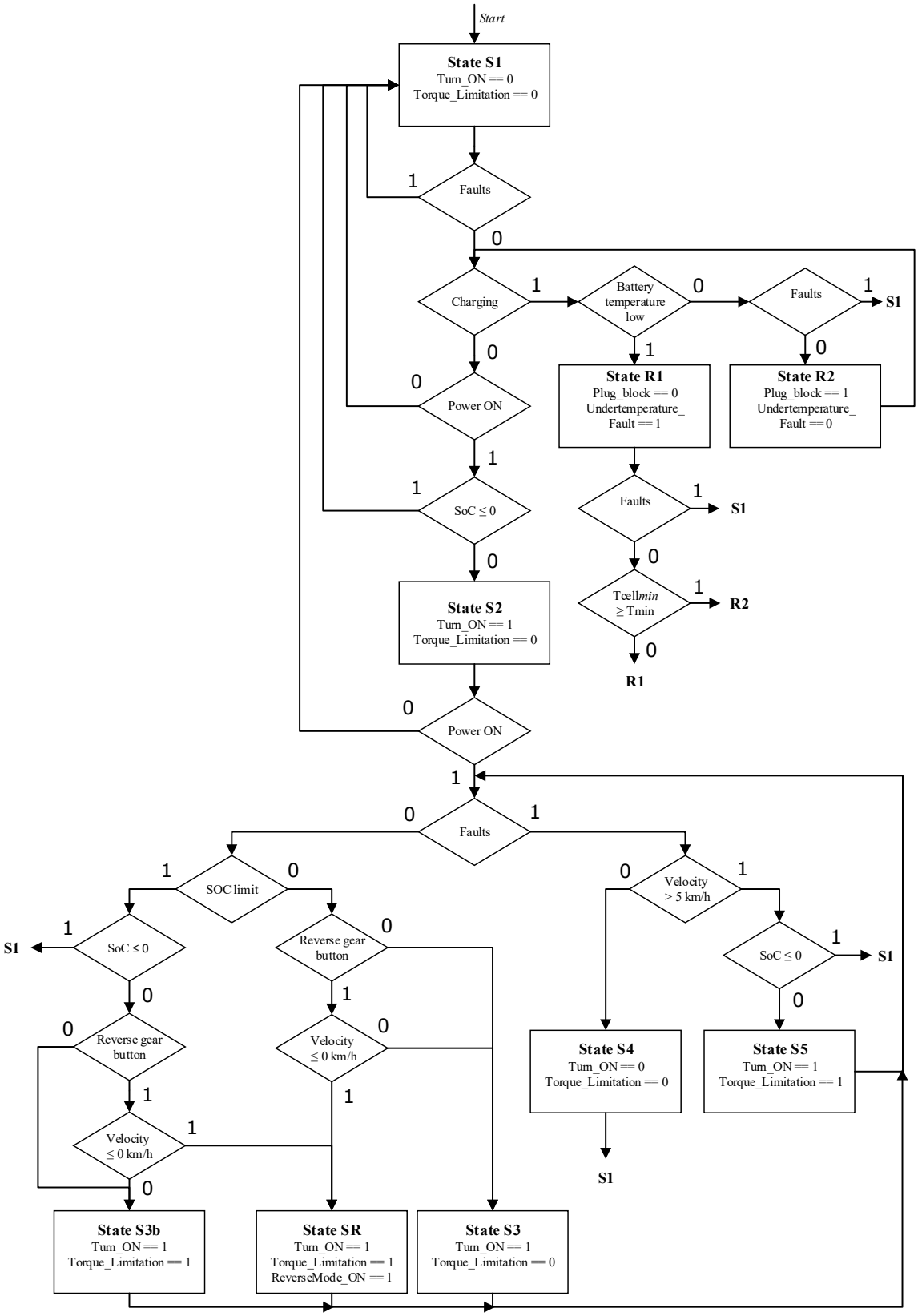

Figure 6.1: FSM flow chart

State S1

This state is the default state of the system, activated by the other states in the event of a critical fault leading to a potential vehicle shutdown or when the battery reaches a low charge level. Output boolean variables are set as follows:

- $Turn\_ON == False$; expresses if the vehicle is ready to deliver power, which means that the motor can deliver any amount of torque above 0.
- $Plug\_Block == False$; plug lock signal to start the charging process.
- $ReverseMode\_ON == False$; reverse gear engagement signal.
- $Undertemperature\_Fault == False$
- $TimeLogic\_Flag == True$; signal to avoid calculation of the requested torque.
- $Torque\_Limitation == False$; no maximum torque limitation is present.

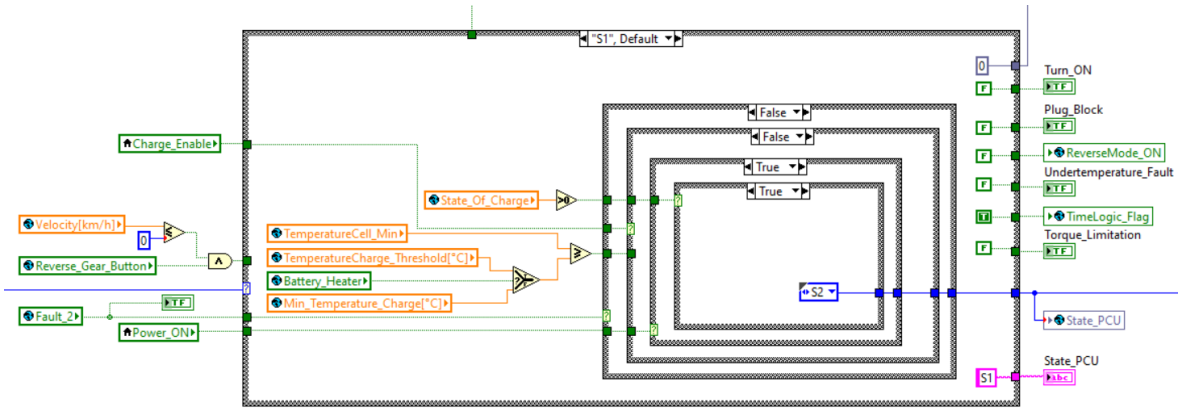

Figure 6.2: State S1

State R1

State that indicates when the battery needs to be recharged, but you cannot proceed because $TemperatureCell\_Min < MinTemperature\_Charge$. Where the first variable indicates the minimum temperature among all battery cells and the second the minimum temperature allowed during the charging process. The state R1 can be triggered by the state S1 with the condition:

$$Fault\_2 == False \quad \&\& \quad Charge\_Enable == True \quad \&\& \\ TemperatureCell\_Min \geq MinTemperature\_Charge$$

The $Charge\_Enable$ and $Fault\_2$ signals are set in a previous subVI. In this state, the fault $Undertemperature\_Fault$ is set and will be handled by the battery management algorithm. The other variables are configured as in S1. This state allows transition to R2 only when the temperature-related safety condition is confirmed or to S1 if a fault occurs during the battery heater action.

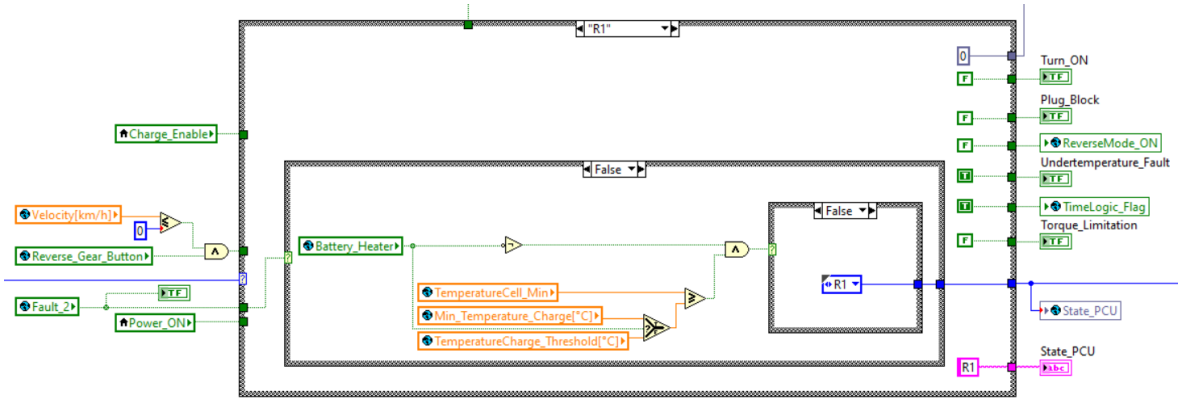

Figure 6.3: State R1

State R2

State of the vehicle charging phase. Here, the charging socket lock signal is activated ($Plug\_Block == True$). The conditions for switching from R2 to other states are:

- To enter S1, a fault must be detected or the battery state of charge must be zero. It is possible to enter even if the $Power\_ON$ signal is not verified, although there are no faults and charging is successful.
- Transition to R1 occurs only if, during the charging phase, the temperature-related safety condition fails.
- To enter S2, you must have the following variables set as follows: $Charge\_Enable == False$, $Power\_ON == True$, $State\_Of\_Charge > 0$.

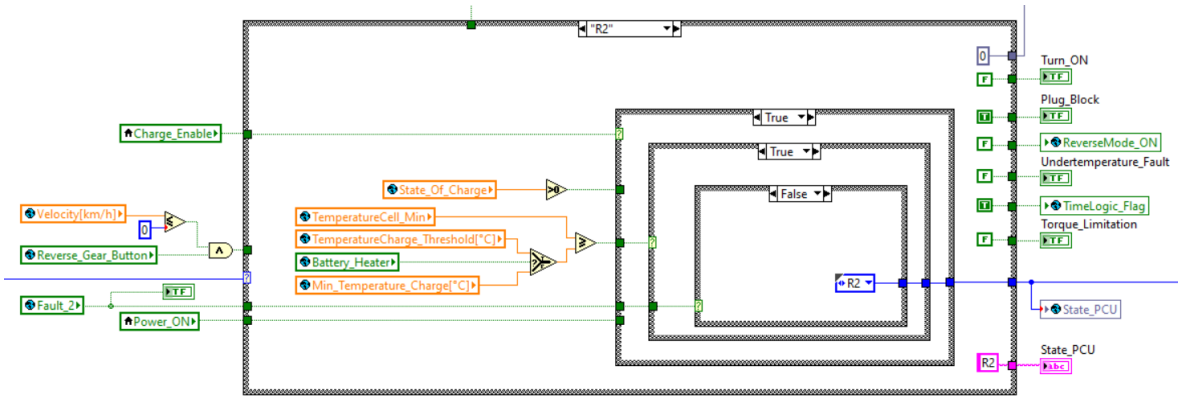

Figure 6.4: State R2

State S2

It is a transition state; this state is not visible in the indicator during the execution of the algorithm. It is used to distinguish S1 and S3 states. The triggered signal is:

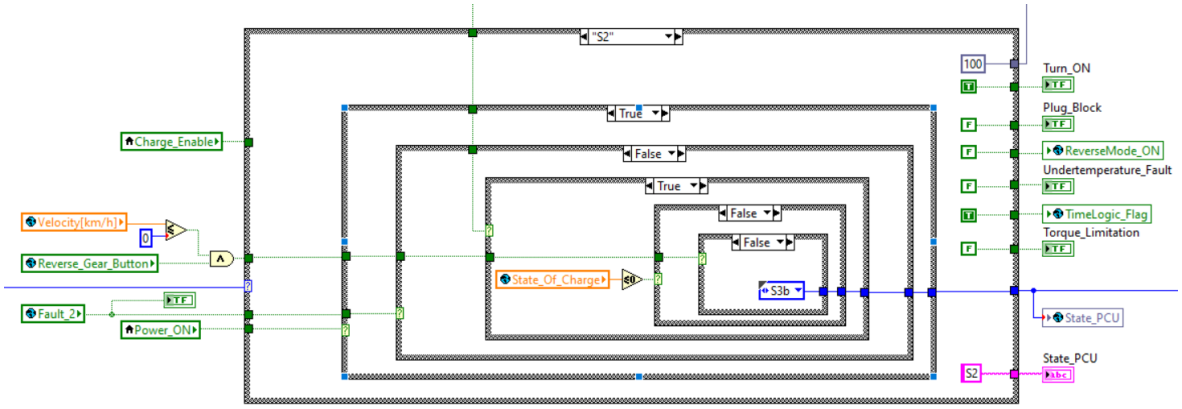

Figure 6.5: State S2

$Turn\_ON == True$.
Unlike S1, in this state the vehicle is powered, but there is no torque request. All states except R1 and R2 can be accessed from S2, as can be seen from the code below.

```
if(Power_ON == 0) {
    State_PCU = S1;
} else {
    if(Fault_2 == 1) {
        if(Velocity[km/h] > 5) {
            if(State_Of_Charge <= 0)
                State_PCU = S1;
            else
                State_PCU = S5;
        } else
            State_PCU = S4;
    } else {
        if(SOC_Alarm == 1) {
            if(State_Of_Charge <= 0)
                State_PCU = S1;
            else {
                if(Reverse_Gear_Button == 1 && Velocity[km/h] <= 0)
                    State_PCU = SR;
                else
                    State_PCU = S3b;
            }
        } else {
            if(Reverse_Gear_Button == 1 && Velocity[km/h] <= 0)
                    State_PCU = SR;
                else
                    State_PCU = S3;
        }
    }
}
```

State S3

The S3 state is critical for vehicle operation. Used during the motoring, coasting and braking phases under normal operating conditions. In this state, the VCU processes analog signals from the throttle and brake pedals, computing the torque request to be transmitted to the inverter ($TimeLogic\_Flag == False$). In this case, there is no torque limitation except that given by excessive speed and temperature. All states except R1, R2 and S2 can be reached.

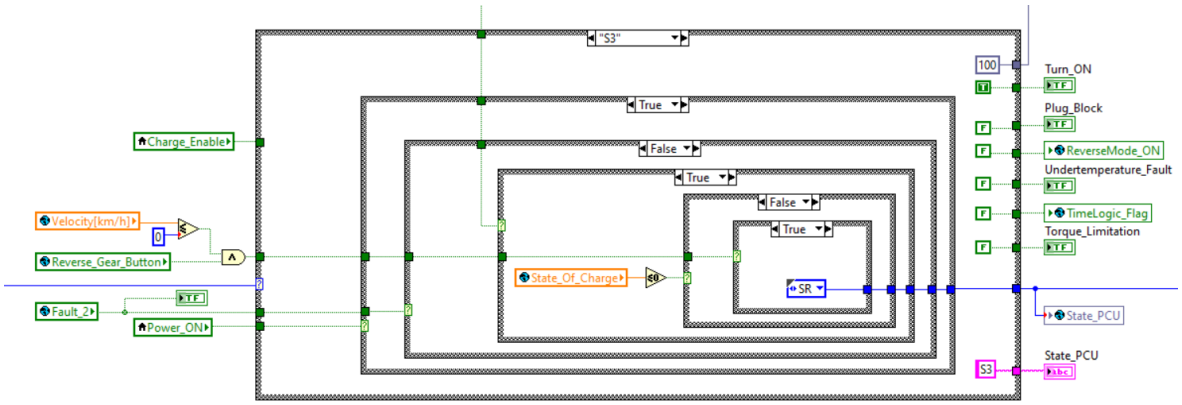

Figure 6.6: State S3

State S3b

The S3b state is a modified version of S3, representing a energy-saving state. Here, a maximum torque limitation is imposed due to the charge state falling below a specific threshold ($Torque\_Limitation == True$). This limitation ($Torque\_Max\_SOC[\%Nm]$) was set at 50% of the maximum value.

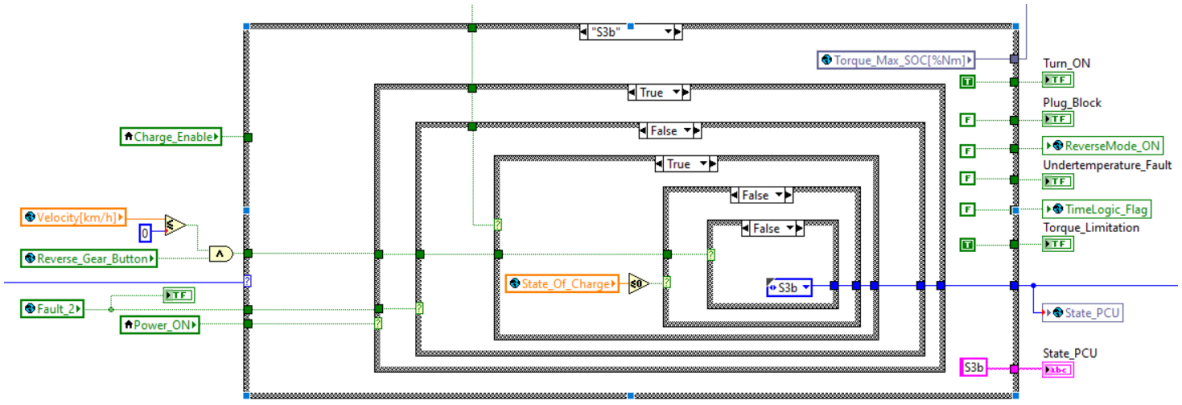

Figure 6.7: State S3b

State SR

Similar to S3, this state is used for reverse gearing ($ReverseMode\_ON == True$). The requested torque is calculated using a different curve from that used in the forward phase. To switch to SR instead of S3, as we have already seen, it is necessary to check the following condition: $Velocity[km/h] <= 0 \quad \&\& \quad Reverse\_Gear\_Button == True$. Also in SR, all states except R1, R2 and S2 can be reached.

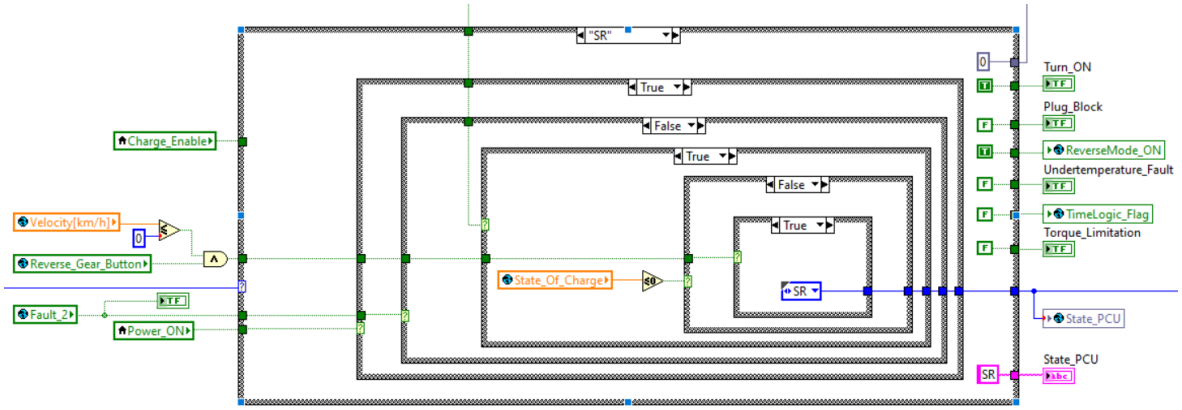

Figure 6.8: State SR

State S4

It is the second transition state present in the FSM. It is the transition state that allows the VCU to project directly to the default state S1. It occurs whenever a fault is present while the vehicle is running and the speed is less than 5 km/h; therefore, the vehicle can be shut down and stopped.

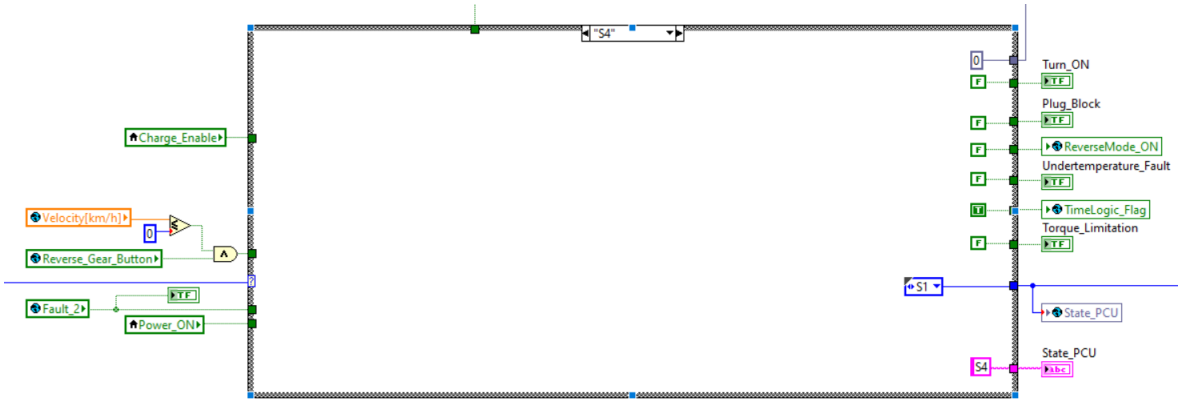

Figure 6.9: State S4

State S5

In the event of a fault, while the vehicle is running at a speed greater than 5 km/h, it can enter S1 if the state of charge is zero; otherwise, it enters the S5 state. In this state the torque limitation is active ($Torque\_Limitation == True$) and is defined as 5% of the maximum torque ($Torque\_Max\_Faults[\%Nm]$). All possible states except R1, R2 and S2 can be reached directly from S5.

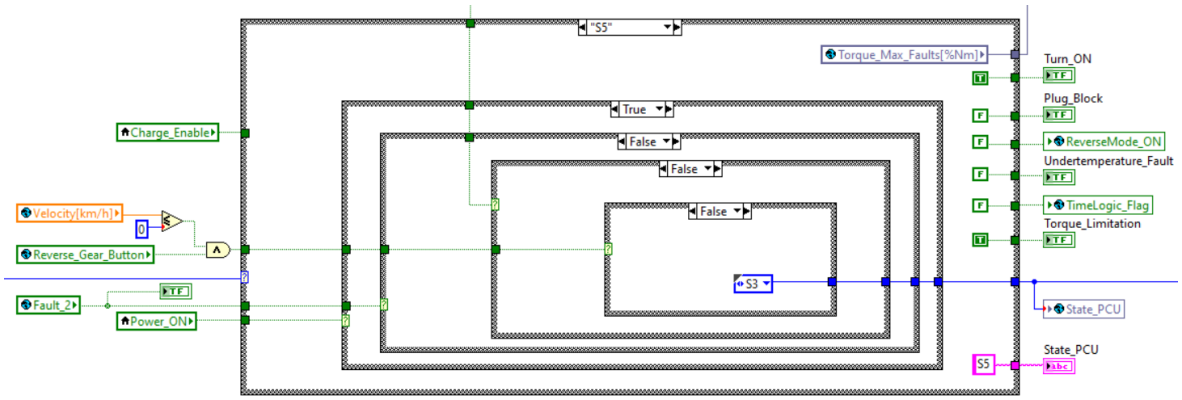

Figure 6.10: State S5

As seen in the previous figures, each state sets a specific restriction on the maximum deliverable torque. When the limit is equal to 100, there is no constraint on the maximum torque. However, these are not the only limitations of the system, as the FSM operates simultaneously with other continuously active torque limiting algorithms.

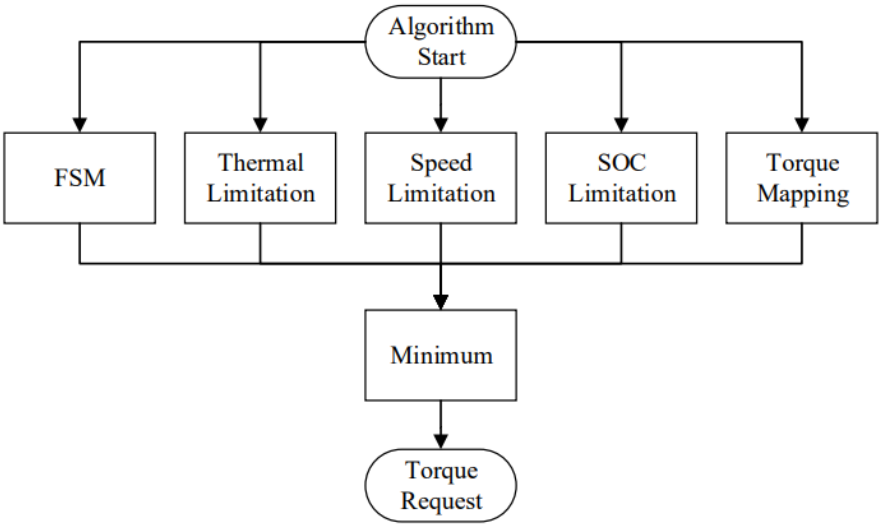

Figure 6.11: Torque limitation procedure

6.1.2 Throttle-Torque Mapping

Under normal vehicle operating conditions, in the absence of faults and when torque is not limited by any of the other limiting subVIs, the relationship between throttle and torque is expressed as a function of current vehicle speed. As seen in the requirements analysis chapter, the profile is divided into three regions. The scheme discussed above and illustrated in figure 5.2 is implemented in the following sections, analyzing one profile at a time.

Acceleration profile

During the acceleration phase, the torque request is determined by the curves shown in the figure 6.12. When the throttle pedal is fully depressed, the torque is always the maximum that can be requested (T_{max}), so all the lines must intersect at the point (100%, T_{max}). The other point of each line is its intersection with the torque axis (T_i). T_i is a function of vehicle speed (v) according to the following relationships:

$$T_i = T_c - Kv \tag{6.1}$$

$$K = \frac{T_c - Torque\_0}{v_{max}} \tag{6.2}$$

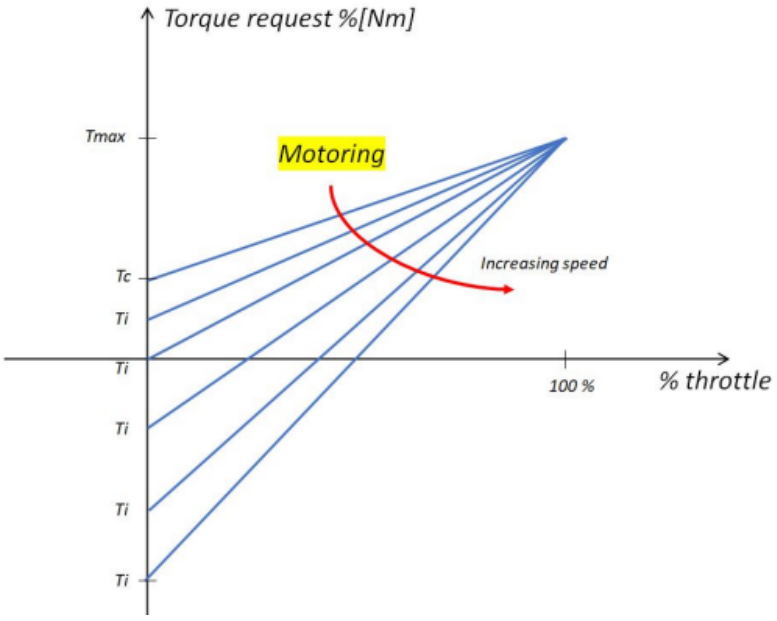

Figure 6.12: Acceleration profiles

$$v_{lim} = \frac{D \cdot T_{max} + T_c}{K(1 - D)} \tag{6.3}$$

where K defines the sensitivity of the accelerator, indicating how hard it must be depressed to reach a given speed. Small values of K imply that slight pedal movement results in significant acceleration, and vice versa. The limit velocity is the velocity that

the vehicle can reach under ideal conditions with a certain displacement of the throttle pedal. The creep torque (T_c) represents the maximum value of T_i and is reached at 0 km/h, the minimum speed within the acceleration profile. For this project, the speed is limited to the range between 0 km/h and 100 km/h, so K is set equal to 1.

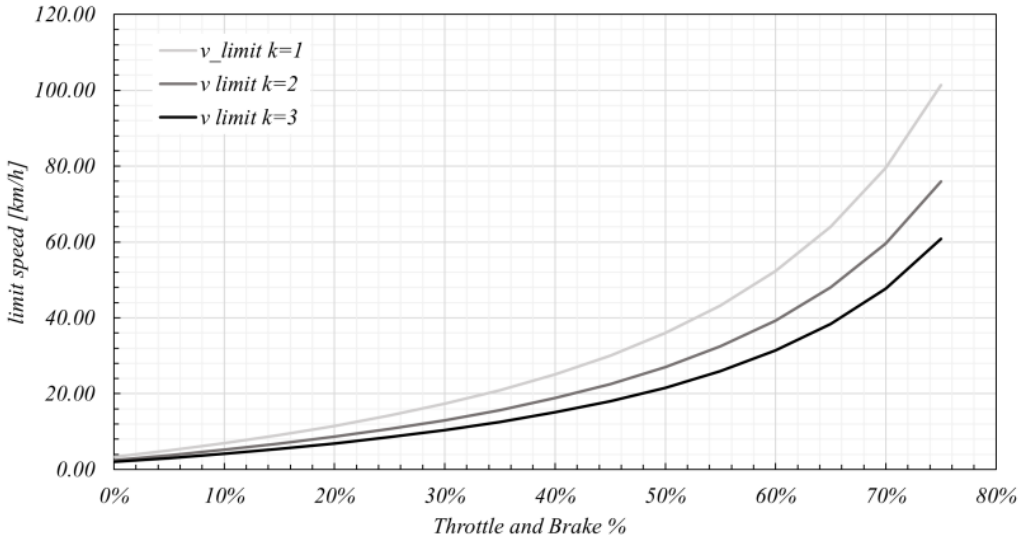

Figure 6.13: Limit velocity for different K; $T_{max} = 88Nm$, $T_c = 10\%Nm$

Having chosen K, the requested torque T_{req} is calculated using the equation of the line passing through T_{max} and T_i:

$$T_{req} = \begin{cases} T_i + D(T_{max} - T_i) & \text{if } T_{fb} \geq 0 \\ 0 & \text{if } T_{fb} < 0 \end{cases} \tag{6.4}$$

where:

$$D = \frac{\%throttle}{100} \tag{6.5}$$

is the displacement of the throttle pedal. T_{fb} is the torque requested at the previous iteration ($T_{req}(t-1)$) and is used to detect whether the torque is greater than 0. Otherwise, the algorithm would compute negative values.
Torque request decreases with increasing speed for the same amount of throttle pedal pressure. This behavior is consistent with the characteristics of the electric motor. In this project, only the constant-torque region of the real motor graph, figure 5.4, was considered, so all lines intersect at T_{max}.

The $Torque\_Profile$ subVI, which handles the throttle mapping, processes the following inputs:

- $Turn\_ON$ and $ReverseMode\_ON$, outputs of the FSM, which must be true and false, respectively, to enable forward torque computation.
- $Torque\_Max$, T_creep, T_0 and other constant parameters needed to calculate the requested torque. T_{fb} to compute if the algorithm should use the acceleration profile or the coasting one.

- $Brake[\%]$ and $Throttle[\%]$, values of the accelerator and brake pedal, respectively.
- Parameters to check whether the brake has been applied, thus disabling torque generation to avoid the simultaneous occurrence of non-zero acceleration and braking parameters. In the standard torque calculation procedure, the brake always takes priority over the throttle, setting it to 0 when activated.

To prevent small unintended movements of the brake pedal from deactivating torque generation, a small hysteresis block is added. As a result, a minimum threshold of 7% must be exceeded for torque deactivation to occur. The threshold is subsequently reduced to 2% to allow torque demand when the brake pedal is fully released. The transition between the two thresholds is triggered by the variable $Brake\_ON(t-1)$ indicating the value of the last braking cycle.

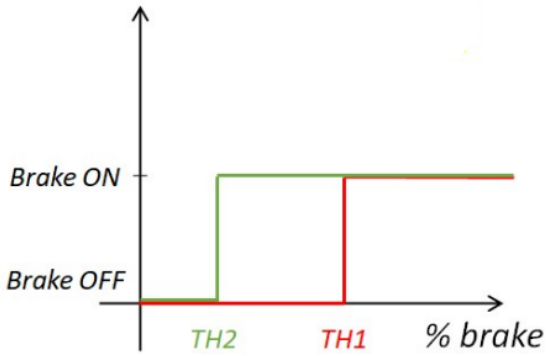

Figure 6.14: Brake hysteresis

Coasting profile

During coasting, when the throttle pedal is released, the system is designed to recharge the battery by generating regenerative negative torque. Coasting curves cannot be a continuation of motoring curves because, otherwise, the negative torque would be too high and cause severe shocks to the vehicle. Therefore, new straight lines passing through the points (100%, T_{max}) and (0%, T_0) are identified to have a smoother ride. The equation identifying the torque curves of the coasting phase is:

$$T_{req} = \begin{cases} T_0 + D(T'_{max} - T_0) & \text{if } T_{fb} < 0 \\ 0 & \text{if } T_{fb} \geq 0 \end{cases} \tag{6.6}$$

where:

– T'_{max} is a value with no physical meaning, used as a mathematical construct. To avoid abrupt movements of the vehicle during the transition from motoring to coasting, the two profiles must coincide, for each speed, when $T_{req} = 0$. By equating the value of D in equations 6.4 and 6.6, the value of T'_{max} can be determined as follows:

$$T'_{max} = \frac{(T_{max} - T_i)T_0}{T_i} + T_0 \tag{6.7}$$

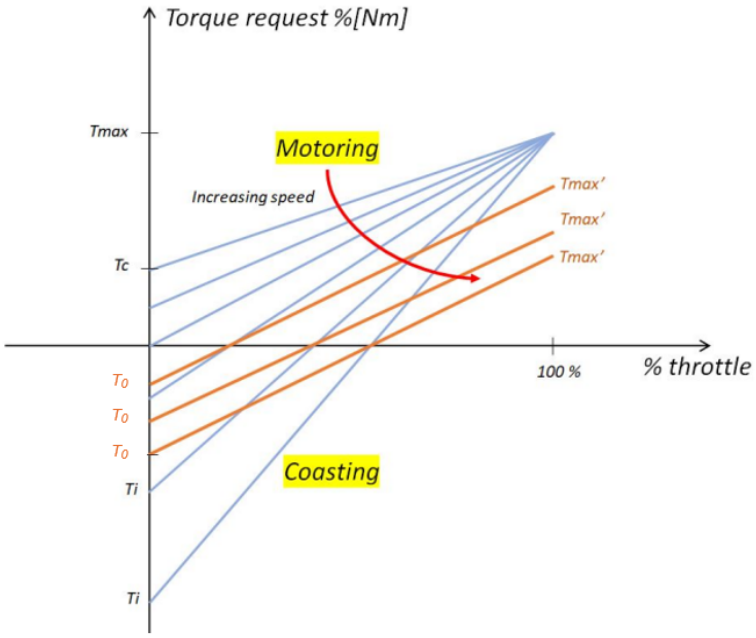

Figure 6.15: Coasting profiles

– T_0 represents the maximum negative torque that can be required at a specific speed during coasting phase and with 0% throttle/brake. As shown in figure 6.16, its magnitude is influenced not only by the speed but also by the driving mode chosen.

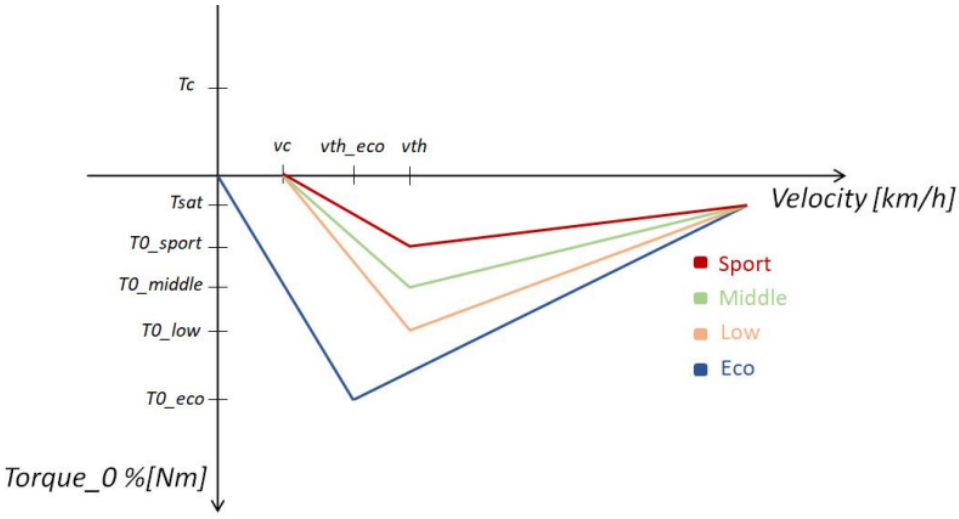

Figure 6.16: T_0 profiles

The selection of driving mode affects not only the maximum negative torque, but also the creep torque, as shown in the table below. The T_0 profile, as a function of speed, has a first increasing phase in modulus followed by a second decreasing phase. The

Mode	Torque_0	$\mathbf{T_{creep}}$	Velocity_threshold
ECO	$T0\_eco = T_{min}$	0	12 km/h
LOW	$T0\_low = 0.8 \cdot T_{min}$	T_c	25 km/h
MIDDLE	$T0\_middle = 0.6 \cdot T_{min}$	T_c	25 km/h
SPORT	$T0\_sport = 0.5 \cdot T_{min}$	T_c	25 km/h

Table 6.1: Driving modes parameters

minimum T_0 value ($Torque\_0$) for each mode is defined with respect to the minimum available torque T_{min}. To calculate the values of T_0, another function is needed. As stated in the requirements analysis, the coasting torque must be small for both low and high speeds, resulting in the following behavior:

$$T_0 = \begin{cases} \dfrac{v - v_c}{v_{th} - v_c}(Torque\_0 - T_c) + T_c & \text{if } v \leq v_{th} \\ \dfrac{v - v_{th}}{v_{max} - v_{th}}(T_{sat} - Torque\_0) + Torque\_0 & \text{if } v > v_{th} \end{cases} \tag{6.8}$$

v_c is the creep-off velocity, set at 5 km/h. v_{th}, which depends on the driving mode, is the threshold velocity at which T_0 begins to decrease and as such is also the speed at which maximum regenerative torque can be obtained. T_{sat} represents the saturation torque and is reached at maximum velocity. It allows the vehicle to slow down and pass on curves with higher regenerative torques.
This function is implemented in a dedicate subVI called $Torque\_0$.

Braking profile

During the braking phase, the system is designed to generate regenerative torque. As mentioned above, this phase takes precedence over the previous two. A braking variable, $Brake\_ON(t)$, has been defined to instantaneously interrupt the torque request while driving or coasting as soon as the brake pedal is pressed sufficiently. The equations governing these profiles are simpler because braking torque does not depend on speed:

$$T_{req} = T_{fb} + B(T_{min} - T_{fb}) \tag{6.9}$$

where:

$$B = \frac{\%brake}{100} \tag{6.10}$$

is the displacement of the brake pedal. T_{min} is the minimum negative torque that the motor can apply to stop the car and is a fixed value set at 60% of maximum available torque. The only variable value is T_{fb}, torque computed in the previous cycle, which is used as the starting point of the braking profile. If this value is not lower than 0, brake activation will be mapped with $T_{fb} = 0$, as shown in the figure 6.17.

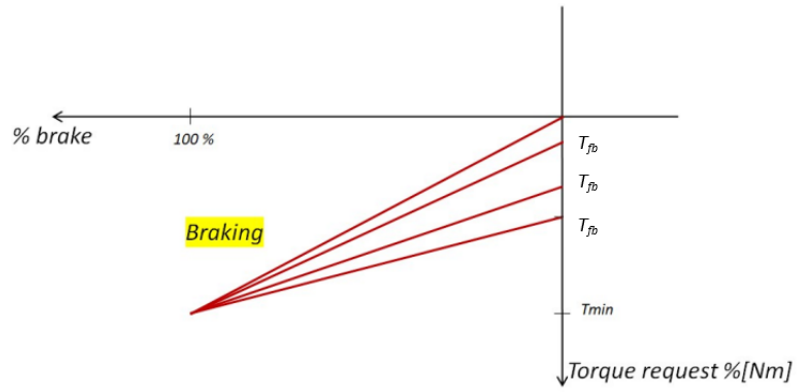

Figure 6.17: Braking profile

Reversing profile

In the reverse gear state, the throttle pedal mapping used during the acceleration phase is switched to a new mapping. For the design of torque curves, the following requirements are identified:

- As stated in the requirements chapter, the vehicle speed is between 0 km/h and -20 km/h; the minus sign indicates that the vehicle is moving in the opposite direction of forward motion.
- The creep torque T_c is set to -10%Nm. The creep torque defined here differs from that in the previous paragraphs in that it refers to reverse creep torque.
- Useful torque is negative, positive torque is used for coasting phase.

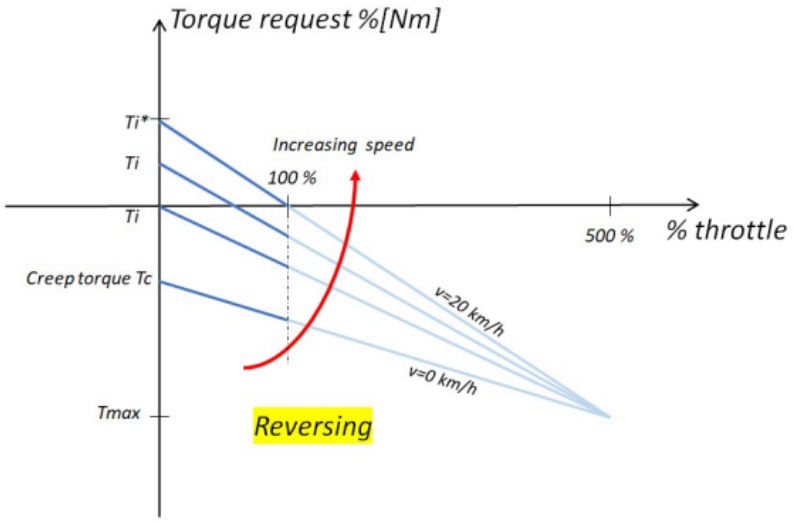

Figure 6.18: Reversing profile

The vehicle always starts reversing at the speed of 0 km/h. The generated torque is negative and decreases in modulus with increasing speed as can be seen in figure 6.18. For speeds above 10 km/h, coasting can be initiated by releasing the throttle pedal. During this phase, the torque generated is positive and causes the car to decelerate to a minimum speed characterized by zero torque. Afterwards, brake application becomes necessary to bring the vehicle to a complete stop. The torque profiles are approximated by linear functions, and the equation representing them is as follows:

$$T_{req} = T_i - \frac{\%throttle}{500}(T_i - T_{max}) \tag{6.11}$$

where:

- $T_{max} = -40\%Nm$; represents the theoretical maximum reverse torque. Although this value is unattainable, it serves as a convergence point for torque profiles at different speeds. The hypothetical throttle value for generating this torque is 500%. This quantity is obtained by inverting the following equation:

$$T_{max} = T_i^* - \frac{\%throttle}{100}T_i^* \tag{6.12}$$

  with $T_i^* = 10\%Nm$, that is the maximum torque value provided at a speed of -20 km/h when the throttle pedal is at 0%.

- T_i represents the torque value obtained when the throttle pedal is not pushed. Its values are distributed between -10%Nm and 10%Nm and depend on the reverse speed. It is computed as follows:

$$T_i = T_i^* - \frac{(T_i^* \cdot v_{max}) - (T_i^* \cdot v) - (T_c \cdot v_{max}) + (T_c \cdot v)}{v_{max}} \tag{6.13}$$

As with the forward driving phase, braking takes priority over acceleration in the reverse driving phase. As we have seen for throttle mapping, the reverse gear algorithm is also implemented in the $Torque\_Profile$ subVI.

6.1.3 Torque Limitation Functions

As shown in figure 6.11, several functions monitor various vehicle parameters during operation and generate a torque limitation if the corresponding conditions are met. Torque limiting values can result from the following conditions:

- An increase in shaft speed.
- An increase in motor temperature.
- Presence of a fault or low state of charge.

Since the torque limitation values can vary in different subVIs, the algorithm employs a dedicated subVI, called $Min\_Computation$, to select the smallest limitation among them, providing the final output.

Speed limitation

This limitation is implemented to reduce torque in relation to motor speed, considering the original speed of the vehicle. A second-order polynomial, passing through three specific points, is used to establish the speed limit for each torque value in the range from 0 Nm to 88 Nm. The points chosen for interpolation, carried out in *Torque_Speed_Limitation* subVI, are:

- p1(1700 rpm, 88 Nm): maximum speed attainable with maximum torque. This value is set lower than the value given in the motor data sheet to ensure a robust safety margin.
- p2(2000 rpm, 44 Nm): maximum speed value that can be reached with the rated torque. Again, the value is slightly lower than that given in the data sheet.
- p3(2500 rpm, 0 Nm): maximum motor speed value, in accordance with the maximum linear speed set for this project, of 100km/h.

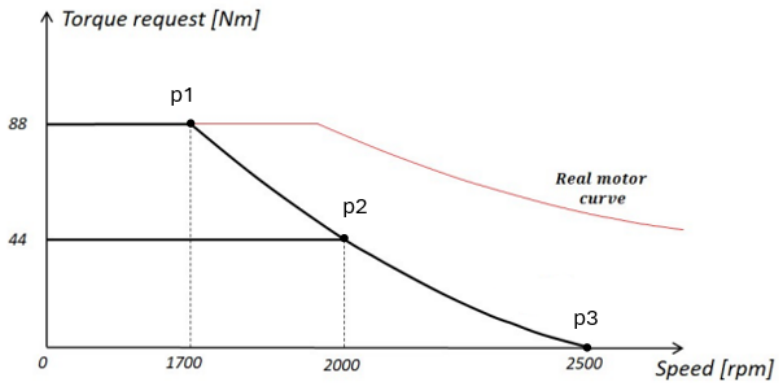

Figure 6.19: Torque-speed limitation

The expression of the obtained polynomial, after calculating the coefficients thanks to a polynomial fit, is:

$$T_{speed\_limit} = 7.33 \cdot 10^{-5}\omega_{rpm}^2 - 0.418\omega_{rpm} + 586.8 \tag{6.14}$$

Limits for all other speed values are derived accordingly.

Thermal limitation

This limitation is activated when the motor produces more than its rated torque and reaches the critical operating temperature. As specified in the data sheet, the motor under consideration belongs to a type F insulation class, which indicates that its components can maintain its performance up to a maximum temperature of 155°C. Therefore, it is essential to reduce the torque to the rated level as the temperature increases to avoid overheating, which could damage the motor. In general, the stator

windings are the hottest area of the motor; however, because the temperature sensors are distant from these components, it is prudent to set a maximum operating temperature slightly below 155°C. So, a linear temperature limitation is implemented with the following relations:

$$T_{temp\_limit} = \begin{cases} T_{max} & \text{if } T < T_{th1} \\ T_{max} - \dfrac{T_{max} - T_{max\_cont}}{T_{th2} - T_{th1}}(T - T_{th1}) & \text{if } T_{th1} \leq T \leq T_{th2} \\ T_{max\_cont} & \text{if } T > T_{th2} \\ 0.05 T_{max} & \text{if } T > T_{fault} \end{cases} \tag{6.15}$$

T represents the motor temperature, and T_{th1} and T_{th2} the two thresholds set at 105°C and 120°C, respectively. For temperatures below T_{th1}, the available torque is the maximum one. Between T_{th1} and T_{th2}, the torque decreases linearly until it reaches T_{max_cont}, which is 44 Nm. For higher temperatures than T_{th2}, the motor can continuously apply the rated torque. If the temperature continues to rise, reaching the limit value (T_{fault}), the torque is set to 4.4 Nm, triggering the *Motor_Overtemperature_Fault* error variable to prevent thermal failure.

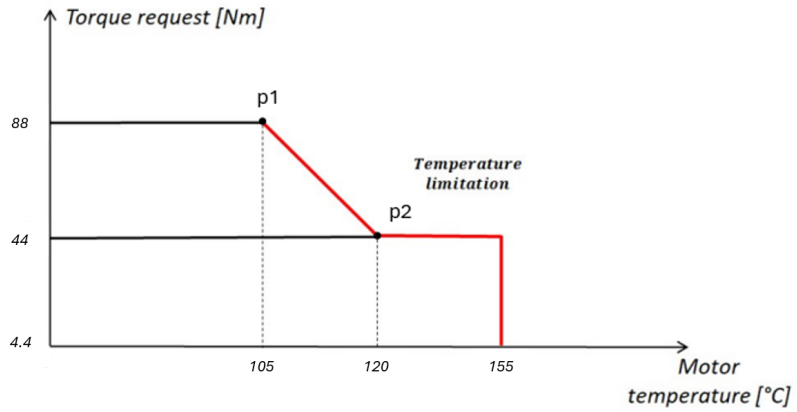

Figure 6.20: Torque-temperature limitation

The described function is implemented in a dedicated subVI, *Thermal_Limitation*, and determines the maximum available torque based on the measured motor temperature. The final value is then proportional to the maximum torque T_{max}, since, as seen in the previous sections, all torque values within the algorithm are expressed as a percentage ratio between the two.

FSM torque limitation

As explained in section 6.1.1, FSM is used to generate torque limits depending on the current state of the vehicle.

The first limitation that the state machine imposes is that due to a low state of charge. When the state of charge of the battery falls below a certain value (20%), an

automatic Boolean signal, SOC_Alarm, is generated. This signal is used to limit the maximum deliverable torque. The mechanism for triggering the Boolean low-charge warning signal involves a hysteresis loop. SOC_Alarm is set to true when the SOC falls below a specific threshold, and returns to false when the SOC exceeds another threshold, higher than the initial one (30%). This approach was implemented to prevent the alarm from going off due to a simple regenerative braking or coasting phase.

The second, more stringent limitation arises from the occurrence of a fault. As stated in the FSM description, the maximum torque limit value is set to 0 only if the fault occurs at a speed below a certain threshold. If the speed is too high, the maximum torque is set to a very low value to allow the driver to perform a safety maneuver followed by a subsequent stop.

6.1.4 Enabling Charging and Startup

The $Charge\_Enable$ subVI, is the one that handles the charging enable and startup phase. This subVI cooperates with the battery management algorithm, receiving the estimated state of charge value and monitored voltage values. About charging, the vehicle can be recharged when the following conditions are simultaneously met:

1. $SOC < 90\%$; the state of charge of the vehicle is less than 90%. During the charging process, this control persists and the 90% value is replaced by the 100% value to allow the battery to reach full charge.

2. $VoltageCell\_Max < Cell\_Threshold\_2$; the maximum voltage value among the cells is below a certain threshold.

3. $VoltageCell\_Min < Cell\_Threshold\_1 \quad || \quad AvgBatt\_Voltage < AvgVoltage\_Threshold$; the minimum voltage value among the cells is below a certain threshold (smaller than the previous one) or the average battery voltage is below a critical average voltage.

To start charging with the charging station, the $Charge\_Enable$ signal must be switched to true. This signal is the result of a logical AND combination of the above conditions and two additional signals: $Plug\_In$ confirming the presence of the charging connector and $Control\_Pilot$ generated by the charging column to start the process.
After the completion of the charging process, when a balancing phase occurs, the algorithm of this subVI allows the start of a subsequent charging phase. After balancing, especially in the case of significant cell imbalances, there is a SOC decrease of a certain percentage. To show the driver a complete SOC at the end of charging, a short additional charging phase triggered by setting the variable $AfterBalancing\_Charge == True$ is required.

A case structure has been implemented to notify the user of the vehicle status related to charging through a display. This structure activates an LED with different colors depending on the input received:

- Flashing light/dark green LED indicates that the vehicle is charging.

- Fixed green LED indicates that charging cannot be enabled because the previous three conditions are not met.
- Fixed white LED indicates that the battery can be charged.
- Fixed red LED indicates that the battery can be charged but cannot proceed due to a fault or because the temperature of a battery cell is below a critical value.

To activate the latter LED, the algorithm must be able to detect faults. The VCU is programmed to receive critical fault alerts via CAN communication from various vehicle components, such as the motor, or via internal communication from the battery management algorithm, which indicates failures in the battery pack. If any of these faults are present the output variable $Fault\_2$ is set to true.

Regarding startup management, to activate all driving modes, the boolean $Power\_ON$ must be on the true state. This variable acts as a switch for the entire system. To satisfy this condition, no charging connector must be plugged in and the key presence signal (Key) must be on.

6.2 Battery Management Implementation

The main objective of the battery management algorithm is to monitor and control the battery in different operating modes. Ensuring safe and reliable operation in all situations.

6.2.1 Finite State Machine

Again, a finite state machine was used to express the current operating state of the battery. The battery can operate in one of the following modes: Standby mode, Charge mode, Discharge mode and Fault mode. Depending on the current state, the FSM can activate or deactivate output variables that are essential to perform additional tasks. The logic of the battery state machine is illustrated below.

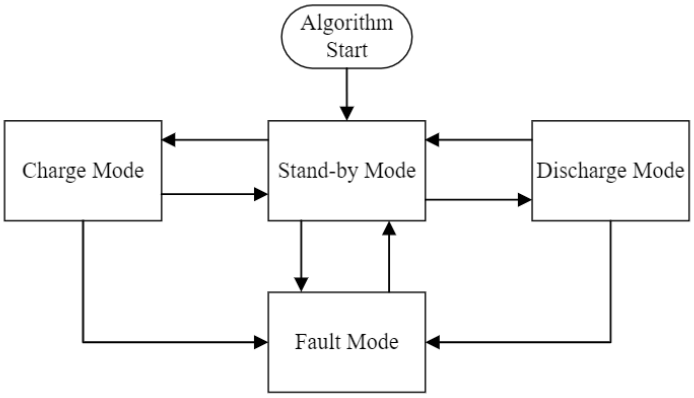

Figure 6.21: Battery FSM logic

As we shall see, the battery finite state machine will receive an input signal (*State_PCU*) indicating the current state of the state machine related to the generation of the torque signal. The interaction between the two FSMs was achieved by associating the states of the battery FSM with those of the powertrain FSM.

Battery State	**Powertrain State**
Stand-by Mode	S1 (NO battery fault), S2, S4, S5 (NO battery fault)
Charge Mode	R2
Discharge Mode	S3, S3b, SR
Fault Mode	S1 (Battery fault), R1, S5 (Battery fault)

Table 6.2: FSMs relationships

Stand-by Mode

This is the initial state of the battery FSM at startup. It represents the only state from which all other states can be accessed, driven by various signals, including *State_PCU* and *Battery_Fault*. Output boolean variables are set as follows:

- $Charging == False$; indicates if the charging phase is started.
- $Balancing\_Enable == False$; balancing phase activation signal
- $Battery\_Heater == True$; battery heater activation signal.
- *Drive_Mode* and *Charge_Mode*; signals used to start the inverter/charger contactors opening or closing procedure.

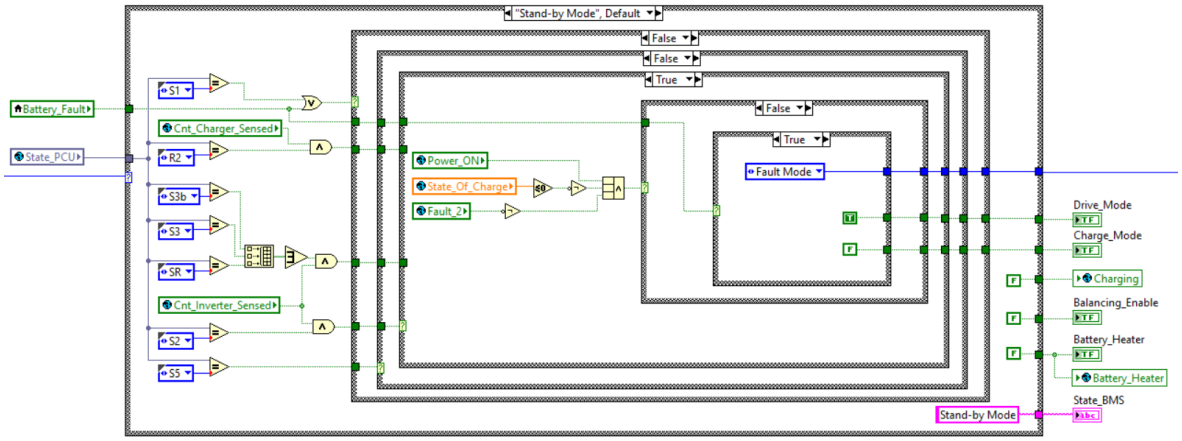

Figure 6.22: Stand-by mode

The last two signals can be configured in two ways: both set to false or one set to true and the other set to false. This configuration depends on the expected future state and the current speed of the vehicle. It is important to note that in no case will both signals be set to the true state at the same time.

Charge Mode

Battery charging state. In the absence of battery-related faults and with the state of the powertrain FSM set to R2, the variables *Charging* and *Charge_Mode* are triggered, initiating the charging process. This state is also intended for the balancing task. When the SOC is 100%, the variable *Balancing_Enable* switches to the true state. From here, all states except the discharge mode can be accessed.

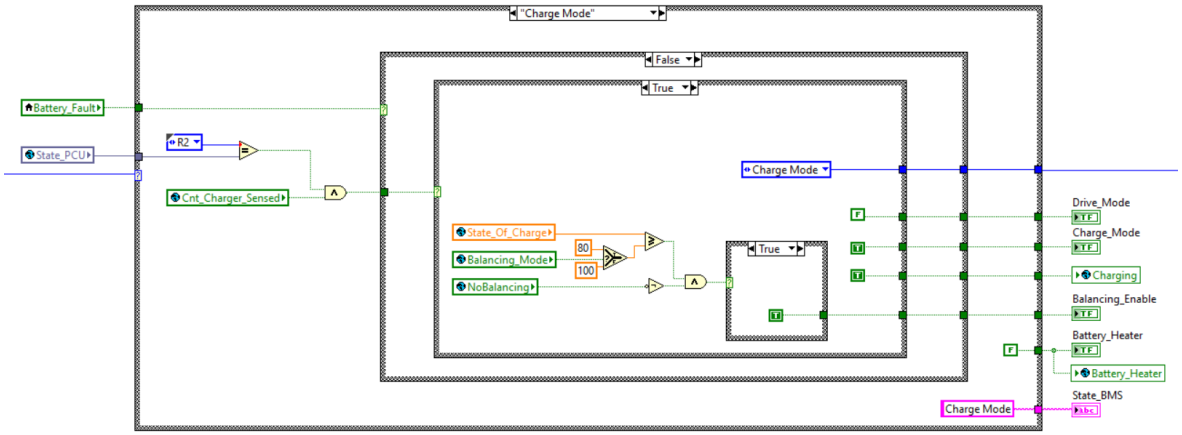

Figure 6.23: Charge mode

Discharge Mode

Discharge mode represents the battery discharge state used during forward and reverse

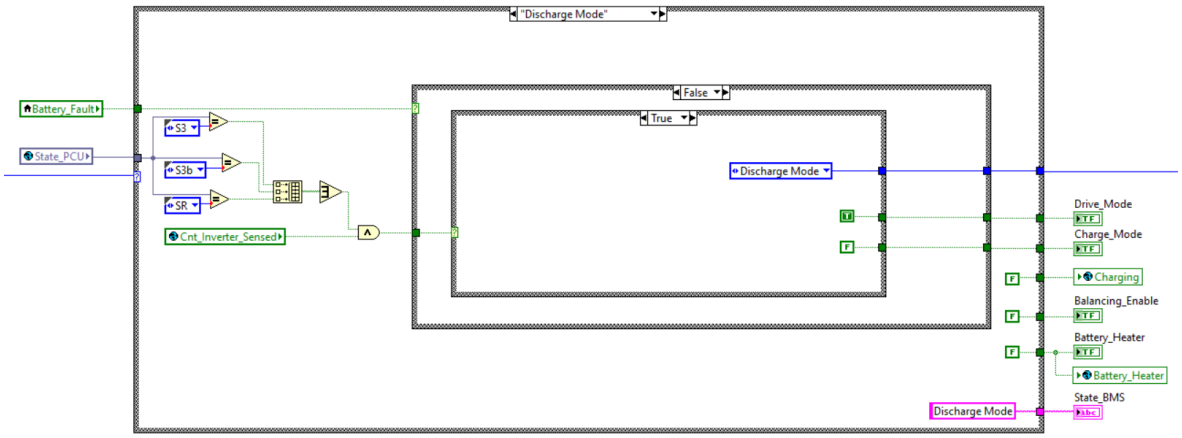

Figure 6.24: Discharge mode

driving under normal working conditions ($Drive\_Mode == True$). It is possible to switch from this state to stand-by when the vehicle is off or when a motor fault occurs. In case of battery failure, on the other hand, the system switches to the fault state. In both scenarios, if the vehicle speed exceeds 5 km/h, the contactors connected to the inverter remain in the closed position, allowing safe deceleration and stopping of the vehicle.

Fault Mode

This is the state in which the battery FSM enters when failures occur in the battery cells or contactors ($Battery\_Fault == True$). In case the following condition occurs, $State\_PCU == R1 \quad \&\& \quad Battery\_Fault == True$, where the battery needs to be recharged but is below a critical temperature, the boolean variable $Battery\_Heater$ is enabled, which allows the warming process to take place.

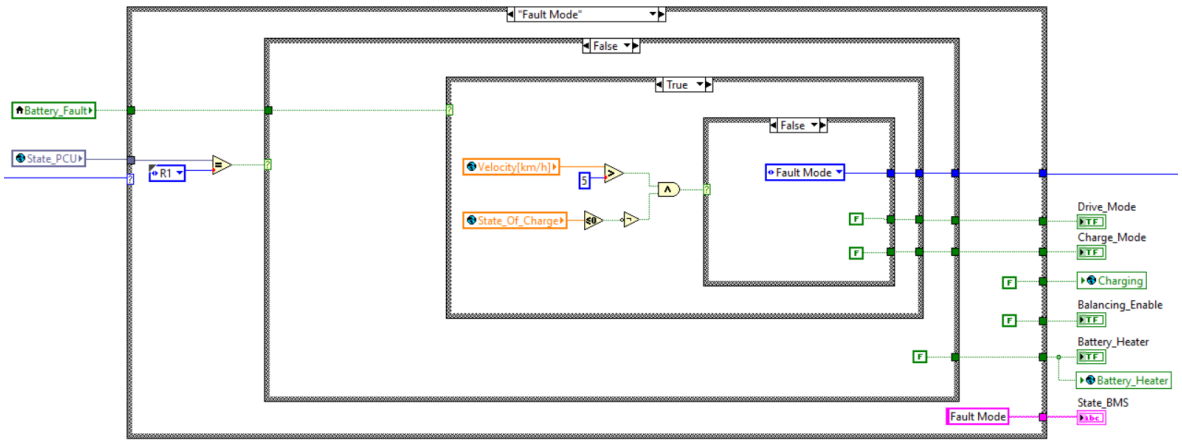

Figure 6.25: Fault mode

As shown in figure 6.21, the stand-by mode is the only state accessible from the fault mode. This occurs either upon resolution of the fault or when the battery heater achieves its purpose, allowing the charging phase to begin.

6.2.2 Contactors Management

The signals responsible for beginning the inverter or charger contactor opening/closing procedure, outputs of the battery FSM, serve as inputs to the $Contactors\_Management$ subVI. This subVI is dedicated on the management and control of contactors. As already seen in the chapter on requirements analysis, the following procedure must be performed to properly close the contactors:

1. Initially both positive and negative contactors are opened.
2. Negative contactor is closed.
3. Pre-charged contactor is closed and the voltage in the connected device begins to rise.

4. When the desired threshold voltage is reached, positive contactor can be close.
5. Pre-charge contactor is opened.

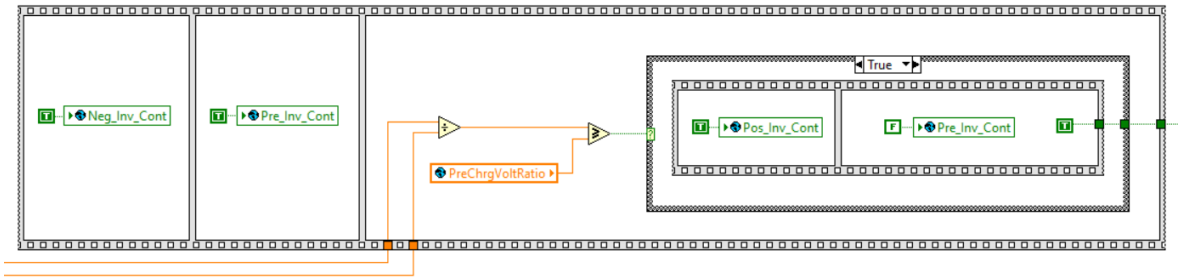

Figure 6.26: Inverter contactors closure procedure

As can be seen from figure 6.26, to perform this sequential operation in LabVIEW, a specific structure called "Flat Sequence Structure" was used. This structure includes one or more frames executed in sequence, ensuring the orderly execution of each frame before or after another.
A procedure almost similar to that described is used to open the contactors.

6.2.3 Fault Monitoring

In each state of the battery FSM, the *Battery_Fault* signal is checked to evaluate the condition of the cells and contactors. This signal is set within the *Fault_Management* subVI following a deep validation process that ensures that all cell parameters are within safe ranges and that contactors are functioning properly.

Initially, the system records the maximum and minimum values of voltage and temperature among all cells, checking them against allowable limits. If these values fall outside the acceptable ranges, a respective boolean variable is flagged as true, indicating the occurrence of a fault. Specifically, with regard to temperature limit checks, the algorithm dynamically adjusts the upper and lower verification limits, as shown in figure 6.27. This adjustment is necessary because of the stricter safety interval to be met during the charging phase than during the discharging phase. The current flowing during charging and discharging is also monitored. Although the maximum allowable values are different (the maximum charge current is usually less than half the maximum discharge current), simultaneous tracking is carried out. This is made possible by the convention that considers the outgoing current from the battery pack to be negative and the incoming current to be positive.
Another check performed concerns the voltage sensors. The sum of the measured voltages across all cells triggers an alarm if the derived value deviates from that of the entire battery pack beyond a certain threshold. This approach makes it easier to identify problems with the instrumentation responsible for cell measurements.

Regarding the validation of proper contactors operation, two blocks have been integrated. They serve to verify that both the pre-charge contactor associated with the

inverter connection and the one connected to the OBC connection do not remain closed for an extended time, exceeding a predetermined time limit. In such a case, the system issues *ChargeContactor_Fault* or *InverterContactor_Fault* warning, thus signaling the detected problem.

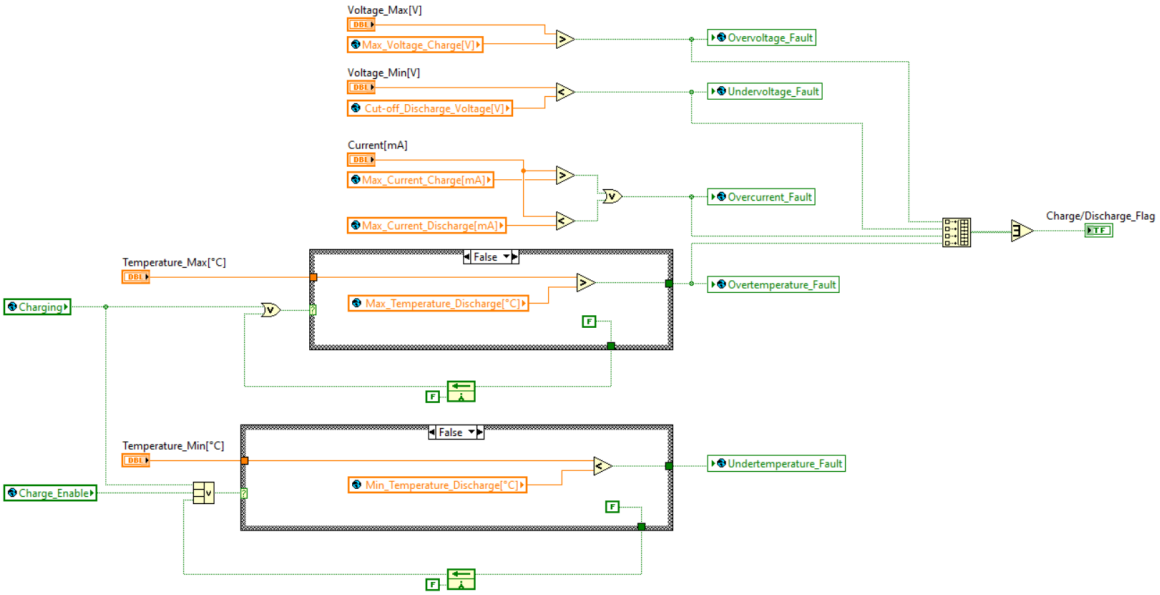

Figure 6.27: Fault detection algorithm

Current limits computation

In addition to fault diagnosis, the battery management algorithm must establish current limits to prevent users from requesting or delivering power beyond these thresholds, thus safeguarding the battery from potential damage. These limits are determined through calculations involving cells voltage and temperature measurements. When temperature and voltage values approach maximum allowable levels, the algorithm linearly limits current to reduce potential risks.
Current_Power_Limits_Management subVI outputs a pair of current limits, one applicable during the charging phase and the other during the discharging phase. The former is obtained by computing the minimum among three different values.

$$Charging\_Limit\_Current = min(i(V_{cell\_max}), i(T_{cell\_max}), i(T_{cell\_min})) \tag{6.16}$$

where $i(V_{cell\_max})$ represents the limit dependent on the maximum measured voltage. It is obtained from the following function:

$$i(V_{cell}) = \begin{cases} i_{max} & \text{if } V_{cell} \leq V_{th\_high} \\ \dfrac{V_{cell} - V_{max}}{V_{th\_high} - V_{max}}(i_{max} - i_{fault}) + i_{fault} & \text{if } V_{th\_high} < V_{cell} \leq V_{max} \\ i_{fault} & \text{if } V_{cell} > V_{max} \end{cases} \tag{6.17}$$

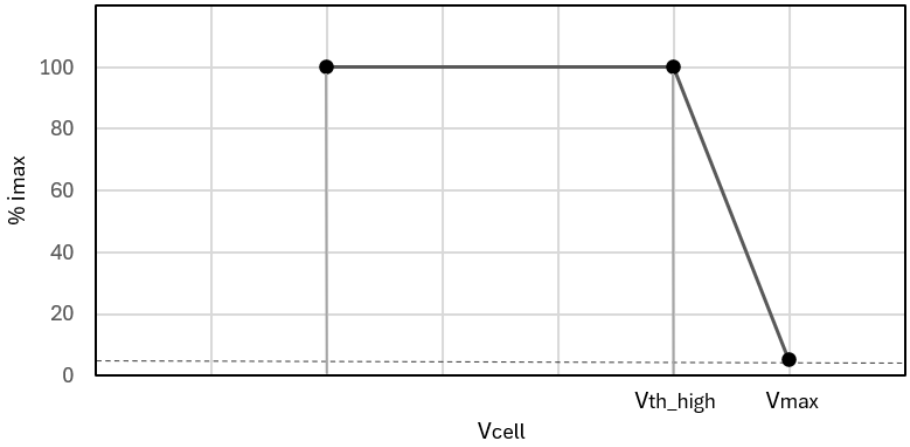

Figure 6.28: Current limitation: charge voltage measurements

Whereas, the last two parameters in equation 6.16 represent the highest and lowest temperature-dependent current limits measured, respectively. They are derived from the function below:

$$i(T_{cell}) = \begin{cases} i_{fault} & \text{if } T_{cell} < T_{min} \\ \dfrac{T_{cell} - T_{min}}{T_{th\_low} - T_{min}}(i_{max} - i_{fault}) + i_{fault} & \text{if } T_{min} \leq T_{cell} < T_{th\_low} \\ i_{max} & \text{if } T_{th\_low} \leq T_{cell} \leq T_{th\_high} \\ \dfrac{T_{cell} - T_{max}}{T_{th\_high} - T_{max}}(i_{max} - i_{fault}) + i_{fault} & \text{if } T_{th\_high} < T_{cell} \leq T_{max} \\ i_{fault} & \text{if } T_{cell} > T_{max} \end{cases} \tag{6.18}$$

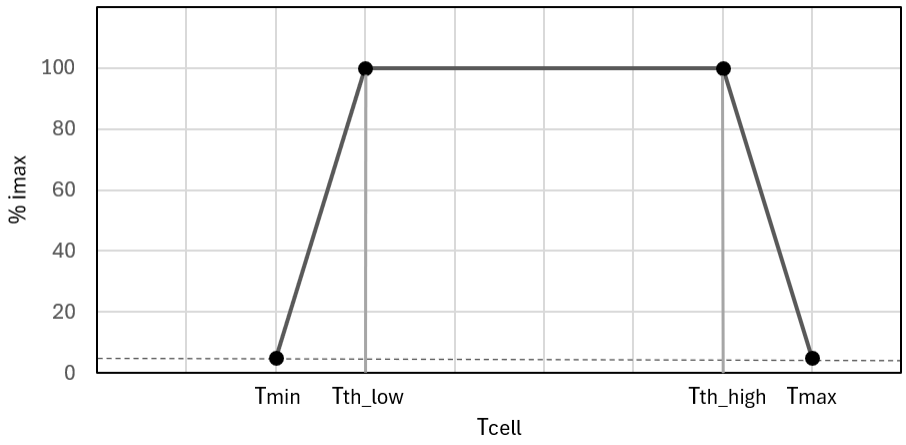

Figure 6.29: Current limitation: temperature measurements

As is evident from the equations and qualitative graphs presented above, beyond the

established safety thresholds, the current undergoes a linear limitation until it reaches the specified limit values. Once these limit values are exceeded, the current is clamped to 5% (i_{fault}) of the maximum available current.
To determine the discharge current limit, the procedure mirrors that of the previous scenario, derived from the minimum of three values.

$$Driving\_Limit\_Current = min(i(V_{cell\_min}), i(T_{cell\_max}), i(T_{cell\_min})) \tag{6.19}$$

The parameters $i(T_{cell\_max})$ and $i(T_{cell\_min})$ are determined as in the previous case, even though the threshold and limit values set in the equations are different. The first parameter, instead, which represents the limit dependent on the minimum measured voltage, is computed as follows:

$$i(V_{cell}) = \begin{cases} i_{fault} & \text{if } V_{cell} < V_{min} \\ \dfrac{V_{cell} - V_{min}}{V_{th\_low} - V_{min}}(i_{max} - i_{fault}) + i_{fault} & \text{if } V_{min} \leq V_{cell} < V_{th\_low} \\ i_{max} & \text{if } V_{cell} \geq V_{th\_low} \end{cases} \tag{6.20}$$

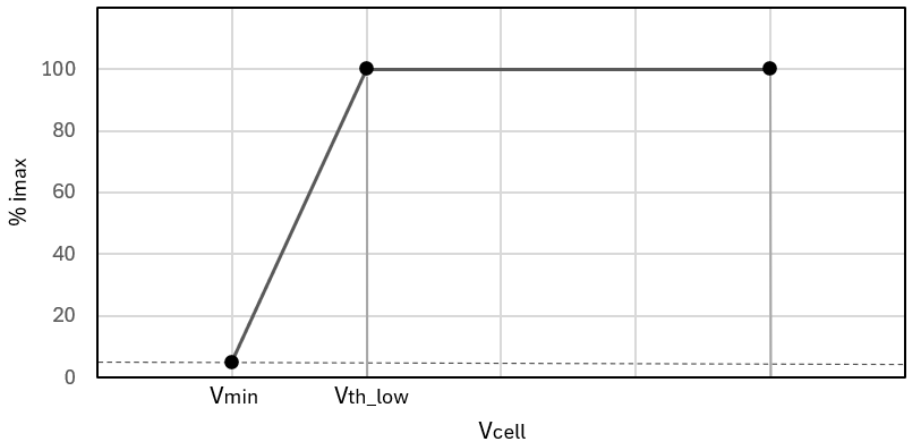

Figure 6.30: Current limitation: discharge voltage measurements

At each iteration, the battery management algorithm calculates current limits. However, in cases where the battery is isolated, i.e. when the contactors connecting to the charger or inverter are open, these limits are overwritten, resulting in output values of 0.

6.2.4 SOC Estimation

Assuming it is possible to measure the current with high precision, the chosen method to estimate the state of charge in this project is Coulomb counting. The decision was influenced by one of the main advantages of this method, namely the ease of implementation. Unlike equation 5.1 outlined in the previous chapter, the implemented algorithm neglects the coulombic efficiency η, setting it constant, equal to 1. As a result,

the updated equation is as follows:

$$SOC(t) = SOC_i + \frac{1}{C_{rated}(T)3600} \int i(t)\, dt \tag{6.21}$$

Since the measured signals are sampled in time, the above function takes its discretized form:

$$\begin{cases} SOC(k+1) = SOC(k) + \dfrac{\Delta t}{C_{rated}(T)3600} i(k) & \text{if } k \geq 1 \\ SOC(k+1) = SOC_i & \text{if } k = 0 \end{cases} \tag{6.22}$$

To implement the nonlinear relationship between rated capacity and temperature, a function generated by polynomial interpolation was used. The subVI *SOC_Estimation* derives the final state of charge of the battery based on the state of charge of individual cells. As an input, in addition to current, this block also receives cell temperatures for capacity calculation. When the total SOC falls below the 20% threshold, the *SOC_Alarm* signal is activated, signaling the need to recharge the vehicle.

6.2.5 Battery Heater Management

As mentioned above, when the vehicle is to be charged and the minimum temperature among all battery cells falls below the minimum allowable, the battery heater is activated to bring the battery pack to the correct temperature. To manage this device, a Proportional–Integral–Derivative (PID) controller was implemented.
PID controller is a control algorithm with a predefined structure, which is calibrated by adjusting specific parameters. From a mathematical point of view, this is a dynamic system that processes an input signal $e(t)$, called "error," obtained as the difference between the reference and the controlled variable, and then outputs a control signal $u(t)$. This control has, in its basic form, a structure that includes the sum of three terms:

$$u(t) = K_P \cdot e(t) + K_I \cdot \int_0^t e(\tau)\, d\tau + K_D \cdot \frac{de(t)}{dt} \tag{6.23}$$

In this case, the error is given by the difference between a threshold temperature and the temperature of the coldest cell:

$$e(t) = TemperatureCharge\_Threshold[^\circ C] - TemperatureCell\_Min \tag{6.24}$$

where the threshold temperature is set higher than the minimum allowable temperature to avoid potential bouncing effects on the *Battery_Heater* boolean variable.
The parameters that identify the PID are K_P , K_I and K_D and are also called controller degrees of freedom. The first, proportional gain, adjusts the amplitude of the system's response in proportion to the current error. A higher K_P value increases the proportional response of the system. The second parameter, takes into account the cumulative sum of errors over time. It helps to correct persistent errors in the system. A bigger value of K_I increases the long-term correction effect. The K_I value is given by the inverse of the time constant integral T_I multiplied by the proportional gain. The last one takes into account the error rate of change over time. This feature aims to prevent excessive oscillations and improve the stability of the system. The derivative parameter K_D is

determined by multiplying the proportional gain by the derivative time constant T_D. A greater value of K_D reduces oscillations by slowing down the system response.
For this application, the PI configuration was used. This means that the value of K_D was set to 0, effectively eliminating the derivative action, while K_P and T_I were chosen by a trial-and-error procedure and subsequently set to 5 and 500, respectively. Such configuration allows for greater accuracy without worsening the degree of system stability, coupled with faster response.

6.2.6 Passive Balancing

Using a passive balancing technique designed for low-power applications, this algorithm was adapted to the specific requirements of the chosen motor, which works with a DC voltage at the terminals of the inverter of about 48 V.
After the end of the charging phase, the *Balancing_Enable* variable triggers the passive balancing operation implemented in *Passive_Cells_Balancing* subVI. This balancing process consists of discharging the cells through a resistor until their voltage falls below a specified threshold relative to the cell with the lowest voltage. The algorithm controls this process by generating a vector containing the balancing switch commands for each cell. Each vector entry is given by the following equation:

$$Cells\_Commands(V_{cell}) = \begin{cases} 0 & \text{if } V_{cell} - V_{cell\_min} < Threshold \\ 1 & \text{if } V_{cell} - V_{cell\_min} \geq Threshold \end{cases} \tag{6.25}$$

A command value of 1 corresponds to closing the switch that connects the cell to the resistor, while a value of 0 corresponds to opening that switch. Once the sum of all the components of the vector becomes equal to 0, i.e. all the switches are open, the balancing phase ends and the *Balancing_Mode* variable changes to the false state.

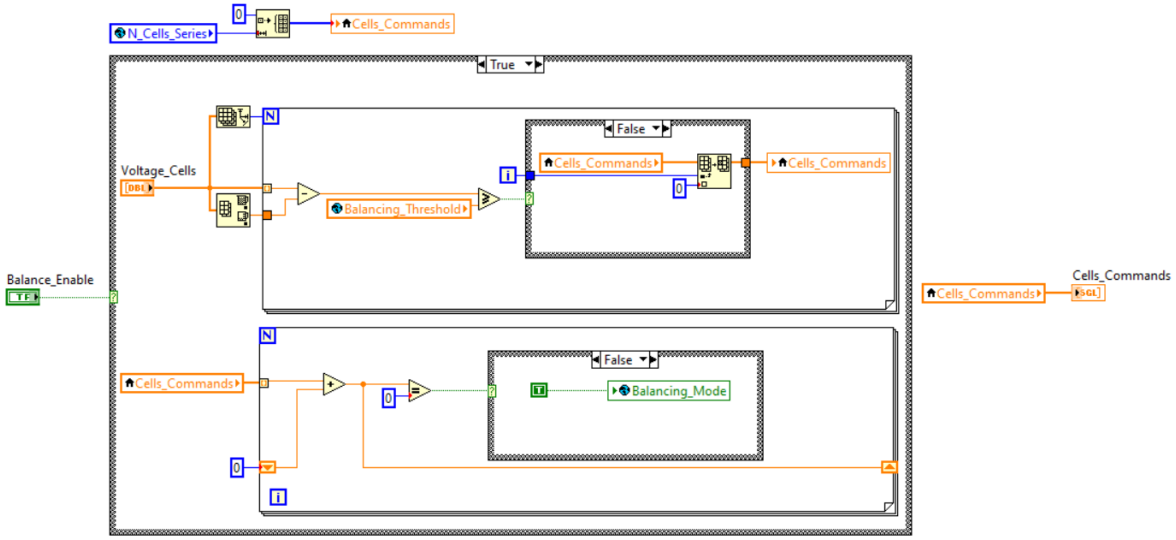

Figure 6.31: Passive balancing algorithm

Chapter 7

Plant Simulation Model

The first step in testing the physical behavior of the system is to create a good LabVIEW model. It is not always necessary for models to represent every internal characteristic of the real system, as long as their output can accurately represent the behavior of interest. As announced in the introductory chapter, a single battery module, containing 12 cells in series, will be modeled to validate all the logic related to the battery management algorithm. In creating the model, it is therefore necessary to take into account the data expected from the control algorithm and the input parameters that, whether or not generated by the actuators connected to the VCU, will allow the battery module to meet the initial conditions and physical behavior it should have in reality.

7.1 Cell Models

Several models have been developed in the literature in recent decades, each of which has different purposes. These models range from those that capture the chemical-physical phenomena characteristic of charge/discharge processes, offering high accuracy but requiring long computational times and specialized knowledge of internal structures and materials, to models that, while easily implemented with limited initial information, provide less accurate data. In general, achieving accurate modeling without introducing computational complexities, and vice versa, remains a challenge. It is essential to understand the strengths and limitations of the major models in order to choose the most suitable one based on the intended application. Although the landscape of models is wide and varied, they can be broadly classified into four main groups:

1. *Electrochemical Models:* these models are distinguished by their high accuracy, as they describe electrochemical processes within the cell through explicit and detailed formulations. However, their accuracy involves the use of numerous nonlinear differential equations, which require significant computational resources. This involves a very in-depth knowledge of the cell (white box model) and the measurement of many parameters, which is often difficult to perform except in specialized laboratories. This complexity makes electrochemical models impractical for real-time battery monitoring applications. Instead, their main utility lies in simulations aimed at improving cell design.

2. *Analytical Models:* these typologies aim to model the operation of a cell with few equations, thus favoring speed of processing at the expense of a high degree of abstraction. Some analytical models make use of simple equations such as Peukert's law. These equations can predict the nonlinear relationship between cell capacity and discharge rate, but do not take into account the recovery effect that is instead considered in the Kinetic Battery Model (KBM).

3. *Stochastic Models:* these models maintain a high level of abstraction, with the goal of representing the charge/discharge and recovery effect phenomena as stochastic Markovian processes. The cell is represented by a discrete Markov chain, with N+1 charge states, numbered from 0 to N. Each state number indicates the charge units currently available in the cell. N indicates the number of charge units immediately available for continuous discharge. The unit of charge is defined as the energy required to transmit a packet of data, reflecting the origins of the model in telecommunications.

4. *Electrical Circuit Models:* in these models, an equivalent circuit is created using ideal components, including voltage generators, resistors, and capacitors. The goal is to reliably replicate the voltage-current relationship of the cell under various operating scenarios. In general, the circuits can be either parameter concentrated or parameter distributed. The following section provides a brief overview of models in the literature that use concentrated-parameter elements.

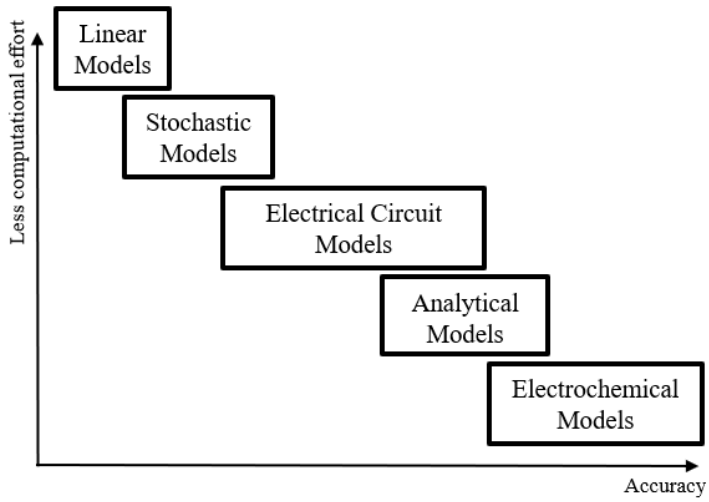

Figure 7.1: Cell models comparison

7.1.1 Electrical Circuit Models

Before going into the main circuit models of a battery cell, it is essential to clarify two phenomena that these circuits must be able to represent.
The first is the **ohmic jump**. When a cell, and more generally a battery is in steady

state, i.e. in no-load condition for a sufficiently long period of time, it presents a certain voltage level. However, when going to supply a load, there is a sudden drop in voltage at its terminals, which cannot be due to a simple change in the value of the OCV (Open Circuit Voltage) curve, since in the first few instants it can be assumed that the SOC remains unchanged. Moreover, the greater the magnitude of the current drawn, the greater the magnitude of this sudden voltage drop, known as the ohmic jump. This treatment is doubly valid when suddenly going from a load condition to a no-load condition, in which there is a sudden increase in voltage at the battery terminals.
The second one, is the phenomenon of the **recovery effect**. It occurs when the available energy is less than the difference between the energy charged and the one consumed because of the consumption of energy from the edge of the cell due to uneven distribution of charge. A cell with the same initial conditions allows a higher capacity to be drawn if the discharge, with the same current supplied, is carried out by steps separated by pauses in which the battery is left in no-load condition, rather than by a continuous discharge. Furthermore, during such pauses it is observed that the voltage at the cell terminals tends to return to the value expressed by its OCV curve for the value of the SOC at which one is, provided the duration of such a pause is sufficiently long.
Among the most widely used circuit models, we have:

a) The R_{INT} model is the simplest model and consists of an ideal voltage generator, representing no-load voltage, and a series resistor. The inclusion of this resistor makes it possible to model the ohmic jump phenomenon, but not to accurately simulate the recovery effect. For such a simple model to give good results on the estimated voltage, at least as far as the ohmic jump is concerned, the value of both circuit elements must depend on the SOC and the cell temperature.

b) Thevenin's model, often referred to as the "first-order model," is an evolution of the R_{INT} model, introducing a parallel RC circuit in series with the resistor to emulate the dynamic behavior of the cell (due to various physico-chemical phenomena), i.e. the recovery effect, by means of a first-order exponential transient.

c) In the PNGV (Partnership for a New Generation Vehicle) model, a capacitor is added to the Thevenin model in series with the voltage generator to represent the change in open-circuit voltage during the current storage period, and its value reflects the capacity of the cell.

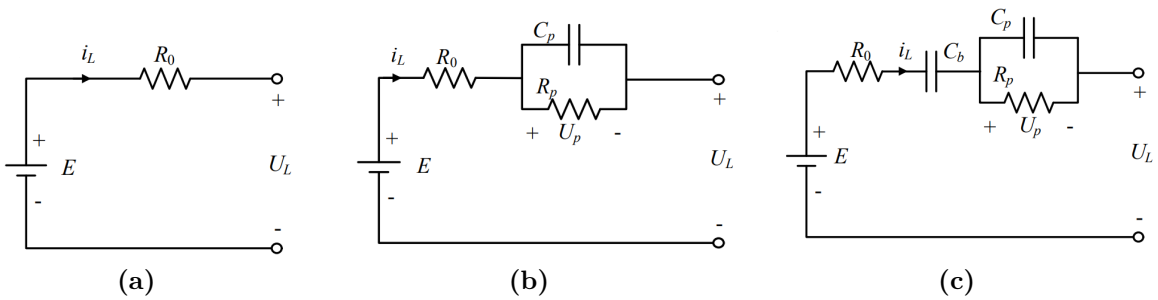

Figure 7.2: Equivalent circuit models: (a) R_{INT}; (b) Thevenin; (c) PNGV

7.2 Developed Electrothermal Model

Based on the above, in this project we chose to model the 12 cells of the battery module with a Thevenin equivalent circuit models. The choice to adopt this circuit configuration was made because it is able to represent the main phenomena occurring within a cell. Moreover, as we will see later, the values of various electrical circuit parameters are commonly considered functions of cell temperature and state of charge. This is because these factors significantly influence the behavior of the cell. The correlation between the parameters and the state of charge required the inclusion of a SOC estimator alongside the actual model, as seen in figure 7.3. The SOC estimator employed integrates the current delivered/absorbed by the cell, considering the change in capacity as a function of temperature. This approach is in line with the classical definition of SOC (see equation 6.21). In conclusion, the electrical model was completed with a simple thermal model that estimates the cell temperature from the room temperature, the temperatures of adjacent cells and the energy information provided by the electrical model, i.e. the power lost due to the Joule effect.

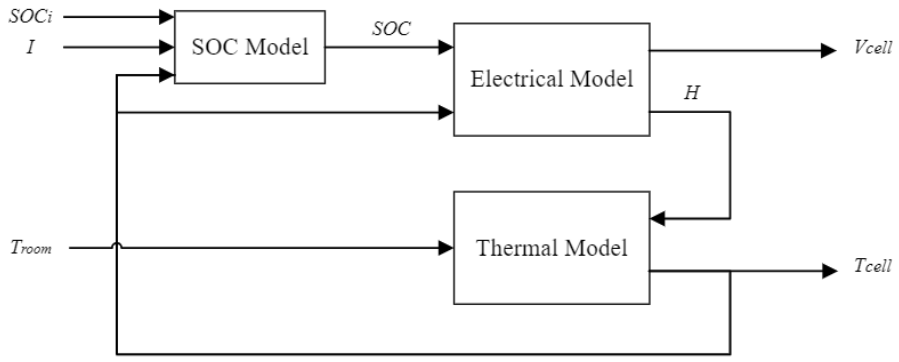

Figure 7.3: Electrothermal model: block diagram

7.2.1 Cell Electrical Model

As mentioned above, the equivalent circuit model chosen is Thevenin's, characterized

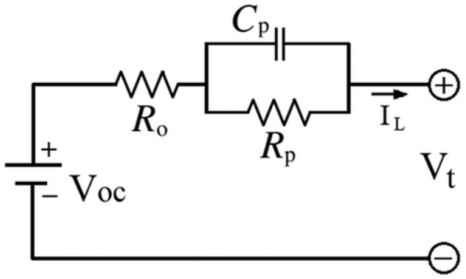

Figure 7.4: Thevenin cell model

by a voltage generator, a series resistor and a parallel RC block connected in series to the previous components. According to the electrical circuit, the relationship between terminal voltage and current can be expressed by the following equations:

$$\begin{cases} \textit{Terminal voltage:} & V_t = V_{OC} + V_o + V_p \\ \textit{Open-circuit voltage:} & V_{OC} = f(SOC, T) \\ \textit{Voltage on ohmic resistor:} & V_o = R_{o(SOC,T)} I \\ \textit{Voltage on polarization resistor:} & I_{C_p} = C_{p(SOC,T)} \dfrac{dV_p}{dt} \\ \textit{Cell current:} & I = I_{C_p} + I_{R_p} \end{cases} \tag{7.1}$$

That is, the dynamic voltage can be described by the following differential equation:

$$\frac{dV_p}{dt} = -\frac{V_p}{R_{p(SOC,T)} C_{p(SOC,T)}} + \frac{I}{C_{p(SOC,T)}} \tag{7.2}$$

The overall differential equation is:

$$\frac{dV_t}{dt} = -\frac{V_t}{R_{p(SOC,T)} C_{p(SOC,T)}} + R_o \frac{dI}{dt} + \frac{R_{p(SOC,T)} + R_o}{R_{p(SOC,T)} C_{p(SOC,T)}} I + \frac{V_{OC}}{R_{p(SOC,T)} C_{p(SOC,T)}} \tag{7.3}$$

where I is the cell current, V_t is the terminal voltage and V_{OC} represents the open-circuit cell voltage. The presence of the resistor R_o represents the ohmic jump. When switching from no-load to load conditions, or vice versa, the incorporation of this resistor in series with the generator allows for instantaneous voltage changes at the circuit terminals, reflecting the actual behavior of the cell. The parallel RC group (R_p and C_p) is responsible for describing the recovery effect. In the transition from load to no-load, they induce a transient that leads to a gradual increase in voltage over time, exceeding the simple ohmic jump. This occurs when the capacitor gradually discharges through the parallel resistor until the cell voltage equals that of the no-load characteristic, assuming a sufficiently long rest period. Finally, the presence of resistors in series with the ideal voltage generator, which result in voltage drops, also allows for the rate discharge effect. At higher currents, given the same initial conditions and values of the various parameters, the cut-off voltage is reached sooner, resulting in a reduction of the available dischargeable capacitance.

Passive balancing circuit model

To account for the passive balancing circuit as well, the previous circuit model is modified by adding a switch and resistor in a parallel configuration with respect to the cell. When the switch is closed, during balancing operations, the current I_b flowing through the cell is given by the following equation:

$$I_b = \frac{V_t}{R_{shunt}} \tag{7.4}$$

R_{shunt} is the shunt resistance and its value was set at 500 Ω. This choice was made to obtain, during the balancing phase, a very low current (about 8.4 mA) so as not to excessively discharge the cell.

7.2.2 Parameters lookup

The parameters characterizing equation 7.1, V_{OC}, R_o, R_p and C_p, depend non-linearly on temperature and state of charge. To estimate them, standard tests can be performed on the cell, such as capacitance test, Dynamic Discharge Performance (DDP) test, and Hybrid Pulse Power Characterization (HPPC) test. These tests should be done at different SOC and temperatures. In this project, unlike the motor, a dedicated battery was not available for testing. Consequently, the necessary data were provided by an analysis conducted by the Vrije Universiteit Brussel and Erasmus University College Brussels on a lithium polymer cell, in which parameter estimation for the Thevenin cell model was performed using the Matlab/Simulink parameter estimation tool [32]. The analyzed Li-Po cell present the following characteristics:

Specification	**Value**
Rated Capacity	12 Ah
Rated Voltage	3.7 V
Max. Charge Voltage	4.2 V
Discharge Cut Off	2.75 V
Max. Charge Current	2 C
Max. Discharge Current	5 C
Charge Temp. Range	10 to +45°C
Discharge Temp. Range	-20 to +60°C

Table 7.1: Li-Po cell characteristics

The data obtained from the previous analysis were used for interpolations, allowing the trend of the four circuit model parameters as a function of SOC and temperature to be derived. The results of these interpolations are shown in the figures below. The green plots represent the trends of the four parameters as a function of SOC at the temperature of 25°C. The blue plots represent these trends at 5°C, while the red plots illustrate the trends at 40°C.

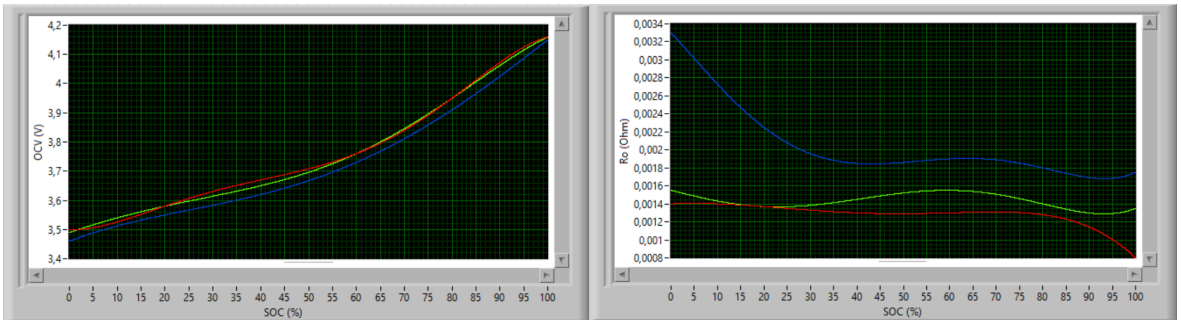

(a) **(b)**

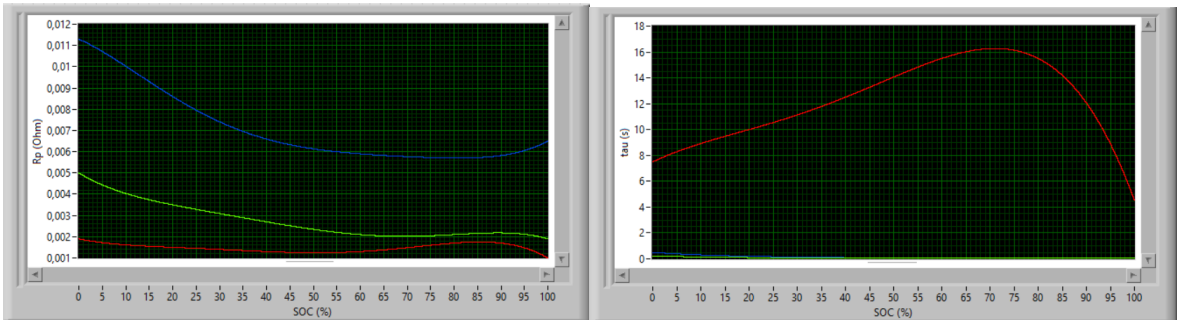

(c) **(d)**

Figure 7.5: (a) V_{OC}; (b) R_o; (c) R_p; (d) τ

The *Parameters_Lookup* subVI of the LabVIEW model handles the update of the parameters in the cell electrical model. This block placed after the SOC estimator and before the electrical model, receives the temperature and SOC as input and outputs the four corresponding values.

7.2.3 Cell Thermal Model

The thermal model is used to estimate temperature changes that affect the capacity, state of charge and voltage of the cell under various operating conditions. A simplified model, developed on the basis of the following approximations, was considered:

- Cells exchange heat with their surroundings and adjacent cells, without considering a cooling system. Heat generated by the battery heater during operation is taken into account.
- Each battery cell is assumed with uniform temperature distribution.
- Heat propagation is considered only along the horizontal and vertical axes of the cell.
- Heat transmitted by radiation is neglected, focusing exclusively on the processes of heat conduction and convection.

The model used, which is also circuit-based, is illustrated in the figure 7.6. The power dissipated by the Joule effect within the cell is symbolized by a current generator, its heat capacity corresponds to a capacitor, and the thermal resistances in the various directions are represented as resistors. In this circuit, temperatures are made analogous to potential differences, all measured with reference to the ground, which is aligned with the room temperature set at 25°C.
The parameters that characterize the thermal model, such as capacitance and resistance, are related to the previously mentioned lithium polymer cell. As anticipated, to make the twelve-cell module, these were connected in series and packed inside a case usually composed of an aluminum alloy characterized by thermoplastic materials. The figure below illustrates the thermal model for the first and last cell of the twelve in the module. The model for all intermediate cells becomes equivalent when resistance R_{b2a} is replaced

with resistance R_{b2b}. This is because the intermediate cells along the horizontal direction exchange heat only with adjacent cells and not with their surroundings.

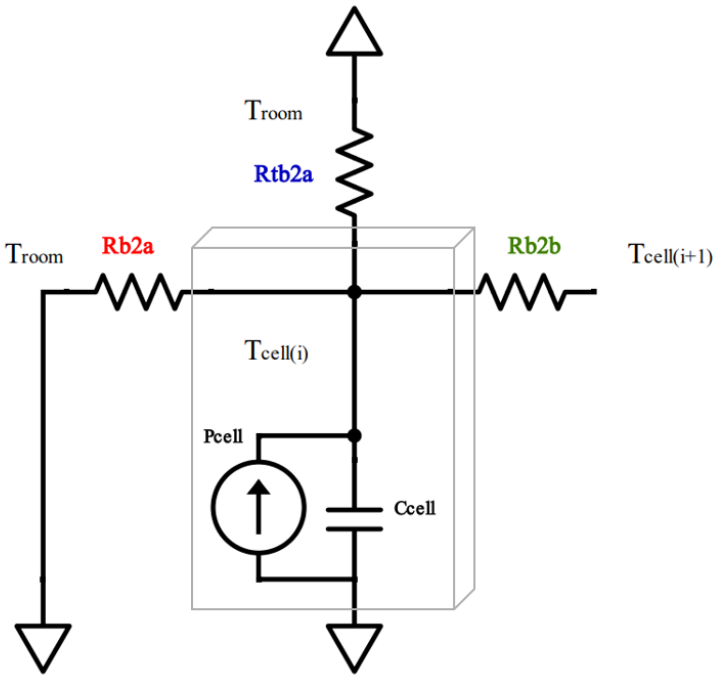

Figure 7.6: Thermal cell model

The heat balance of a each battery module cell with internal heat generation and external conduction is expressed as follow:

$$mC_{cell}\frac{dT_i}{dt} = P_{cell} + \frac{T_{room} - T_i}{R_{b2a}} + \frac{T_{room} - T_i}{R_{tb2a}} + \frac{T_{i+1} - T_i}{R_{b2b}} \tag{7.5}$$

where m is the total mass of the cell, while C_{cell} indicates the specific heat calculated using the mass fractions of the different components of the cell, including cathode, anode, separator and electrolyte.

$$C_{cell} = \frac{\sum(C_p m)_j}{\sum m_j} \tag{7.6}$$

R_{tb2a} considers the resistance, along the vertical direction, to both convective heat exchange with the surrounding air and conductive heat exchange with the aluminum alloy case surrounding the module. Along the horizontal direction, R_{b2a} considers the resistance to the same heat exchanges as in the previous case, but with a different heat exchange surface area of the cell, while R_{b2b} models the resistance to conductive heat exchange with the adjacent cell.

$$\begin{cases} R_{tb2a} = R_{conv} + R_{cond} = \dfrac{1}{hA_{xz}} + \dfrac{L}{K_{Al}A_{xz}} \\ R_{b2a} = R_{conv} + R_{cond} = \dfrac{1}{hA_{yz}} + \dfrac{L}{K_{Al}A_{yz}} \\ R_{b2b} = R_{cond} = \dfrac{x}{K_{cell}A_{yz}} \end{cases} \tag{7.7}$$

In the equation 7.7, K_{cell} and K_{Al}, expressed in $\frac{W}{Km}$, represent the thermal conductivity constants of the cell and alloy, respectively. While, h indicates the air convection coefficient, assumed to be 5 $\frac{W}{Km^2}$. The geometric parameters L, x and A represent the case thickness, thickness and heat transfer areas of the cell.
Going back to the heat balance equation (7.5), T_i denotes the temperature of the cell under consideration, while $T_{(i+1)}$ is the temperature of the adjacent cell. The total heat generated by the cell (P_{gen}) is the sum of three components: battery heater heat, irreversible and reversible heat.

$$P_{cell} = H_{gen} + H_s + H_{heater} \tag{7.8}$$

The heat generated by the battery heater H_{heater} is considered only during battery heating; for all other situations, it is equal to 0. On the other hand, the first term H_{gen}, describes the loss mechanisms resulting from the conversion of electrical energy into heat. This irreversible part of the generated heat can be expressed as:

$$H_{gen} = (V_t - V_{OC})I \tag{7.9}$$

For electrochemical processes such as lithium batteries, reversible heat must also be considered.

$$H_s = \frac{IT\Delta S_{(SOC)}}{zF} \tag{7.10}$$

where T is the absolute temperature expressed in K, ΔS is the change in entropy, F is the Faraday constant, and z is the number of electrons transferred per ion.
In the LabVIEW model, heat generation is simulated using the dedicated subVI, *Heat_Generation*. Its output serves as input to the *Cell_Thermal_Model* subVI, in which the thermal model is realized.

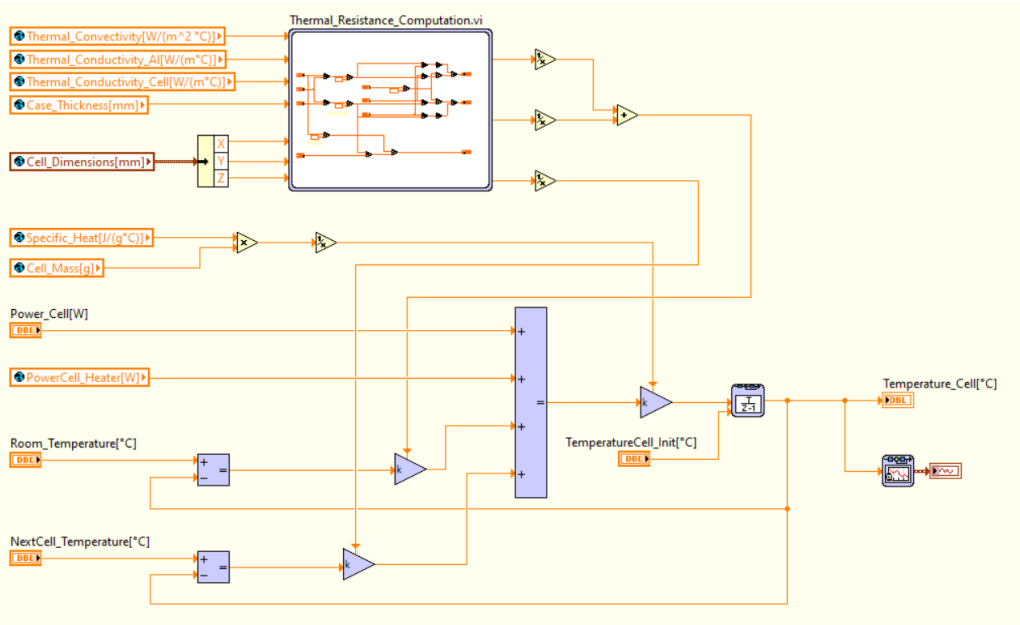

Figure 7.7: LabVIEW thermal cell model

Chapter 8

Tests and Results

After the development of the VCU algorithms described in chapter 6, a testing phase is carried out to validate the logic implemented in LabVIEW. First, a test phase is carried out to validate the state transitions logic of both FSMs. Next, the battery management algorithm is verified. So, a MIL test is performed using the plant model simulated in the previous chapter, providing a comprehensive analysis of the operation of the entire system.

8.1 Finite State Machines Testing

The finite state machines must be checked first. The algorithm must be able to switch between states deterministically when relative transition requirements are met. Using LabVIEW, state machines' input variables can be easily controlled to test state transitions. The following tests were performed:

Transition from S1 to R2 (Standby Mode to Charge Mode). The transition occurs when the following conditions are met:

1. All critical faults are set to false ($Fault\_2 == False$).
2. The SOC and cells voltage are configured to obtain the $Charge\_Enable$ signal in the true state.
3. Both $Plug\_In$ and $Control\_Pilot$ boolean signals are set to true.
4. The minimum temperature among all cells is set to a value greater than 10°C.

Transition from S1 to R1 (Standby Mode to Fault Mode). This is the transition related to the activation of the battery heater; it occurs when the following conditions are met:

1. The first three conditions of the previous case must be set.
2. The minimum temperature among all cells is set to a value smaller than 10°C.

Transition from S1 to S3 (Standby Mode to Discharge Mode). The conditions of transition to driving mode are verify when:

1. $Fault\_2 == False$.
2. Both $Plug\_In$ and $Control\_Pilot$ boolean signals are set to false.
3. The Key signal is set to true ($Power\_ON == True$).
4. The SOC is set to a value greater than 20%.
5. $Reverse\_Gear\_Button$ is not engaged.

Transition from S3 to S5 (Discharge Mode to Fault/Standby Mode). This occurs in the presence of a fault at a speed greater than 5 km/h. To test this transition, the vehicle was brought into the S3 state (discharge mode) and both motor and battery overtemperature faults were simulated. Transition conditions are fulfilled when:

1. The vehicle speed is set at a value higher than 5 km/h.
2. $Power\_ON == True$.
3. $Fault\_2 == True$

To first test the fault related to motor overtemperature, the motor temperature is fixed at a value higher than 155°C. As a consequence:

- The $Motor\_Overtemperature\_Fault$ signal is triggered.
- The battery FSM goes into standby mode.

While, to test the fault related to battery overtemperature, we set the temperature of one of the cells to a value higher than 60 °C. In this way:

- The $Overtemperature\_Fault$ signal is triggered.
- The battery FSM goes into fault mode.

Test results indicate that all transitions occur without any unexpected events, confirming proper communication between the two finite-state machines, that of the powertrain and that of the battery.

8.2 Plant Simulation

In this section, the battery management algorithm is tested. After completing the LabVIEW model for the battery module consisting of the twelve cells in series, the system was integrated with the control algorithm to ensure effective response to the inputs generated. Three tests were performed:

1. Battery discharge testing.
2. Thermal management testing.
3. Balancing phase testing.

8.2.1 Battery Discharge Testing

This first test aims to validate the accuracy of the previously constructed battery electrothermal model. For this purpose, the battery is subjected to a discharge process, with a constant current of 12 A (1 C), from a fully charged state to 0%. At this preliminary stage of testing, as a safety precaution, the charge and discharge current limits, shown in table 7.1, were lowered to 0.5 C and 1 C, respectively.

Examining the resulting graph, figure 8.1, in which battery voltage is plotted as a function of SOC, it can be seen that even at 0% SOC, it never reaches the knee zone marked by the cut-off voltage. This initial result confirms what was expected, as battery cells near the cut-off voltage are subject to deterioration, swelling and reduction in charge capacity.

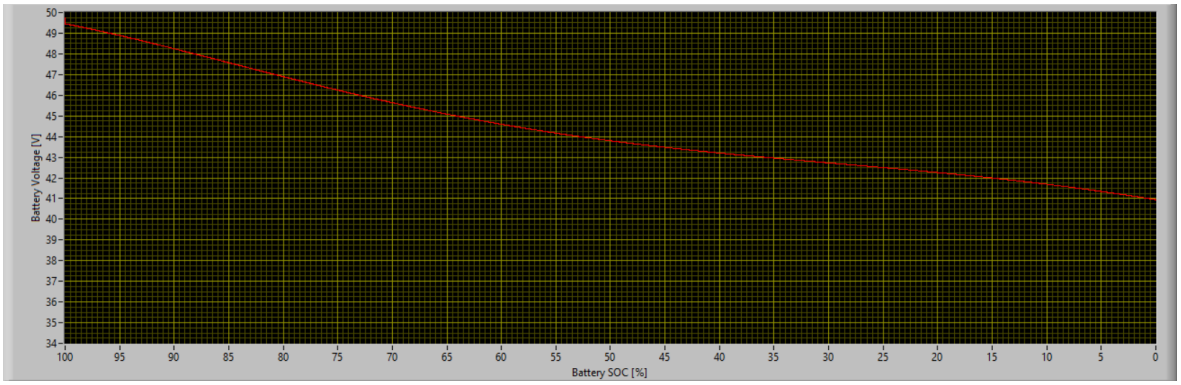

Figure 8.1: Battery discharge test

Another expected significant result is that during the initial section of the discharge phase (100% to 70% SOC), the battery supply voltage decreases from 49.5 V to 45.5 V. Subsequently, in the remaining part until 0% SOC is reached, the battery presents an equal loss of voltage, forming a plateau zone; a characteristic behavior observed in lithium batteries.

8.2.2 Thermal Management Testing

The main purpose of the thermal management test is to validate the proper operation of the battery heater in the pre-charge phase. As mentioned above, this device is controlled through a PI controller whose task is to bring the cell temperatures, which have fallen below the minimum allowable value, back to an established threshold value. For this test, the simulated room temperature is 4 °C, and the values of initial cell temperatures are configured in the table below:

Ti_1	Ti_2	Ti_3	Ti_4	Ti_5	Ti_6	Ti_7	Ti_8	Ti_9	Ti_{10}	Ti_{11}	Ti_{12}
6 °C	6 °C	7 °C	7 °C	7 °C	8 °C	8 °C	7 °C	7 °C	7 °C	6 °C	6 °C

Table 8.1: Initial cell temperatures for testing

Once these parameters were specified and the PI controller coefficients were set, the subVI of battery heating management was simulated using the battery module thermal model. The test results are shown in figures 8.2 and 8.3.

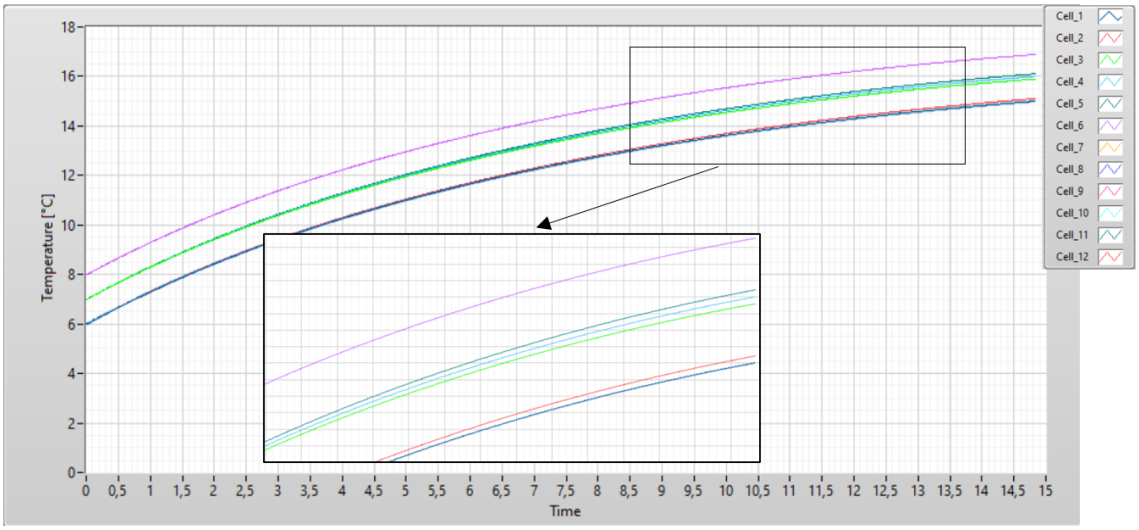

Figure 8.2: Temperatures plot

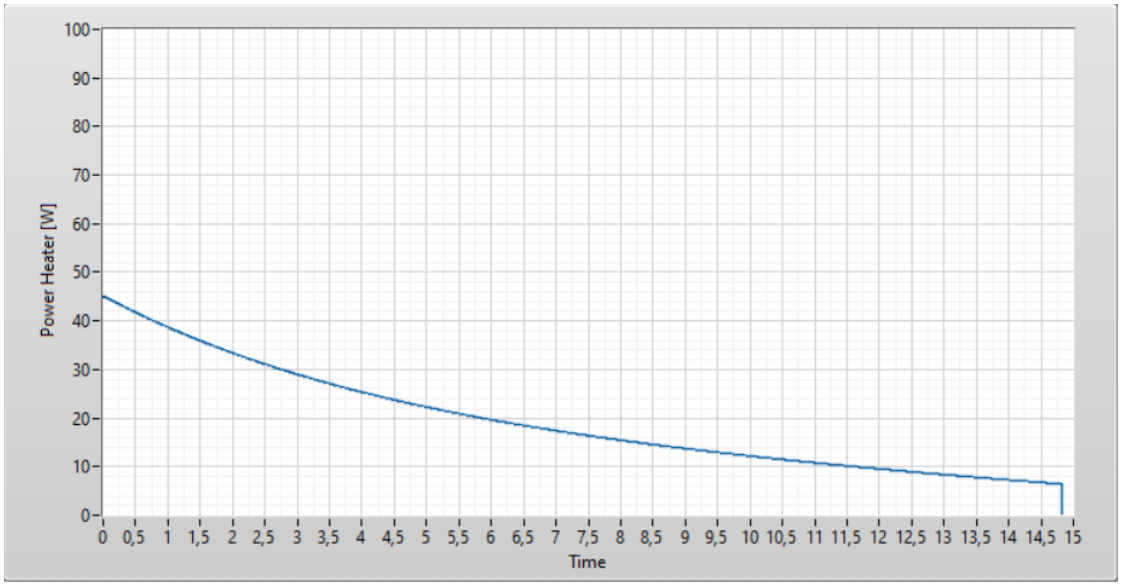

Figure 8.3: Power heater plot

As shown in the initial graph, the cell temperatures increase from their initial values to the PI controller's reference temperature of 15 °C, due to the power provided by the battery heater. Such power decreases with increasing cell temperature, until it reaches 0 W exactly when all cells reach the set temperature.
It is important to note that the heat provided by this device thermodynamically affects all cells equally. This uniformity is attributed to the examination of a single battery

module with only 12 cells in series. However, it should be noted that in the scenario of a battery composed of multiple modules, having larger sizes, the closeness to the heater would result in greater heating for the cells closer than for those farther away. Nevertheless, even more distant cells would be affected by the action of the heater because of the heat transfer between them.

8.2.3 Balancing Phase Testing

The objective of this final test is to validate the correct execution of passive cell balancing at the end of the charging phase. For this purpose, the temperature of one of the twelve cells characterizing the battery module was lowered to a very low value. As a result, at the end of the charging process, this cell have a lower voltage than the others, creating an imbalance scenario among the cells. The obtained cell voltages are shown in the table below:

V_1	V_2	V_3	V_4	V_5	V_6	V_7	V_8	V_9	V_{10}	V_{11}	V_{12}
4.16 V	4.16 V	4.01 V	4.16 V	4.16 V	4.16 V	4.16 V	4.16 V	4.16 V	4.16 V	4.16 V	4.16 V

Table 8.2: Cell voltages after charging

As can be seen from the table, the cell affected by abnormal temperature is the third one. Upon reaching this condition, subVI, which regulates passive balancing, is simulated. The cell voltage trends obtained from the simulation are shown in figure 8.4. As illustrated, cells with higher voltages discharge through a resistor, decreasing their potential until it aligns with that of the cell with the lowest voltage. Once this equilibrium is reached, the balancing phase ends and all switches are moved to the open position (0).

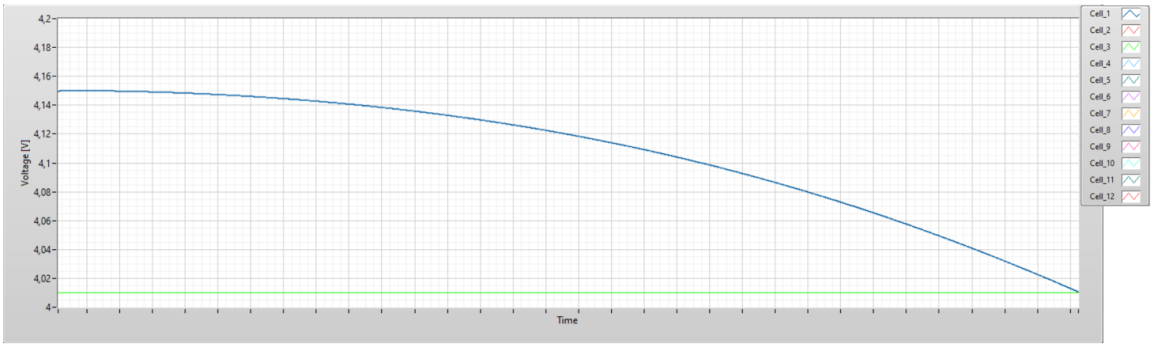

Figure 8.4: Cell voltages plot during balancing

8.3 Conclusions

The implemented algorithm meets all the defined requirements, presenting improvements and optimizations over the previous version. The SW structural design provides a unified modular algorithm that allows communication in the same control unit between battery management logic and powertrain management logic through the use of global variables. This type of structure makes it possible to potentially separate the two logics into two separate control units by replacing global variables with CAN signals. A further refinement that could be applied concerns the algorithm for SOC estimation. This involves the integration of an Extended Kalman Filter to mitigate the limitations and inaccuracies associated with the Coulomb counting technique.
The next step will involve using the CAN interface already implemented in previous projects to enable communication between the VCU and surrounding devices. This will facilitate the continuous transmission of signals, such as current limits calculated by the algorithm.
Once all the actual components of the system, including the VCU, battery emulator, inverter, and electric motor, are available, the test bench will be assembled. This configuration will allow the first HIL tests to begin.

Bibliography

[1] ETIP SNET. *E-mobility deployment and impact on grids*. 2022. URL: https://smart-networks-energy-transition.ec.europa.eu/system/files/2022-12/ETIP%20SNET%20E-Mobility%20White%20Paper_pdf.pdf.

[2] Sotecna Soc. Coop. *DIGITALIZZAZIONE ED ECONOMIA CIRCOLARE NELLE IMPRESE COOPERATIVE*. 2018. URL: https://www.mimit.gov.it/images/stories/documenti/allegati/coop/SF_Recupero_AutomezziCiclomotori_TrasformazioneMezziverdi.pdf.

[3] MINISTERO DELLE INFRASTRUTTURE E DEI TRASPORTI. *DECRETO 1 dicembre 2015, n. 219*. 2015. URL: https://www.gazzettaufficiale.it/eli/id/2016/01/11/15G00232/sg.

[4] Wei Liu. *HYBRID ELECTRIC VEHICLE SYSTEM MODELING AND CONTROL*. 2017.

[5] U.S. Department of Energy's Vehicle Technologies Office (AFDC). *How Do All-Electric Cars Work?* URL: https://afdc.energy.gov/vehicles/how-do-all-electric-cars-work.

[6] Roberto Boni. *Quel che conta è la posizione*. 2021. URL: https://www.quattroruote.it/news/tecnologia/2021/09/17/tecnica_quel_che_conta_e_la_posizione.html.

[7] Sajib Chakraborty, Mikel Mazuela, Dai-Duong Tran, Javier A. Corea-Araujo, Yuanfeng Lan, Argiñe Alacano Loiti, Patrice Garmier, Iosu Aizpuru, and Omar Hegazy. *Scalable Modelling Approach & Robust Hardware-in-the-Loop Testing of an Optimized Interleaved Bidirectional HV DC/DC Converter for Electric Vehicle Drivetrains*. 2020. URL: https://www.researchgate.net/publication/342368239_Scalable_Modelling_Approach_Robust_Hardware-in-the-Loop_Testing_of_an_Optimized_Interleaved_Bidirectional_HV_DCDC_Converter_for_Electric_Vehicle_Drivetrains.

[8] EVENERGI. *ELECTRIC BATTERY MANAGEMENT*. URL: https://www.evenergi.com/electric-battery-management/.

[9] EVERSAFE; Marcus Wisch. *Recommendations and Guidelines for Battery Crash Safety and Post-Crash Safe Handling*. 2014. URL: https://www.diva-portal.org/smash/get/diva2:1367933/FULLTEXT01.pdf.

[10] CRC Press. *Hybrid & Electric Vehicles*. URL: https://www.routledge.com/rsc/downloads/CRC_Hybrid_Vehicles_Freebook.pdf.

[11] Constantin Paul Roman, Ionel Staretu, and Laurean Bogdan. *Torque And Speed in the Actuating of Mechatronic Systems, a Case Study*. 2015. URL: https://www.researchgate.net/publication/292156233_Torque_And_Speed_in_the_Actuating_of_Mechatronic_Systems_a_Case_Study.

[12] NXP Semiconductors. *Permanent Magnet Synchronous Motor Control*. URL: https://www.nxp.com/docs/en/brochure/BBPRMMAGSYNART.pdf.

[13] Bilal Akin and Manish Bhardwaj. *Sensorless Field Oriented Control of 3-Phase Permanent Magnet Synchronous Motors*. 2013. URL: https://www.ti.com/lit/an/sprabq3/sprabq3.pdf?ts=1705176481189.

[14] Xiaoli Sun, Zhengguo Li, Xiaolin Wang, and Chengjiang Li. *Technology Development of Electric Vehicles: A Review*. 2019. URL: https://www.mdpi.com/1996-1073/13/1/90.

[15] e Station. *NOZIONI DI BASE SULLA RICARICA DEI VEICOLI ELETTRICI*. URL: https://www.e-station.it/guida-alla-ricarica-html.

[16] Bruno Do Valle, Christian T. Wentz, and Rahul Sarpeshkar. *An Area and Power-Efficient Analog Li-Ion Battery Charger Circuit*. 2011. URL: https://www.researchgate.net/publication/249319678_An_Area_and_Power-Efficient_Analog_Li-Ion_Battery_Charger_Circuit.

[17] Salvatore Musumeci. *Energy sources in HEVs and EVs*. 2022.

[18] Scott Lemon and Allan Miller. *Electric Vehicles in New Zealand: Technologically Challenged?* 2013. URL: https://www.researchgate.net/publication/319162842_Electric_Vehicles_in_New_Zealand_Technologically_Challenged.

[19] Heide Budde-Meiwes, Julia Drillkens, Benedikt Lunz, Jens Muennix, Susanne Rothgang, Julia Kowal, and Dirk Uwe Sauer. *A review of current automotive battery technology and future prospects*. 2013. URL: https://www.researchgate.net/publication/258177713_A_review_of_current_automotive_battery_technology_and_future_prospects.

[20] Bosch. *Bosch presents the powertrains of the future*. 2015. URL: https://www.bosch-press.nl/pressportal/nl/en/press-release-600.html.

[21] Rui Martim Salgado, Federico Danzi, Joana Espain Oliveira, Anter El-Azab, Pedro Ponces Camanho, and Maria Helena Braga. *The Latest Trends in Electric Vehicles Batteries*. 2021. URL: https://www.researchgate.net/publication/351906536_The_Latest_Trends_in_Electric_Vehicles_Batteries.

[22] Jian Duan, Xuan Tang, Haifeng Dai, Ying Yang, Wangyan Wu, Xuezhe Wei, and Yunhui Huang. *Building Safe Lithium-Ion Batteries for Electric Vehicles: A Review*. 2019. URL: https://link.springer.com/article/10.1007/s41918-019-00060-4.

[23] POWERSIM. *LITHIUM-ION BATTERY MODEL*. URL: https://powersimtech.com/resources/general-psim-use/lithium%e2%80%90ion-battery-model/.

[24] ACCURE. *Ultimate Guide to Battery Aging - How to Prevent Aging in Battery Energy Storage*. 2023. URL: https://www.accure.net/battery-knowledge/blog-battery-aging.

[25] Alma Automotive. *Micro Rapid Controller & Logging Environmen*. URL: https://alma-automotive.it/products/miracle2/.

[26] Ondrej Spinka, Martin Rezac, and Jan Rathousky. *Evolution of a powertrain manager for electric and hybrid-electric vehicles*. URL: file:///C:/Users/HP/Downloads/Evolution%20of%20a%20Powertrain%20Manager%20for%20Electric%20and%20Hybrid-Electric%20Vehicles%20-%20Porsche%20Engineering%20Magazine%2002-2015%20.pdf.

[27] Benevelli. *SMAC SERIE TECHNICAL DATA SHEET 3-PHASE SYNCHRONOUS MOTOR*. 2023.

[28] Surachai Wongfookeat and Thanatchai Kulworawanichpong. *Outrush Current Control by Hot Swap Controller for Battery Protection in Elecrical Vehicle*. 2017. URL: https://www.researchgate.net/publication/321122895_Outrush_Current_Control_by_Hot_Swap_Controller_for_Battery_Protection_in_Electrical_Vehicle.

[29] Ashwin Kumar Karnad. *Battery Management System for an xEV - Part 1, Basic BMS requiremnets*. 2020. URL: https://ashwinschronicles.github.io/BMS_for_an_EV_intro.

[30] A.M.S.M.H.S.Attanayaka, J.P.Karunadasa, and K.T.M.U.Hemapala. *Estimation of state of charge for lithium-ion batteries - A Review*. 2019. URL: https://www.researchgate.net/publication/332637264_Estimation_of_state_of_charge_for_lithium-ion_batteries_-_A_Review.

[31] Stephen W. Moore and Peter J. Schneider. *A Review of Cell Equalization Methods for Lithium Ion and Lithium Polymer Battery Systems*. 2001. URL: https://www.americansolarchallenge.org/ASC/wp-content/uploads/2013/01/SAE_2001-01-0959.pdf.

[32] Mohamed Daowd, Noshin Omar, Bavo Verbrugge, Peter Van Den Bossche, and Joeri Van Mierlo. *Battery Models Parameter Estimation based on Matlab/Simulink*. 2010. URL: https://www.researchgate.net/publication/234046440_Battery_Models_Parameter_Estimation_based_on_MatlabSimulink.